Aerial LTE Demonstration Report

Maxwell K. Maurice
Samuel L. Ray

NIST

National Institute of Standards and Technology

U.S. Department of Commerce

NISTIR 8380

Aerial LTE Demonstration Report

Maxwell K. Maurice
Samuel L. Ray
Communications Technology Laboratory

July 2021

U.S. Department of Commerce
Gina M. Raimondo, Secretary

National Institute of Standards and Technology
*James K. Olthoff, Performing the Non-Exclusive Functions and Duties of the Under Secretary of Commerce
for Standards and Technology & Director, National Institute of Standards and Technology*

Abstract

In this paper, we investigate a Long Term Evolution (LTE) network mounted on an airborne small unmanned aircraft system (sUAS) to provide broadband connectivity to smartphone devices on the ground. The use case is a public safety scenario where users require broadband connectivity in an isolated area. We evaluate practical constraints for the delivery platform and the LTE system. We propose research questions on how the orbit of a fixed-wing sUAS would affect the coverage area provided by the airborne small cell, and we describe the test plan used to investigate our questions. We present data on multiple field experiments and provide recommendations for future realistic deployments.

Key words

Table of Contents

List of Tables

List of Figures

iv

Definitions

LTE Attach is the successful connection, authentication, and registration of a device to a cellular network.

A **small unmanned aircraft system** is an unmanned aircraft weighing less than 55 pounds on takeoff, including all items that are on board or otherwise attached to the aircraft. The system can also refer to its associated elements (including communication links and the components that control the small unmanned aircraft) that are required for safe and efficient operation of the small unmanned aircraft in the national airspace system.

Acronyms

3GPP Third Generation Partnership Project

4G 4th Generation

5G 5th Generation

AGL Above Ground Level

CSU Colorado State University

CSV comma-separated values

DHS Department of Homeland Security

DS Deployable System(s)

EPC Evolved Packet Core

EVM Error Vector Magnitude

FAA Federal Aviation Administration

FDD Frequency Division Duplex

GPS Global Positioning System

HMDN Highly Mobile Deployed Networks

LTE Long Term Evolution

MANET mobile ad hoc network

MIMO Multiple Input Multiple Output

NGFR Next Generation First Responder

NPSBN National Public Safety Broadband Network

NUC Next Unit of Computing

PSCR Public Safety Communications Research

RF Radio Frequency

RFA Radio Frequency Authorization

RSRP Reference Signal Received Power

RSRQ Reference Signal Received Quality

RSSI Received Signal Strength Indicator

sUAS small unmanned aircraft system(s)

UAS unmanned aircraft system

UE User Equipment

1. Introduction

1.1. Project Background

The Highly Mobile Deployed Networks (HMDN) project falls within the Department of Homeland Security (DHS) portfolio of the Public Safety Communications Research (PSCR) Division. Deployable systems (DS) are a critical component for providing broadband coverage for Next Generation First Responders (NGFR) under the Nationwide Public Safety Broadband Network (NPSBN). The availability of DS is a critical need for remote areas where complete coverage is not feasible and areas where installed resources are compromised. Under this project, PSCR conducts research into DS interconnectivity to create a mobile ad hoc network (MANET) of networks to enhance interoperability between public safety agencies in incident areas.

As DS are highly mobile and rapidly deployable in nature, it should be expected that these systems will operate in a wide range of environments, in the proximity of other deployed and fixed in-band systems, in places with limited or no backhaul connectivity, and in areas where access to protected frequencies such as band 14 may be unavailable. Therefore, this project proposes to identify solutions for realizing public safety's goal of utilizing broadband services in diverse environments. Our research focuses on many aspects of deploying a broadband network for public safety use. Topics include deployment feasibility, wireless access technologies, local and distributed computing resources, and broadband service availability and quality.

1.2. Objectives

This report aims to outline aerial broadband coverage testing conducted in 2020 and 2021 by PSCR staff. We describe our experimental plan in sections 2, 3, and 4, Proposed Experiment, Test Plan, and Equipment, respectively. In section 5, we describe the field tests we conducted from July 2020 to February 2021. We summarize the results in section 6 and provide our recommendations for future work in section 7.

2. Proposed Experiment

2.1. Overview

The purpose of this experiment is to observe the coverage quality of various smartphones connected to an LTE system mounted on an orbiting sUAS. Specifically, this experiment will measure LTE reference signal received power (RSRP) as the system moves in an orbital path at several predetermined distances. Research data will provide insight into the best practices for deploying an aerial LTE communication system for the public safety deployable use case.

In previous research efforts, PSCR identified the sUAS as an ideal delivery platform for hosting a DS [1]. sUAS can position communication systems high above an operational area and provide line of sight wireless links to users on the ground. One challenge with using sUAS for hosting DS is flight time, or endurance. In a survey conducted by PSCR, 183 first responders answered the following question:

> *If drones could stay in the air indefinitely and a drone was [sic] able to provide continuous cellular broadband coverage for first responders in areas where coverage was not available, approximately how long would*

1

you anticipate needing the drone to stay in the air during such a mission?[2]

The survey results indicated that the public safety requirement for sUAS to support broadband communications is greater than 120 minutes. Although only 183 first responders responded to the survey, the majority stated a need for over 120 minutes of flight. The results of the survey question for the sUAS endurance need by first responders are shown in Fig. 1.
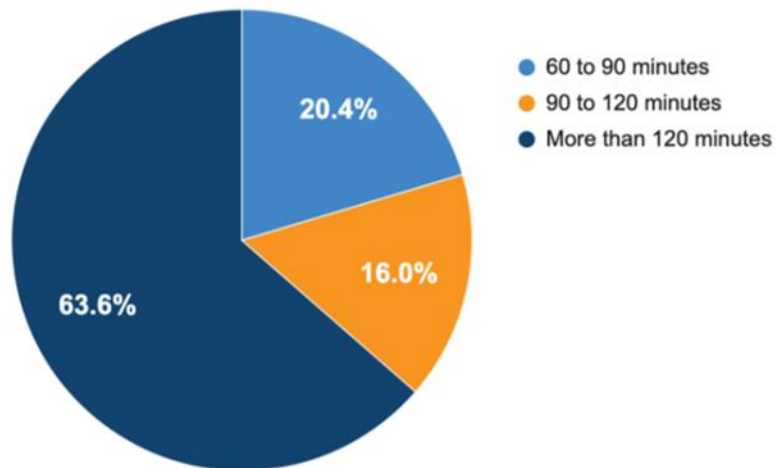
Fig. 1. sUAS endurance need by first responders [2]

Major factors contributing to sUAS endurance time are the size of the sUAS, design type, and payload mass. In previous evaluations, PSCR researchers identified these three factors for further investigation into sUAS feasibility; we continue to use these design elements for our experiments.

The total mass of an sUAS for our research and evaluation was constrained to be under 25 kg (approximately 55 pounds). This criterion comes from the Federal Aviation Administration (FAA) requirements for small unmanned aircraft use by government and commercial operators. These FAA regulations, also referred to as Part 107, are the basis for how public safety entities use sUAS. Part 107 rules dictate that the overall weight of an sUAS must be under 55 pounds, and a special exemption is required for any drone exceeding the weight limit. An exemption may not always be obtained by public safety, and given that uncertainty, our research focused on the use case for drones under the weight limit. The flexibility offered by operating under Part 107 regulations offers the best fit for the public safety DS use cases [3], [4].

From interviews with public safety personnel, the most common drone designs used by public safety agencies were multi-rotor systems. The same drone survey conducted by PSCR asked the following question:

> *If a drone (that can provide continuous cellular broadband coverage) could be either an untethered multi-rotor drone that can take off and land vertically, an untethered fixed-wing drone that can take off and land*

horizontally, or an untethered hybrid drone that can take off and land vertically and fly horizontally, would you choose one type over another?

Of the respondents who answered this question, 74.6% expressed a preference for the platform type or drone design. Independent of their answer to the previous question, respondents then indicated their preferred drone type giving the following preferences (percentages total to 101% due to rounding error):

- Either they had no preference or did not give a relevant answer (46%)

- Preferred multi-rotor UAS (29%)

- Preferred fixed-wing UAS (1%)

- Preferred hybrid UAS (14%)

- Vertical takeoff and landing capability is crucial to their missions (regardless of whether the aircraft was a multi-rotor system or a fixed-wing system) (11%)

From the survey, 29% preferred multi-rotor sUAS. That result and several other factors were sufficient for us to continue constraining our research to multi-rotor systems. Multi-rotor drones are easier to pilot than traditional winged aircraft, are cheaper to produce, and have a more extensive manufacturer base. Additionally, because public safety has adopted multi-rotor systems more than any other type of design, it seemed reasonable to research these systems instead of fixed-wing systems or hybrid systems.

The third major factor we looked at for sUAS endurance time was the payload mass. Although many DS exist within the market, and custom solutions can be built with or without certain features, a reasonable DS payload mass is around 4.5 kg (10 pounds).

The design of a multi-rotor sUAS weighing under 55 pounds (including a 4.5 kg payload) is a technically challenging effort. Moreover, it is even more difficult to design an sUAS to meet these requirements while maintaining flight capability for over 120 minutes. To push the sUAS industry and the current capabilities of an sUAS, PSCR is conducting the First Responder UAS Endurance Challenge [5], seeking to crowdsource sUAS designs that fit these constraints. The challenge is currently ongoing and will conclude in 2021.

Revisiting the major sUAS flight endurance factors, we investigated other sUAS design types in addition to multi-rotor systems. The relationship of aircraft design type to aerial efficiency is noted in [6]. Multi-rotor systems have the lowest efficiency for staying airborne when compared to helicopter systems or fixed-wing systems. One reason fixed-wing systems are more energy efficient is that they obtain lift from forward motion and wing geometry. Because fixed-wing systems by design are more energy efficient, it is expected that fixed-wing systems would generally have longer endurance times than multi-rotor systems. This expectation led PSCR to ask questions about the feasibility of using a fixed-wing system, instead of a multi-rotor system, to host a DS.

2.2. Research Questions

Using fixed-wing systems to provide broadband connectivity to first responders, we encounter a new deployment configuration for an aerial DS. The significant differences in utilizing a fixed-wing system over a multi-rotor system are the following:

1. Fixed-wing drones must be in lateral motion for flight.

2. The use of fixed-wing drones introduces rapidly varying distances to the ground receivers.

These two characteristics introduced by fixed-wing drones may have unintended consequences for providing broadband service. To understand the link characteristics, we propose to investigate a specific scenario involving several LTE connections to users on the ground from a fixed-wing aircraft at various orbital radii. We will collect connectivity data to answer the following:

1. Motion may have unintended effects on the link between an eNodeB and User Equipment (UE). Does eNodeB motion cause link degradation to a UE on the ground?

2. Rapidly varying distances between an eNodeB and a UE will cause fluctuating link qualities. What does this link look like between an eNodeB and a UE on the ground?

3. It can take several seconds for a UE to attach to a network when an eNodeB reference signal is first picked up. If the distance between an eNodeB and UE changes quickly, then a UE may not be able to attach to the network in time. Alternatively, there is a case where a UE does attach, but the eNodeB moves away from the UE, so the connection is only used for a brief period. This case would lead to a limitation on the amount of data exchanged by the LTE network and the UE. In certain cases, the small amount of data exchanged by the LTE network and the UE would have the same effect as if the phone never connected to the LTE network. The delay in attaching to the LTE network would shrink the realized coverage area provided by the system. What would the new effective coverage area be?

By analyzing data from several aerial experiments, we can answer these questions and provide data on optimizing a fixed-wing drone operation. Further, by conducting several experiments, we plan to provide the public safety community with valuable recommendations.

As an additional note, for the remainder of this report, we will be using the term *attach* to describe the successful authentication and connection of a UE to the LTE network.

2.3. Authorizations

Before continuing, it is important to provide a brief account of the frequency authorizations PSCR staff obtained for the experiments. PSCR owns specialized LTE equipment that operates only in band 14, a restricted spectrum that is owned by FirstNet and leased to AT&T. For initial testing, PSCR applied for several Radio Frequency Authorizations (RFA) for Gypsum, Colorado, that were approved in March 2019. The RFAs only cover the Gypsum area. When testing had to move to Fort Collins, Colorado, PSCR staff contacted a federal liaison spectrum manager from FirstNet, who coordinated the request with AT&T for

special permission to use band 14 without an RFA. PSCR was granted an exception for testing band 14 at Christman airport in Fort Collins with the same notice and contact/communication mechanism that PSCR used for the Gypsum RFAs.

3. Test Plan

The test plan below outlines the specific tests for the aerial experiment. Tests included ground-based control measurements as well as various aerial tests.

3.1. Close-range Baseline Test

The close-range baseline connectivity test will collect data on ideal connectivity to the eNodeB for each phone. This test involves the LTE system connected to each smartphone at a close range. Figure 2 shows a diagram of the test setup.
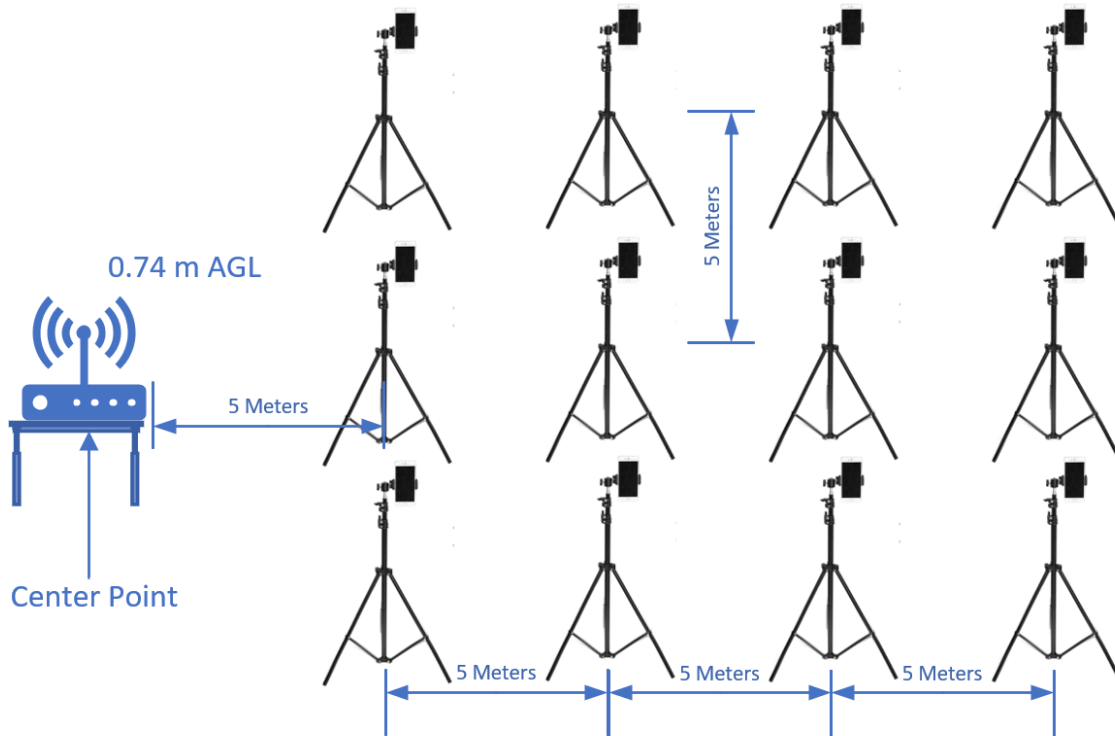
Fig. 2. Baseline test setup diagram

We placed the LTE system at the center of our test range, also known as the central point, elevated approximately 0.74 m from the ground. The height was based on the portable table used for the test. The LTE eNodeB antenna is oriented downrange toward the smartphones using a tripod to maintain its orientation. Specifically, the eNodeB antenna will have its gain maximum in the direction of the smartphones. We provide more information on the LTE eNodeB antenna in Sec. 4.2. Figure 3 shows this test setup in Gypsum, Colorado during a test in August.

Fig. 3. Baseline test setup antenna orientation

Four rows of smartphones will be mounted on tripods 5 m apart in a small grid. The phones will be raised to 1.3 m above ground level and oriented vertically with the screens facing the LTE system. Three different smartphones, anonymized for this report, will be in each of the four rows. Loaded on each phone is the NetMonitor Pro Android application, which monitors and reports cellular connectivity metrics. The application will run on each phone to collect connectivity data during the test. Section 4.4 provides more information on the NetMonitor Pro application. The primary measurement recorded is the eNodeB reference signal received power (RSRP). This measurement can be loosely translated to coverage quality and is a predictable quantity used widely by telecom operators. We will run the experiment for approximately 20 minutes to capture any connectivity fades that the phones may experience over time. We will use a handheld spectrum analyzer at the center point to measure error vector magnitude (EVM) and Doppler shift data if any exist.

This test ensures that the phones are connecting to the LTE network properly before an aerial test. The close-range baseline test will also reveal any issues with the phones connecting to the LTE system. The expectation is that all phones will remain attached and connected to the LTE system throughout the test and will measure an RSRP above -100 dBm. This -100 dBm criterion is based on the free space path loss calculation which is approximately 56 dB for the phones in the fourth row. A phone that reads a connection below -100 dBm most likely has an issue and will be removed from the experiment. This test would provide an opportunity for backup smartphones to be substituted.

3.2.   Full-range Baseline Test

The full-range baseline test involves placing phones down range to collect connectivity data without any movement or altitude advantages. Phones will stay in their same rows, but row spacing will be increased from 5 meters to 300 meters. Figure 4 and Fig. 5 show the diagram of this test setup and the physical location of each smartphone at the Christman test site. More information on the test location will be described in a later section.
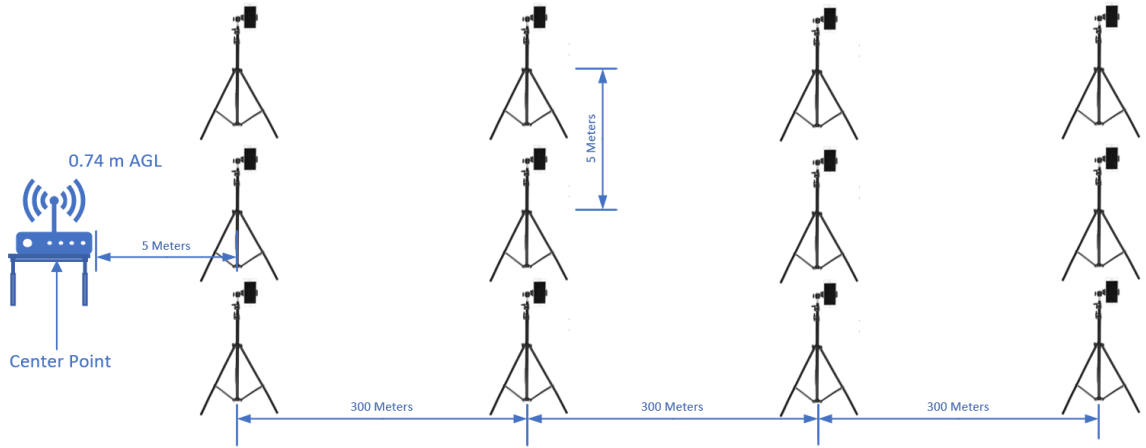
Fig. 4. Full-range baseline test diagram

Fig. 5. Google Maps full-range baseline test setup at Christman airport

Although it is unknown what the connection quality will be between the LTE system and each phone, we can estimate the path loss between the system and each row, as well as the

7

ideal RSRP level. Table 1 shows the calculated path loss and predicted RSRP levels for each row.

Table 1. Estimated Path Loss and Ideal RSRP.

Row	Distance	Free Space Path Loss	Ideal Predicted RSRP
Row 1	5 m	44.1 dB $\pm$ 0.3 dB	-42.5 dBm $\pm$ 0.6 dB
Row 2	305 m	79.782 dB $\pm$ 0.005 dB	-78.2 dBm $\pm$ 0.5 dB
Row 3	605 m	85.731 dB $\pm$ 0.003 dB	-84.2 dBm $\pm$ 0.5 dB
Row 4	905 m	89.229 dB $\pm$ 0.002 dB	-87.7 dBm $\pm$ 0.5 dB

The predicted RSRP values are derived from measured LTE system output power of 1.1 $\pm$ 0.5 dBm and ideal line of sight free space path loss calculation. As noted in previous research [1], line of sight is critical for high-frequency broadband communication links. In most ground-based deployment cases, line of sight cannot be obtained, so it is not expected that this test will yield the ideal predicted RSRP values for phones in the more distant rows. This ground-based test will provide another baseline for comparison with flight tests at similar distances, where line of sight communications will be enabled by the sUAS. In other words, this test will provide data to demonstrate why it is necessary to host the system on a drone in the first place. If all phones in this test could connect to the LTE network with no issues and adequate connection quality, then a drone with an LTE system would not be needed.

3.3. Aerial Tests

The aerial tests involve mounting the LTE system to a fixed-wing aircraft that follows a prescribed circular path around the center point of the test range. The phones for the test will remain in the same place as in the full-range baseline test and will log connectivity data. The altitude of the aircraft will be set near the maximum altitude for Part 107 regulations, just below 122 m (400 feet). Although the optimal speed of the aircraft will be determined during the trial, the aim is for the pilot to conserve as much energy as possible for prolonged flight endurance time. The aircraft has a stall speed of 13.0 m/s and a cruise speed of 18.9 m/s, so it is assumed to fly somewhere in this range, with consistent speed for all tests. Three flight paths, described below, will be implemented.

3.3.1. 350-Meter Test

In the 350-meter test, the aircraft's orbital radius will be set to 350 meters which will place the aircraft into a 5- to 10-degree bank relative to the ground. Figure 6 provides a diagram of this experiment.
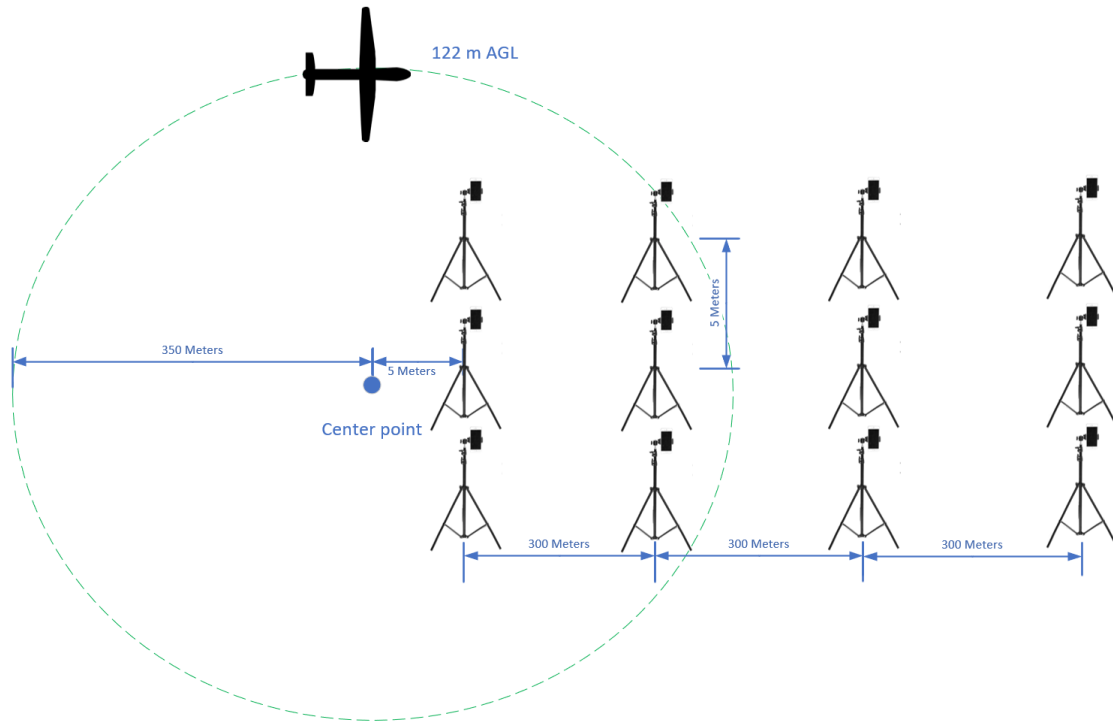
Fig. 6. 350-meter test diagram

We expect a varying connectivity pattern for each row of phones, as described in Sec. 3.4. The orientation of the antenna on the fixed-wing aircraft is described in Sec. 4.2. The test will run for as long as the aircraft can remain in the sky.

3.3.2. 650-Meter Test
In the 650-meter test, the aircraft's orbital radius will be set to 650 meters. Other than the orbital radius, this test is identical to the 350-meter test.

3.3.3. 850-Meter Test
In the 850-meter test, the aircraft's orbital radius will be set to 850 meters. Again, this test is identical to the two previous orbital tests, except for the change in radius. Originally this test was planned for a 950 m orbit; however, due to flight restrictions at Christman airport, the orbital radius was reduced.

3.3.4. Additional Trials
Depending on the available time and the outcome of the previous three flight tests, we may perform additional flight tests for more data. A 200 m trial may be executed, along with iterations of the previous flight tests. Figure 7 shows the aerial map for the three flight tests.
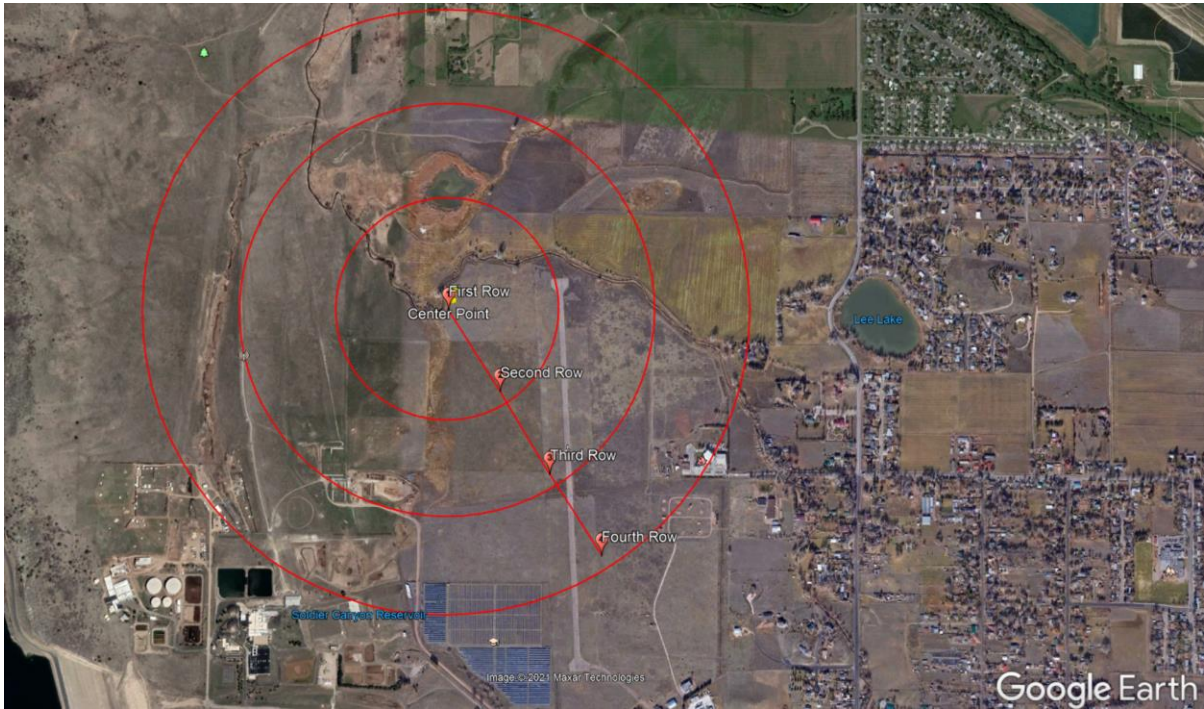
Fig. 7. Google Maps summary of all three flight trials

3.4. Expectation

In preparation for the experiment, PSCR staff developed code to predict the distance and path loss between the aircraft and each row of phones on the ground. Appendix A provides a few sample output data plots for the 350-meter test and the 850-meter test for the first and fourth rows. Table 2 summarizes these plots with approximate estimations about the expected connectivity.

Table 2. Approximate Assessment of Connectivity.

Summary	Small Orbit	Large Orbit
Phones close to the center of the orbit	• Overall path loss: ≈79 dB • Small variation: ≈0.2 dB	• Overall path loss: ≈87 dB • Small variation: ≈0.1 dB
Phones far from the center of the orbit	• Overall path loss: ≈86 dB • Sizable variation: ≈7 dB	• Overall path loss: between 70 dB and 90 dB • Large variation: ≈24 dB

In Table 2 above, when phones are far from the center of the orbit and the aircraft is in a large orbit, we see extreme changes in path loss and distance over time. This variability will cause issues in connecting the phone to the LTE system and, if connected, maintaining the connection.

10

4. Equipment

The following section describes the components involved in the experiment and the details surrounding their usage.

4.1.   LTE System

The LTE system, which we anonymized for this report, is a complete virtualized LTE EPC (Evolved Packet Core) and eNodeB radio. The core and radio combine to form a full LTE system. The eNodeB is a Frequency Division Duplexed (FDD) system that receives UE signals (uplink) in the 788 MHz to 798 MHz range and transmits (downlink) in the 758 MHz to 768 MHz range. These paired frequency ranges are known as band 14.

The system contains an Intel Next Unit of Computing (NUC) that runs a virtualized LTE core. The NUC, radio baseband unit, and the RF board require a 12-volt source to supply at least 6 amps. The total system mass is roughly 1.5 kg without a power supply. Figure 8 shows a picture of the LTE system.

Fig. 8. LTE System

The eNodeB of the LTE system is a 2x2 Multiple Input Multiple Output (MIMO) system that can output 1 W of power per antenna port within the 10 MHz downlink channel; however, that level is reached only when every resource block in the LTE signal is at maximum power. Consequently, the coverage area provided by the system cannot be predicted based on a 1 W signal. The RSRP, which is the power measured by the UE in the downlink reference signal, determines the ability of a phone to attach and maintain a connection to an eNodeB. Therefore, the RSRP, instead of the total power output, is used to determine the coverage area of an LTE eNodeB.

The RSRP value we expect to measure for the eNodeB can be calculated by assuming it transmits with its full rated power across the channel, then dividing the total power between all of the resource blocks of the downlink LTE signal, using Eq. (1)

$$RSRP\ (dBm) = RSSI\ (dBm) - 10\log(12 \times RB) \qquad (1)$$

11

The Received Signal Strength Indicator (RSSI) is the maximum output power of the total channel (specified at 1 W or 30 dBm). RB is the number of resource blocks in the channel. A 10 MHz downlink channel corresponds to 50 resource blocks, so our expected RSRP at the transmitter is 2.22 dBm. PSCR staff cabled the eNodeB directly to a handheld spectrum analyzer and measured the RSRP at approximately 1 to 1.5 dBm. Although under the expected level of 2.22 dBm, the difference may be attributed to losses in cabling and connectors.

PSCR staff tested 17 smartphones from three vendors with the LTE system. Every phone was able to attach to the system and reach the internet when the system was cabled to a gateway router.

4.2.   Band 14 LTE eNodeB Antennas

The eNodeB antenna selected for the experiment was the EM-LTE flexible internal strip antenna from MobileMark. The EM-LTE antenna covers both the 695 MHz to 960 MHz band and the 1710 MHz to 2700 MHz band and provides a directivity slightly over 0 dB at 725 MHz. The antenna has a bend radius of 2.5 inches (6.4 cm), allowing it to fit on curved surfaces [8]. The maximum input power to the antenna is 5 watts, within the 1-watt rating of the eNodeB. The antenna dimensions are 1.3 inches (3.4 cm) by 5.4 inches (13.7 cm). Figure 9 shows the EM-LTE flexible antenna.

Fig. 9. EM-LTE Antenna.

After reviewing the planned experiment measurements, namely RSRP values, we decided to use only one antenna for one of the antenna ports on the eNodeB. Specifically, we will use antenna port 0 of the eNodeB, which transmits the reference signal block. By having only one antenna attached to the aircraft, we save in experiment complexity and space management, as the aircraft underside is small compared to the antenna. An additional antenna would only boost data rates, which we did not measure in this experiment. Figure 10 shows the manufacturer antenna pattern and a PSCR-created visualization of the antenna gain.
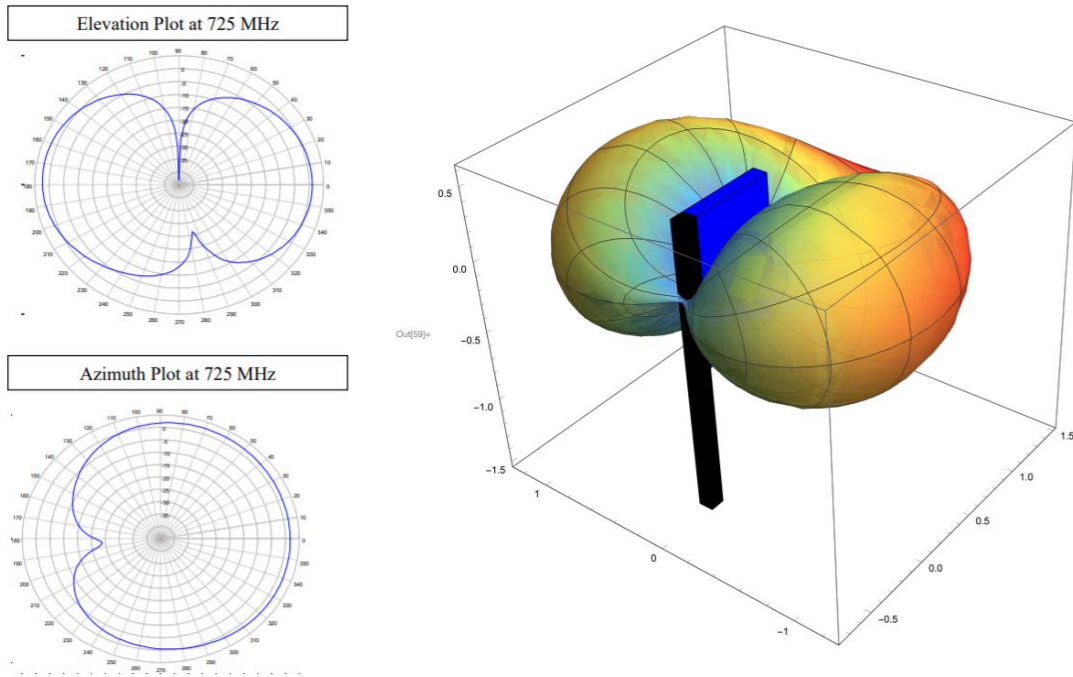
Fig. 10. (a) EM-LTE Antenna gain pattern **(b)** PSCR gain estimation

For the experiment, we will place the antenna as close as possible to the front of the aircraft, away from the motor, to avoid interference from the motor and any other moving metallic sections. This orientation will provide the best possible connectivity to phones on the left and right sides of the aircraft. The major nulls from this orientation would be in front of and behind the aircraft. The antenna will be mounted to the aircraft, as shown in Fig. 11.

Fig. 11. Antenna placement and orientation on sUAS

13

4.3. Albatross Fixed-wing UAV

The sUAS selected for the experiment is the Albatross fixed-wing UAV, owned and operated by the CSU Drone Center at Colorado State University. This sUAS has a mass of 4.4 kg without a battery and is rated to carry a maximum payload of 5.6 kg [7]. The system, developed by Applied Aeronautics, has a wingspan of 3 m and can reach speeds up to 36 m/s (80 mph). The Albatross employs open-source software for its PX4 autopilot system, used for automatic takeoffs and landings. The aircraft is rated for a stall speed of 13.0 m/s and a cruise speed of 18.9 m/s; we assumed it would fly in this range during our tests. During flight trials conducted in July 2020, the system flew for 19 minutes with a replica payload mass of 1.496 kg, using a single battery. Figure 12 shows the aircraft during the July test flight.

Fig. 12. CSU Drone Center Albatross fixed-wing UAV

The CSU Drone Center worked with Applied Aeronautics to increase the efficiency of the drone for this use case. After reviewing some of the flight logs, the Drone Center staff believed that a 30-minute flight time would be obtainable with some drone modifications.

4.4. NetMonitor Pro Tool

For measuring UE LTE connectivity, we will use the NetMonitor Pro cell signal logging application. The tool collects cellular connectivity metrics such as RSRP, Reference Signal Received Quality (RSRQ), Global Positioning System (GPS) data, and other cellular system information. The tool can be used on Android 4.4 and higher devices and provides graphical information for recorded logging sessions. Figure 13 shows results from an example test conducted in Boulder. Note that the application can provide a map of coverage with GPS uncertainty. The color scheme can be customized to show "Good," "Not bad," and "Bad" coverage.

14
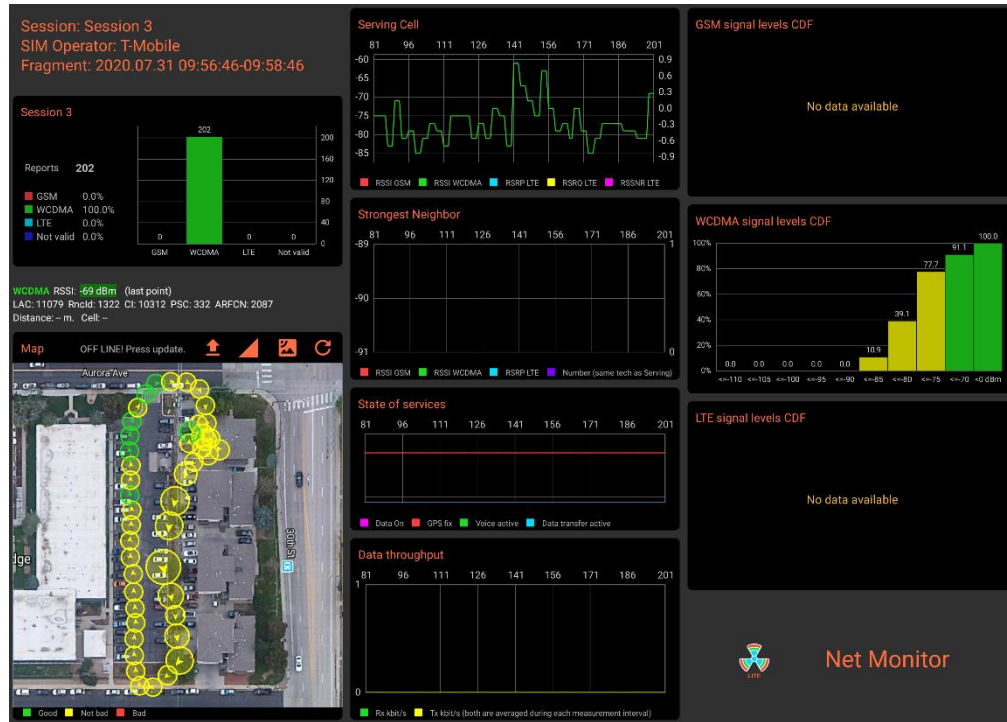
Fig. 13. NetMonitor Pro tool example output

The application stores logged data into a Structured Query Language database or SQLite database in the Android phone. Researchers can export the data into a comma-separated values (CSV) file for further analysis.

In August, tests were conducted on several smartphones to see what occurred when the phones were disconnected from the LTE network and then reconnected. These tests showed that as soon as a phone was reconnected to the LTE network, the application resumed recording, and the next measured point reflected the connection with no lapse in data. This result indicated that the application would measure RSRP near the exact time a phone connected to the network.

4.5. Portable Tripod and Battery Banks

Portable smartphone tripods and portable battery banks will be utilized for the experiment to hold phones in place and to charge the devices. Tripods provide realistic elevation and orientation for the phones, allowing us to simulate users holding the UEs as we measure LTE signals. The 10,000 mA·h battery banks are attached to the tripods and plugged into the smartphones so that devices are charged for the duration of each test. Figure 14 shows the setup in the lab.

15

Fig. 14. Tripod and battery bank setup

4.6. Lufkin 12-1/2-inch Measuring Wheel

A measurement wheel will be used to place the phones relative to one another in each row. The gear-based measuring system has an accuracy of $\pm\,0.01\%$. The position of the phones during the full-range baseline test and flight trials will be determined by using GPS coordinates provided by the phones.

4.7. Rohde and Schwarz FSH8 Spectrum Analyzer

The Rohde and Schwarz FSH8 handheld spectrum analyzer will be used at the center point to measure EVM. The spectrum analyzer can decode and measure over-the-air LTE signal information and report overall transmitter performance.

5. Field Tests

The sections below detail the field tests that PSCR staff conducted from mid-July 2020 until February 2021. Staff conducted the tests in the PSCR lab, Gypsum, Colorado, and Fort Collins, Colorado.

5.1. July Tests

On July 13, 2020, initial flight tests were conducted at Christman airport in Fort Collins with a 1.496 kg replica payload. The tests ensured that the Albatross fixed-wing UAV could fly circular flight paths with the payload properly and safely, as it flew for 19 minutes in the 350 m circular orbit. Figure 15 shows one of the CSU Drone Center pilots placing the replica payload into the Albatross.

Fig. 15. Albatross fixed-wing aircraft with replica payload

5.2. September Tests

On September 18, 2020, PSCR staff conducted a site survey and baseline tests at the Gypsum Creek Ranch airport, a privately owned airport within the boundaries of PSCR's band 14 RFA. After speaking with the airport owners, PSCR and the CSU Drone Center staff were granted permission to use the facilities for experiments. Figure 16 shows the September close-range baseline test setup at the airport.

Fig. 16. Close-range baseline test at the Gypsum Creek Ranch airport

The results of the full-range baseline test are outlined below and revealed that the eNodeB was not operating as expected. The approximate connectivity range of the system for the full-range baseline test showed that only the first row of phones could attach to the network.

A walking test revealed that phones could not detect the eNodeB signal beyond approximately 150 m from the base station, even though line of sight to the LTE system was maintained throughout the test. In the days following the trial, the team determined that the eNodeB was not properly configured by the vendor. Several troubleshooting meetings with the vendor confirmed that the eNodeB was operating at a much lower output power than intended. The eNodeB was reconfigured in late September and validated by PSCR staff.

5.3. October Tests

On October 3, 2020, PSCR staff and the CSU Drone Center pilots arrived at the Gypsum Creek Ranch private airport for testing. PSCR staff conducted both baseline tests; however, we did not conduct aerial tests due to takeoff issues with the sUAS.

Before the September site evaluation, the pilots expressed concerns about the gravel runway and upgraded the landing gear of the Albatross to address the rough surface. After successfully performing pre-flight and taxi tests with the replica payload, the first flight attempt proved unsuccessful. The flight was aborted before the aircraft took off because gravel from the runway started striking the propeller. An inspection of the aircraft revealed that all three blades of the propeller were significantly damaged, presumably when rocks were kicked up by the nose wheel and drawn into the propeller. The Drone Center team had a spare propeller, but given the risk that the same issue could happen again, the team deemed it unsafe to proceed with another flight. The owner of the airport took the flight team around the area to search for another (grass or paved) surface to use as a runway, but we could not find a location that would allow safe takeoff and landing of the aircraft. As a result, we canceled all aerial tests at the Gypsum site.

While flight tests could not be conducted, ground baseline tests provided new information about the LTE system; this information is reported below.

5.3.1. October Close-range Baseline Test

In the close-range baseline test, PSCR staff observed a range of smartphone-measured RSRP values across every device and at all distances. The measurements ranged from -42 dBm to -128 dBm; however, all devices recorded the majority of RSRP values near -55 dBm, indicating a good connection. Figure 17 shows all phone measurements combined into one plot with the mean for each row, the 95% confidence interval of the mean, and error bars that show the middle 90% of the data. The 95% confidence intervals, shown to the right of each mean, were calculated first in linear watts and then converted to dBm. The error bars that extend through the middle 90% of the data provide insight into the density of points for each row. Plots for each phone type are available in Appendix B, which include the mean for each row, the 95% confidence interval of the mean, and error bars that show the middle 90% of the data.

Box labels (left to right above plot):

- Number of points: 2878 / Mean: -49.33 dBm (-49.46,-49.2) / Dropped Connections: 382
- Number of points: 2613 / Mean: -49.05 dBm (-49.15,-48.96) / Dropped Connections: 458
- Number of points: 2619 / Mean: -55.0 dBm (-55.11,-54.89) / Dropped Connections: 161
- Number of points: 3030 / Mean: -54.45 dBm (-54.52,-54.38) / Dropped Connections: 131

Gypsum
Baseline Test 1
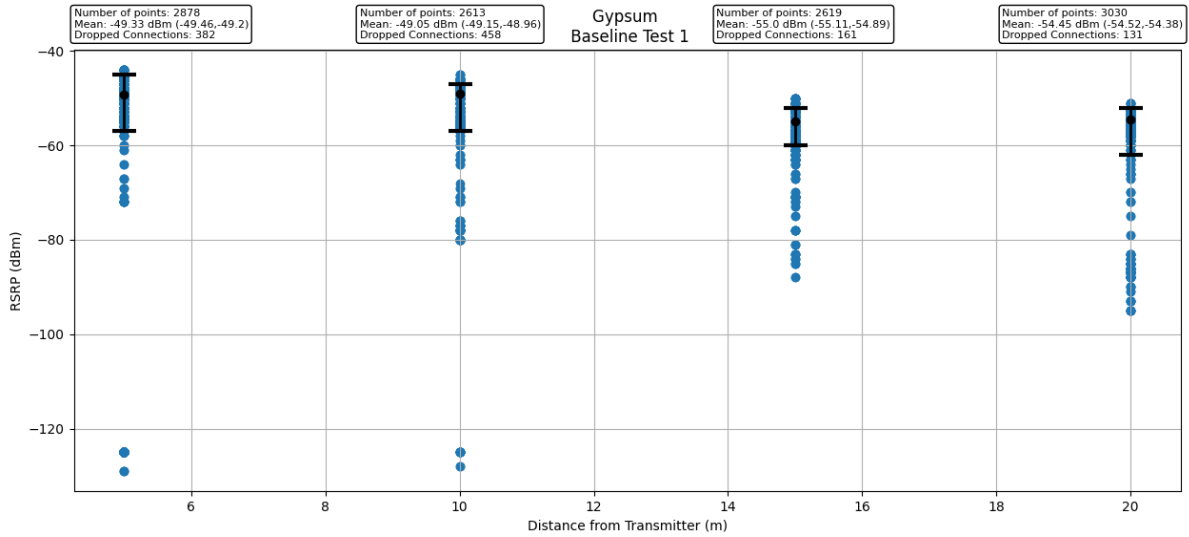
Fig. 17. Plot of all phones in close-range baseline test

Included in Fig. 17 are a number of instances where the NetMonitor Pro tool could not measure LTE connectivity. These instances were recorded in the SQLite database on each phone as points with random or null measurements for certain aspects of the signal such as *eNodeB cell ID* or *network ID*, and they are displayed in each close-range and full-range baseline plot as the number of dropped connections in boxes above the plot. The boxes show data for each row of phones so that the number of dropped connections can be compared between rows. Appendix B includes the number of dropped connections by phone type as well. These points could reflect issues with the application, with the LTE system, or as valid drops in wireless connectivity to the LTE system. Sometimes the drops in connectivity would last for several seconds, and at other times they would come in small bursts lasting only for a few seconds. We observed this behavior also in lab settings under controlled radio environments, such as in an RF shielded enclosure. The drops in connectivity could not be reproduced for a personal device attached to an active commercial network with the app. This issue is discussed further in Sec. 6.2.

For the data collected from the NetMonitor Pro tool, we filtered out only successful measurements from the LTE system. We determined whether a measurement was successful by comparing the known eNodeB cell ID to the one recorded in the phone measurement. For example, some measured points showed the cell ID for a neighboring network site. Although our smartphones would never attach to these neighboring cell sites, the smartphone would cycle through these cell sites to determine whether it could connect. These measured points would be read as dropped connections to our network. In other cases, a measured point would read a nonexistent cell ID such as 2147483647. Again, such points were recorded as dropped connections.

Another note about this test was that the handheld spectrum analyzer used during the experiment measured a nearby AT&T band 14 commercial cell site. The cell site was located near I-70, just north of the airfield. The spectrum analyzer measured the AT&T cell RSRP value at around -120 dBm. While it is unlikely that the low-power LTE system used in our

19

test would interfere with users on the AT&T system, the AT&T cell site did raise the noise floor for our experiment and introduced a low level of interference to the test area.

5.3.2. October Full-range Baseline Test

In the full-range baseline test, we observed that all smartphones in row 1 connected to the LTE system, and only a single type of phone was able to attach from rows 2 and 3. The other two types of phones in the second and third rows did not attach. Finally, all phones in the fourth row failed to attach to the network. In tests conducted in controlled radio environments, phone attachment times to this LTE system ranged from a couple of seconds to around 30 seconds. This test was carried out over several minutes, allowing ample time for any phone within range to attach. Figure 18 shows the full-range baseline test, where the points at 305 m and 605 m are only from one phone type. Again we have included the mean, 95% confidence interval of the mean, and error bars showing the middle 90% of the data.
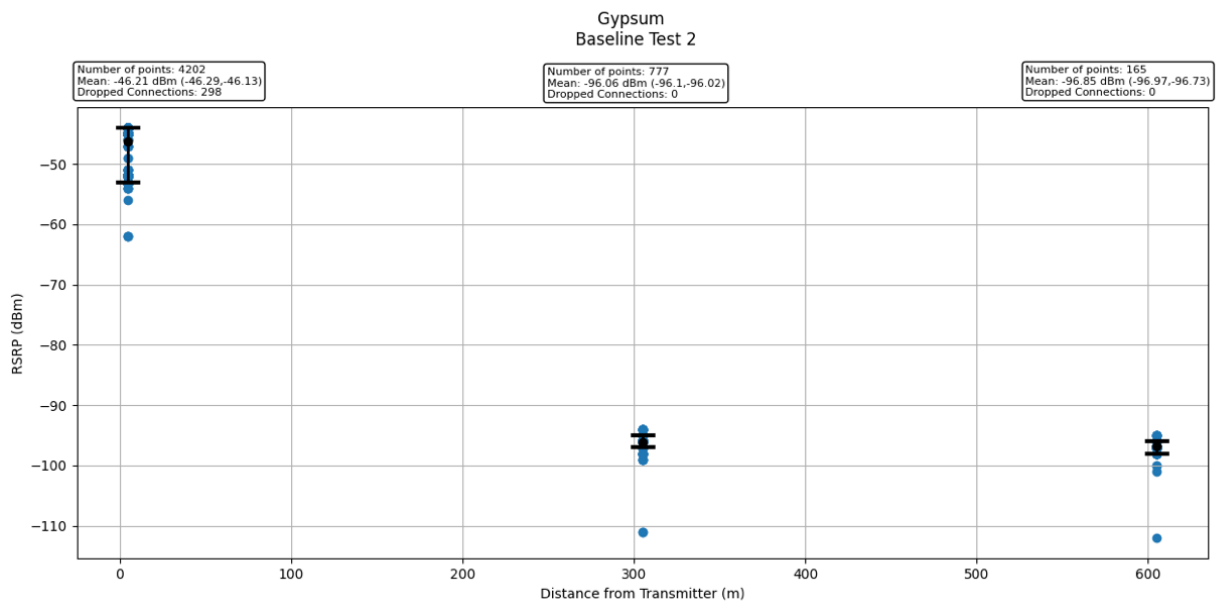
Fig. 18. Plot of all phones for the full-range baseline test

Because the full-range baseline test showed only one type of phone that was able to attach to the network 300 m away, it was decided to carry out an additional walking test as described in the next section.

5.3.3. October Walking Test

As an added informal test to the October experiment, PSCR staff walked with each type of phone along the test site to observe connectivity over distance. Two researchers attached the phones to the network near the LTE system and proceeded to walk in a straight line toward each row of the test site. At all points during this walk, the eNodeB was within visual line of sight to the researchers. Figure 19 shows all the measured RSRP values over distance.

20
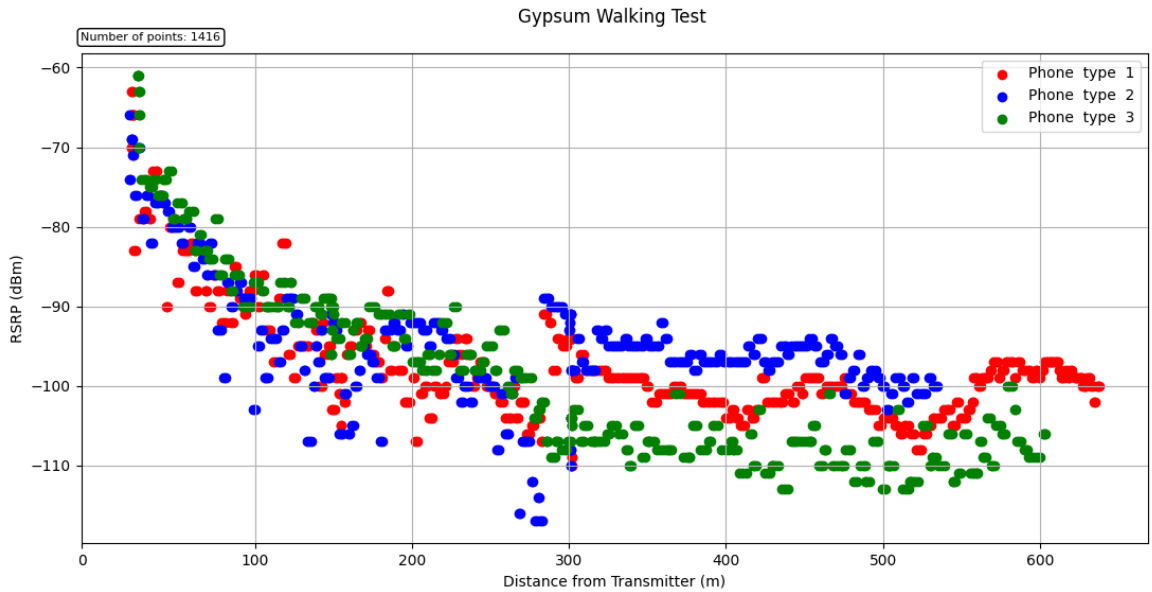
Fig. 19. Plot of all phones for the informal walking test

Plots of RSRP over distance for each phone are in Appendix B. These plots show smartphone connectivity as far out as 600 meters for two of the phones. It is unknown why two types of phones would not attach to the LTE system in their static locations as was the case in the full-range baseline test but could stay attached to the network in the same locations during the walking test. This was the first indication that LTE coverage depends on whether a device is attached to the network or not. This result is further discussed in Sec. 35.

5.4. December Tests

After aerial tests could not be carried out in October, the research team determined that the CSU Drone Center in northwest Fort Collins was the most viable alternate test site. The Christman airport is owned and operated by the CSU Drone Center and is used primarily for drone flights by the center. The property is fully fenced off, and only CSU personnel have gate access. The asphalt runway is approximately 18 m wide and 1200 m long, making it ideal for fixed-wing drone operations. Special permission was obtained from AT&T and FirstNet by PSCR staff to conduct band 14 tests at the airport.

In October, the State of Colorado used the Christman airport for fighting the Cameron Peak fire west of Fort Collins. Because of this development, the CSU Drone Center and PSCR staff could not gain access to the airport for testing until early December.

On December 7, PSCR staff planned to conduct flight tests with the LTE system at Christman airport. However, during a preliminary test flight with the Albatross, the system autopilot landed too hard, breaking one of the landing wheels. Figure 20 shows the damaged Albatross.

Fig. 20. Albatross fixed-wing aircraft on December 7 with detached landing gear

Without proper landing gear, the CSU drone pilots no longer felt safe in piloting the system, and they elected to replace it with a multi-rotor drone which was used in previous experiments by PSCR in the Summer of 2019. The LTE system was mounted to the underside of the drone with the intention of simulating a fixed-wing drone flight by following the same orbits proposed for the experiment. Due to endurance limitations, the multi-rotor drone could only complete one 850 m orbit. As a result, the PSCR research team chose to perform only the 350-meter and 650-meter tests. Due to limitations in the software used to pilot the multi-rotor, the system could not fly continuously in a circular pattern for the 650 m orbit. For the 650 m orbit, the drone had to slow down at points along the circular orbit, so the system was not at a constant speed and not flying in a perfect circle. The effects from this limitation are apparent later in Fig. 26, where the plot of drone distance to each row is not smooth. Also, the maximum speed was restricted to 9.8 m/s (22 mph), so the system did not perfectly emulate the fixed-wing drone pattern. The eNodeB antenna was placed in a similar orientation as was planned for the fixed-wing Albatross. Figure 21 shows the LTE system mounted to the multi-rotor.

Fig. 21. Multi-rotor drone with LTE system

Altogether, the results from the aerial tests seem to provide a fairly accurate representation of a fixed-wing drone flight, with the most significant difference being the speed at which the aircraft moved. As previously mentioned, since the aircraft is in motion, there are cases where UEs do not have enough time to attach to the LTE network. The multi-rotor drone orbits the area at a much slower rate than a fixed-wing vehicle, giving UEs more time to attach. The following sections describe the data collected from the experiment.

5.4.1. December Close-range Baseline Test

The close-range baseline test showed results similar to those from the Gypsum tests, with phones collecting connectivity data at spacing intervals of 5 m. Each row of phones recorded average RSRP values between -52 dBm and -60 dBm. Figure 22 shows the measured RSRP values for all phones within each row for this test. Plots of data from individual phones are included in Appendix B.
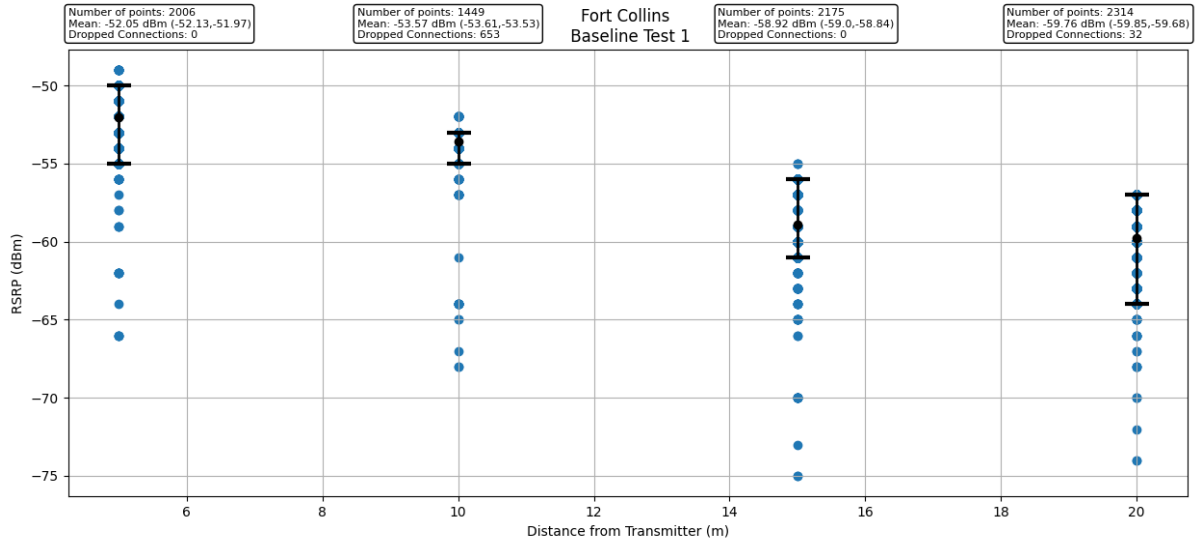
Fig. 22. Plot of all phones in close-range baseline test

In addition to collecting signal information from phones, we placed a Rohde and Schwarz handheld spectrum analyzer next to the system to collect data. The analyzer was placed in the null of the radiating antenna, collecting spectrum metrics such as RSRP, RF Channel Power, SINR, and others. Table reports the means, 95% confidence intervals of the means, and the delineation points where in between resides 90% of all the 154 measurements collected during the test.

Table 3. Handheld Spectrum Analyzer Measurements.

Metric	Mean	95% CI	Middle 90% Range
RSRP	-34.75	-34.87, -34.64	-35.51, -33.727
RF Channel Power	-18.87	-19.01, -18.74	-20.09, -17.563
RSSI	-14.07	-14.19, -13.96	-14.94, -12.96
SINR	35.07	34.85, 35.29	32.91, 37.16
EVM Average	1.67 dB	1.59, 1.75	0.96, 2.55
Frequency Error	0.1047 Hz	0.1040, 0.1055	0.0959, 0.1111

The handheld spectrum analyzer also measured a nearby AT&T band 14 cell site somewhere in the Fort Collins area. The cell site location is unknown; however, the spectrum analyzer measured the RSRP for the site to be around -110 dBm, significantly higher than the interferer identified at the Gypsum site.

5.4.2. December Full-range Baseline Test
The full-range baseline test showed that no phones would connect beyond row 1. Row 2 phones were within line of sight to the transmitter; however, they could never attach to the network. Rows 3 and 4 were not in visual line of sight due to small hills, so it was not surprising that these phones could not attach. Because only the smartphones in row 1

24

attached, the plot was not included in this report as it conveys the same information as the row 1 data in Fig. 22.

5.4.3. December Walking Test

The informal walking tests for the phones revealed that ground-based connectivity only extended for approximately 170 m, much less than the Gypsum walking test. Figure 23 shows the NetMonitor Pro data overlaid on the Android Team Awareness Kit (ATAK) interface, showing one phone losing connectivity at 170 m away from the transmitter. The other two phones used in the walking test lost connectivity at a shorter distance. Considering the problem with the LTE system output power we found in September (see Sec. 5.2), we tested the system again in the lab after the December test day and confirmed that it was operating at expected levels.
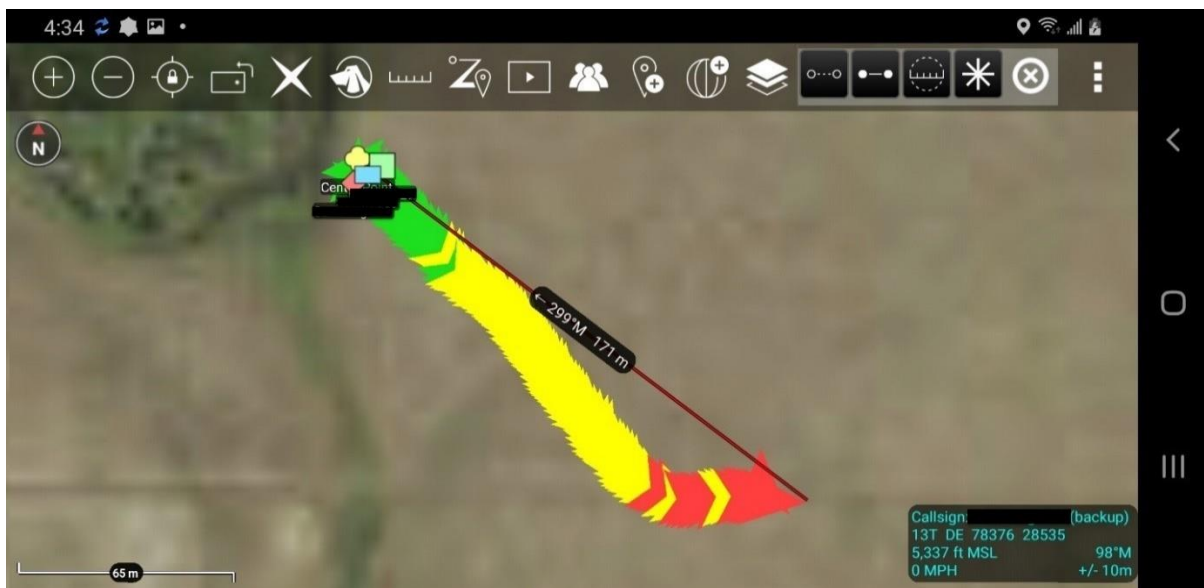
Fig. 23. Ground based walking test for phone type 3

5.4.4. December 350-Meter Test

The 350-meter test revealed much about the connectivity range of the LTE system from an orbiting sUAS. Primarily, we were able to observe that phones retained connections to the network much farther away than in the walking test or the full-range baseline tests. Figure 24 and Fig. 25 show the connectivity of phones in rows 1 and 2 to the LTE system over time. In addition, the distance between the phones and the aircraft is plotted. As a note, although the distances between each phone in the row to the drone are not the same, their differences are small compared to the minimum distance observed. As a consequence, for visualization on a plot, we have only included the distance from the drone to the center phone in the row. The distance was calculated from flight data collected from the drone after the test. Phones in rows 3 and 4 never connected to the LTE network.

Figure 24 shows the measured RSRP from the first row of phones over time. The graph shows an RSRP plot for each phone, as well as a plot of the distance from the drone to the phones. Only one phone in the first row connected to the LTE system during the actual orbit.

Later, when the drone was landing, one of the other phones finally connected. Phone logs did not reveal a reason the other two phones in this row did not connect during the orbit; however, it is possible that the phones were in a cycle to search for other networks during the flight. Another explanation could be that the interfering band 14 LTE system, which was measured at -110 dBm, could have stopped the phones from attaching; however, these phones connected to the LTE system before and after the flight.
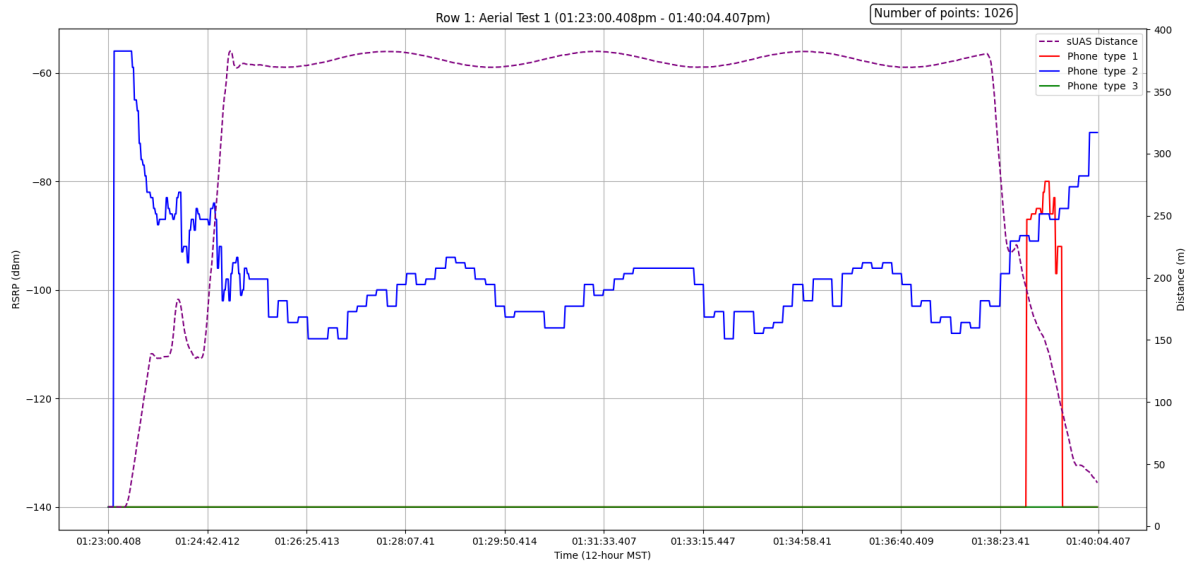
Fig. 24. 350-meter test row 1

Looking at the only connected phone during the 350 m test in Fig. 24 above, we see the predicted cyclic connectivity pattern. As the aircraft took off vertically and began to orbit the center point, we saw a decline in RSRP to approximately -100 dBm, which then varied from -95 dBm to -110 dBm. The total flight lasted around 12 minutes from the beginning of the orbit at 1:25 p.m. until the aircraft started to descend at 1:37 p.m. Overall, from the only connected phone in the center of the aircraft orbit, we saw a sufficiently stable connection to the LTE system.

Figure 25 shows the measured RSRP values for the row 2 phones, where two of the phones connected during one pass but not for the other two passes. Note that the phones were still connected to the eNodeB when the aircraft was at its farthest point away from the row.
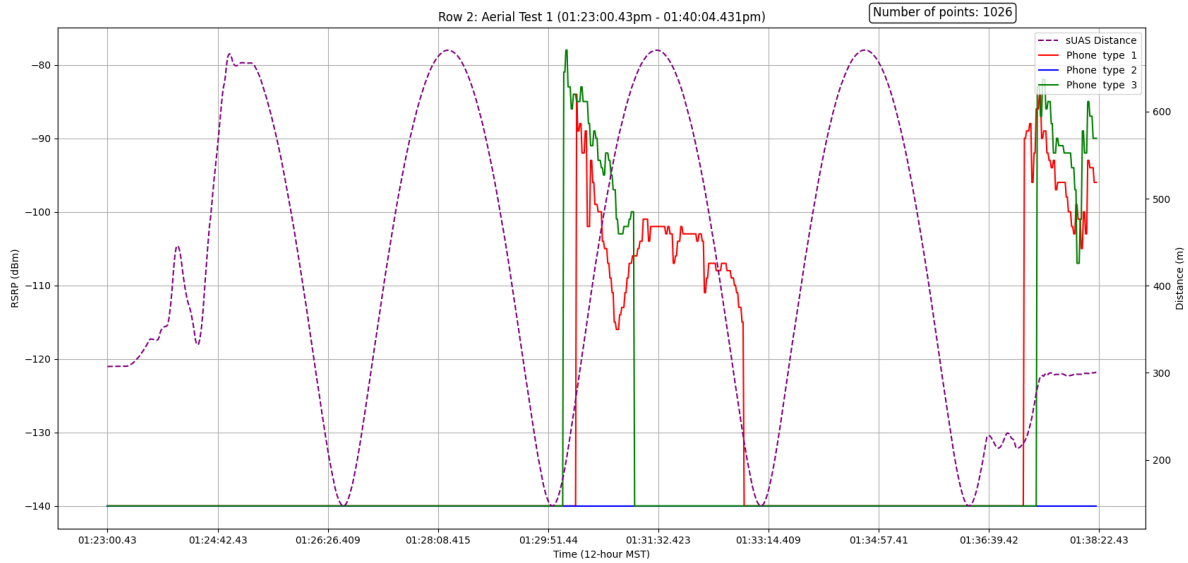
Fig. 25. 350-meter test row 2

The phones in rows 3 and 4 never connected to the LTE network throughout the test. It is unknown whether the reference signal could be detected at this location or if the phones could not connect in time when the aircraft was nearby.

5.4.5. December 650-Meter Tests

After the 350-meter test, we ran the 650-meter test with manual flight controls for the orbit. Using manual control causes the sporadic distance between the sUAS and phones (Fig. 26). For row 1, we observed that all three phones connected to the LTE system during the orbit. After a few minutes, however, one of the phones lost connectivity and never reconnected. The other two phones retained connections throughout the test. This flight lasted approximately 17 minutes, with only two full orbits completed.
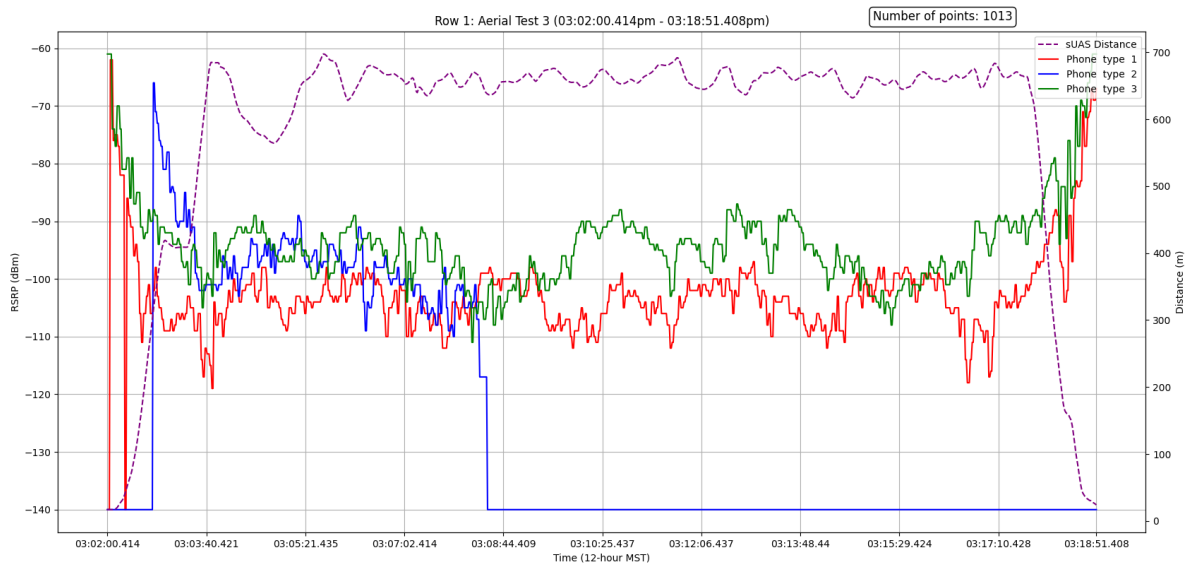
Fig. 26. 650-meter test 2 row 1

27

Phones in row 2 never connected to the LTE system during the orbits, even though the LTE system flew very close to that row, with a minimum distance of only 400 m.

Figure 27 shows results for the phones in row 3, where two devices connected for a brief moment when the orbit was directly overhead. On the first pass, phone type 1 successfully attached for a couple of seconds. On the second pass, phone type 3 attached in a similar manner for only a couple of seconds.
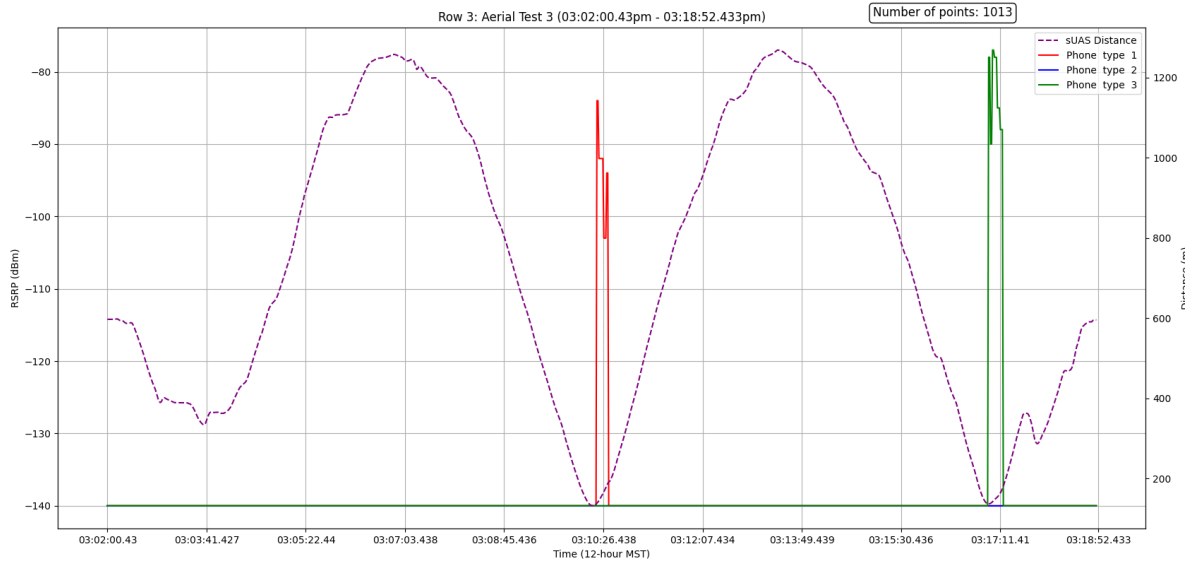
Fig. 27. 650-meter test 2 row 3

Figure 28 shows results for row 4, where one phone was able to attach during one orbit. Phone type 2 attached and stayed attached for approximately two minutes.
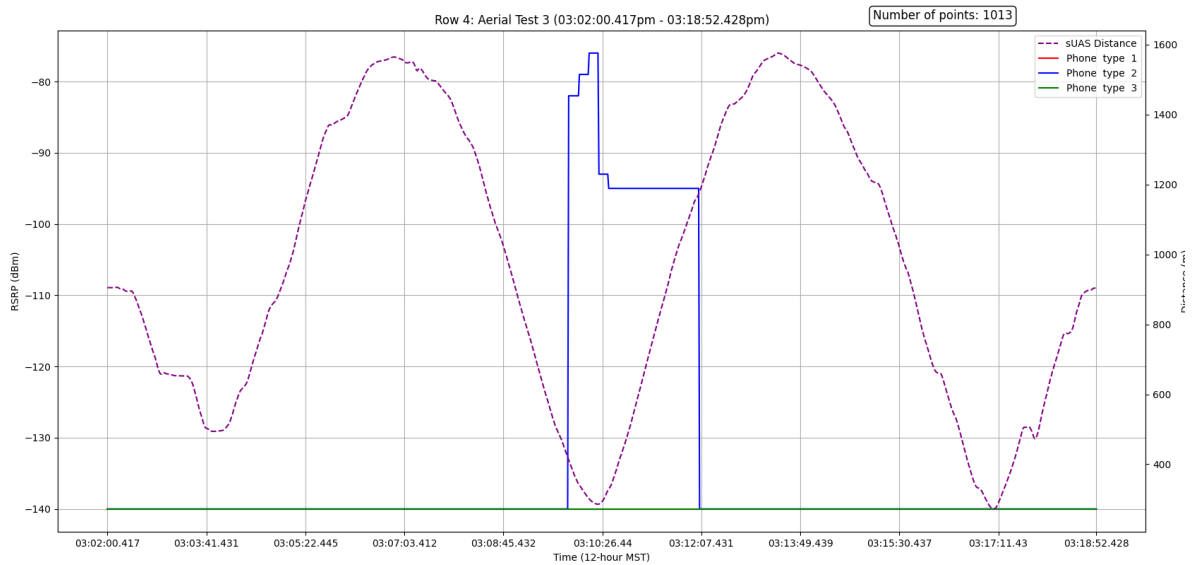
Fig. 28. 650-meter test 2 row 4

5.5. February Tests

Flight experiments conducted by PSCR staff and the CSU Drone Center in December resulted in overall unsatisfactory broadband service to devices on the ground. We believe one of the reasons for this result is that devices attempted to attach to other available commercial cellular networks in the area rather than attaching to the aerial network.

In general, phones that were beyond 305 m from the center of the orbit were disconnected from the LTE network for most of the duration of the flights. Although phones connected consistently to the test network under static conditions during ground baseline tests, aerial test results were inconsistent. In some instances, one or two phones would attach to the aerial network, while the rest of the phones within the same row did not connect. An example can be found in Fig. 24, where phone type 2 connected to the aerial network throughout the entire 12-minute flight, but phone types 1 and 3 did not. Phone types 1 and 3, in this case, were only 5 meters from phone type 2. Detailed process flows for the UE initial attach process can be found in [9] and [10], but the general outline is that devices loop through available network IDs and attempt to attach in a specific order. In our example, phone types 1 and 3 may have been trying to attach to a commercial network instead of the aerial network. As a solution, most phones have the capability to lock to a specific frequency and wireless protocol. When locked, the device only considers a specific cellular technology, such as LTE, and frequency band, such as band 14, when considering the list of available networks. For our case, this configuration can be applied to the phones to restrict them to the specific frequency and technology of the aerial network, yielding more consistent connectivity when testing in the presence of other cellular networks.

In late February, PSCR and the CSU Drone Center conducted more flight tests using phones locked to LTE and to band 14. Because concurrent experiments were being executed, only phone type 1 was used, with a smaller number of phones. Additional changes were made to the tests to accommodate other experiments. For example, the 650 m orbit was reduced to a 600 m orbit. Figure 29 shows the new flight plan, with phones located at positions A, B, C, and D. These points are 300 m from each other, with point C near the center point of the orbit.

Fig. 29. Google Maps flight paths of the multi-rotor drone with phone locations

Several other improvements were implemented to address findings from the December tests. We added a second antenna, allowing connections to both ports of the LTE system. The pilots also used a different flight software application that allowed the drone to fly continuously for an entire orbit. Unfortunately, the drone stopped at the end of each orbit before beginning a new circle. Plots reflect this pause as a constant distance period between the drone and any UE after a complete orbit. The continuous orbit was considered to be better than in the previous experiments where orbits were piloted manually. Finally, the phone located at the center of the orbit was placed on the operations table with its display facing upward rather than on a tripod. Figure 30 shows the equipment table where the center phone was placed.
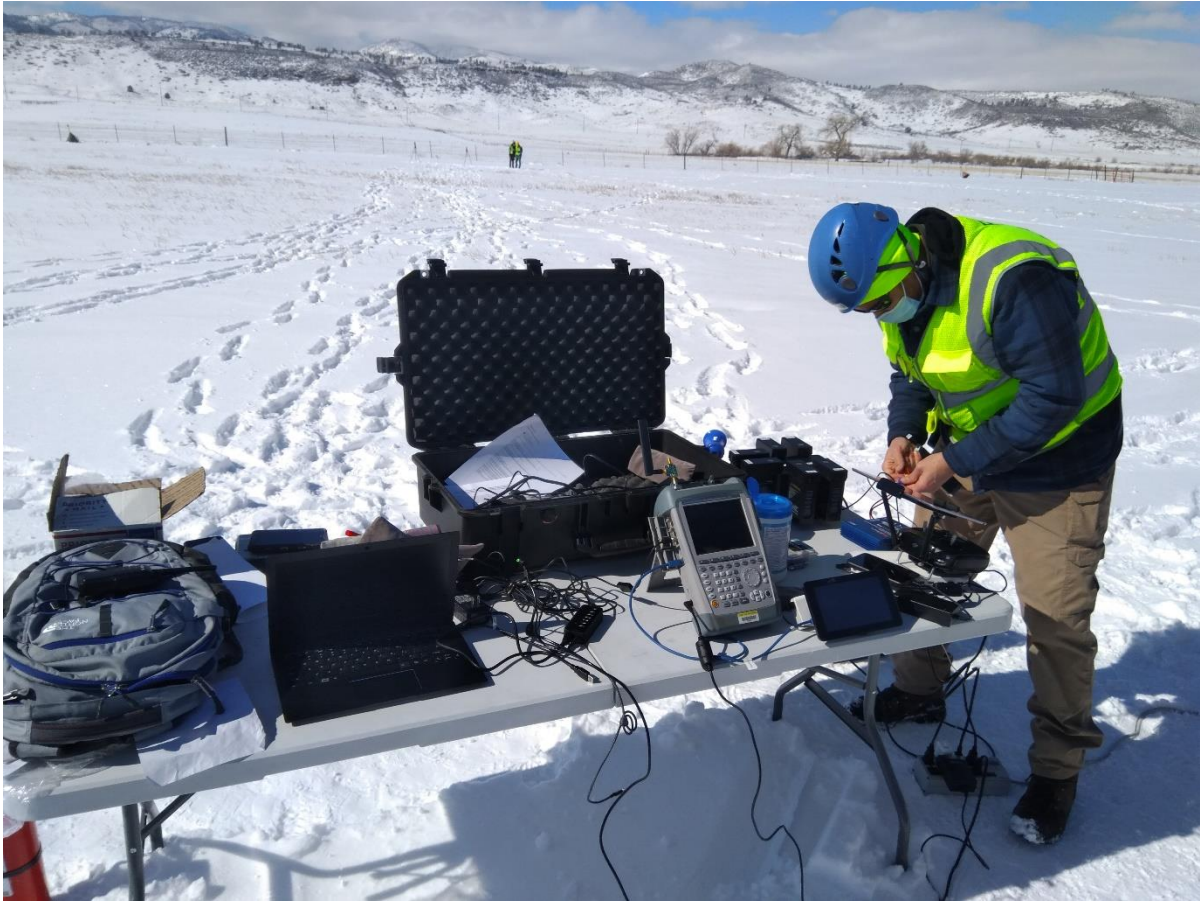
Fig. 30. Equipment table, near the center point where the center phone was placed

Baseline tests were not conducted in this set of tests using band locked phones. All of the aerial test plots from this experiment are shown in Appendix C, and a few sample plots are described in the next section.

5.5.1. February 350-Meter Tests
The 350-meter tests with band locked phones showed more consistent connectivity than the December 350-meter tests; however, the improvement was not as much as we expected. For some of the 350-meter flight tests, we observed continuous connectivity between devices and the LTE network as in the case of Fig. 31.

In other cases, phones lost connectivity to the LTE network for an orbit or two before reconnecting as in the case of Fig. 35, or they never connected to the aerial network. Another finding was that the phone in the center of the orbit, which was not mounted on a tripod, only connected to the aerial network when the drone was at its closest position to the phone, as shown in Fig. 36.

Figure 31 shows the measured RSRP for one of the phones located at point D during one 350 m orbital test. In this test, we saw continuous connectivity between the phone and the LTE network after the phone attached to the network during the first orbit. We observed a cyclic

31

connectivity pattern where RSRP reached a local maximum when the drone was at a minimum distance to the phone.
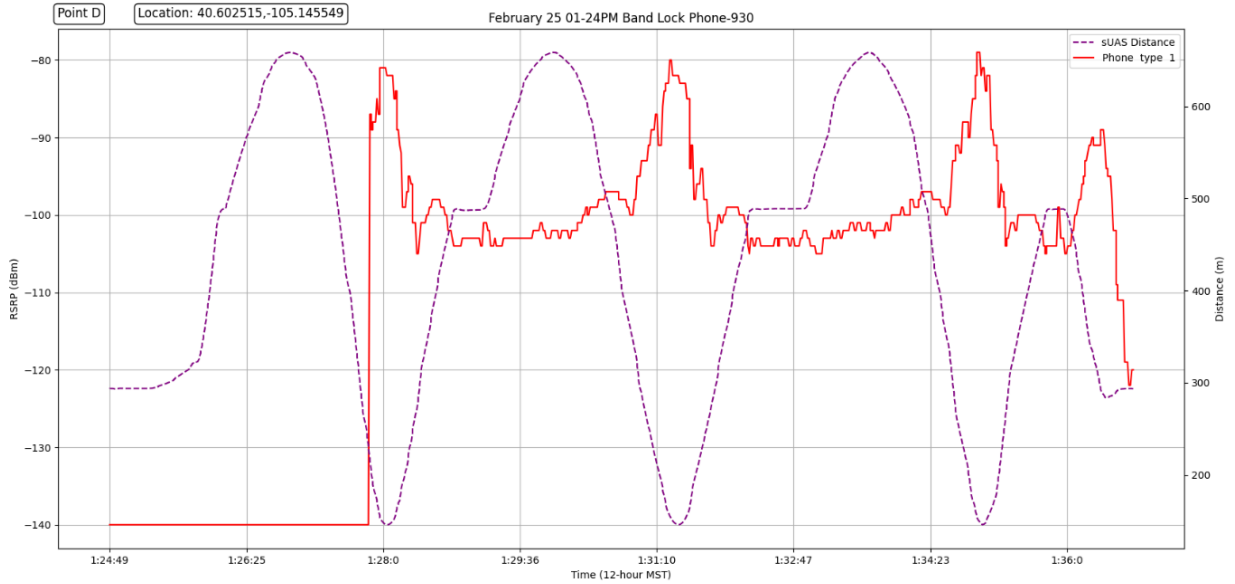
Fig. 31. 350-meter test with consistent connectivity for a phone at point D

Another example of consistent connectivity is shown in Fig. 32, where a phone at point B was connected throughout the entire experiment.
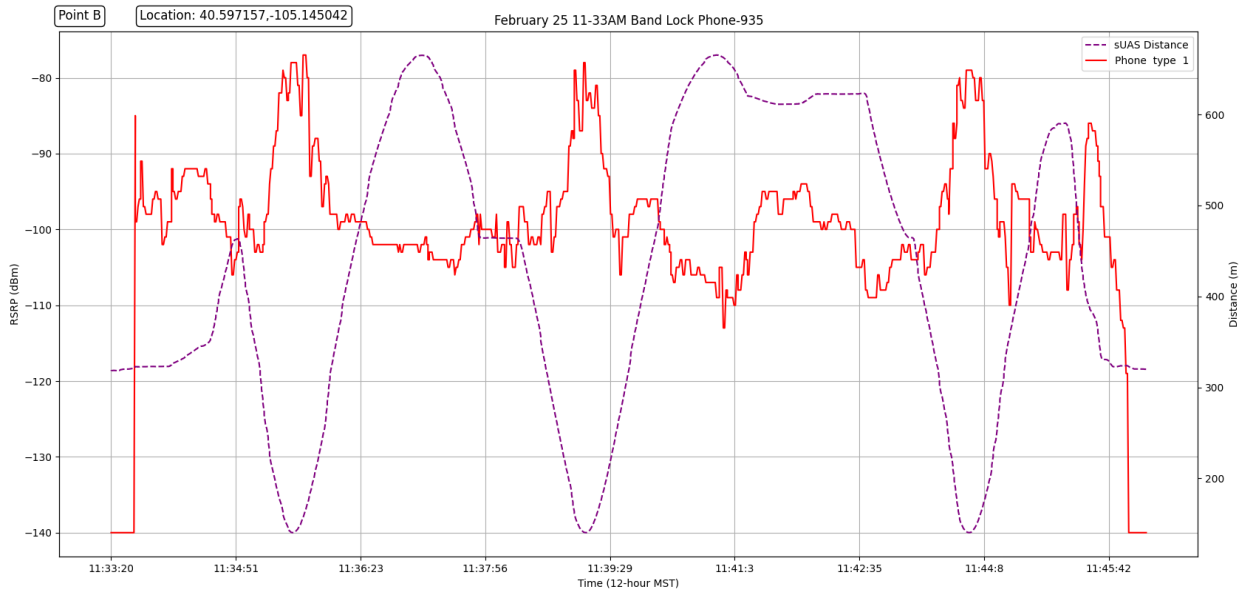
Fig. 32. 350-meter test with consistent connectivity for a phone at point B

Under previous DS research projects, PSCR conducted informal RSRP service quality tests for our band 14 FDD system and concluded that RSRP values at or greater than -100 dBm are generally considered usable for voice, video, and text applications. LTE connectivity for our specific system starts to degrade as RSRP decreases from -100 dBm to -110 dBm, at

32

which point the connection is essentially unusable. Figure 32 has been overlaid with this informal connectivity quality metric to produce Fig. 33, indicating that connectivity is generally good so long as the drone is less than 480 meters from the phone. If the drone is not within 480 meters, we start to observe degraded connectivity.
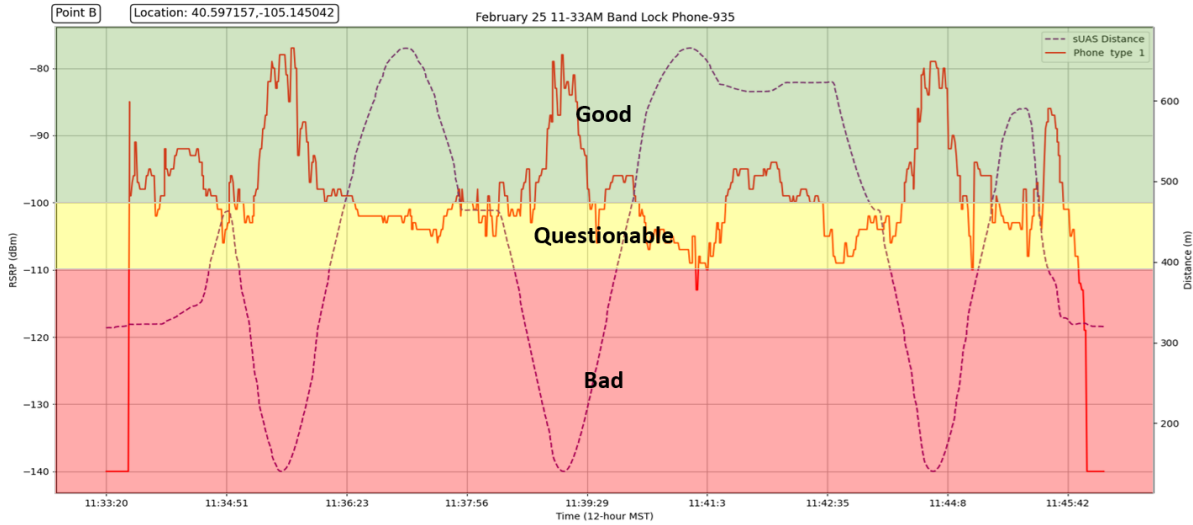
Fig. 33. 350-meter test at point B with service quality

As noted previously, not all tests showed consistent results. Figure 34 shows one phone at point D for a 350-meter flight where the phone only connected when the drone was within 400 m.
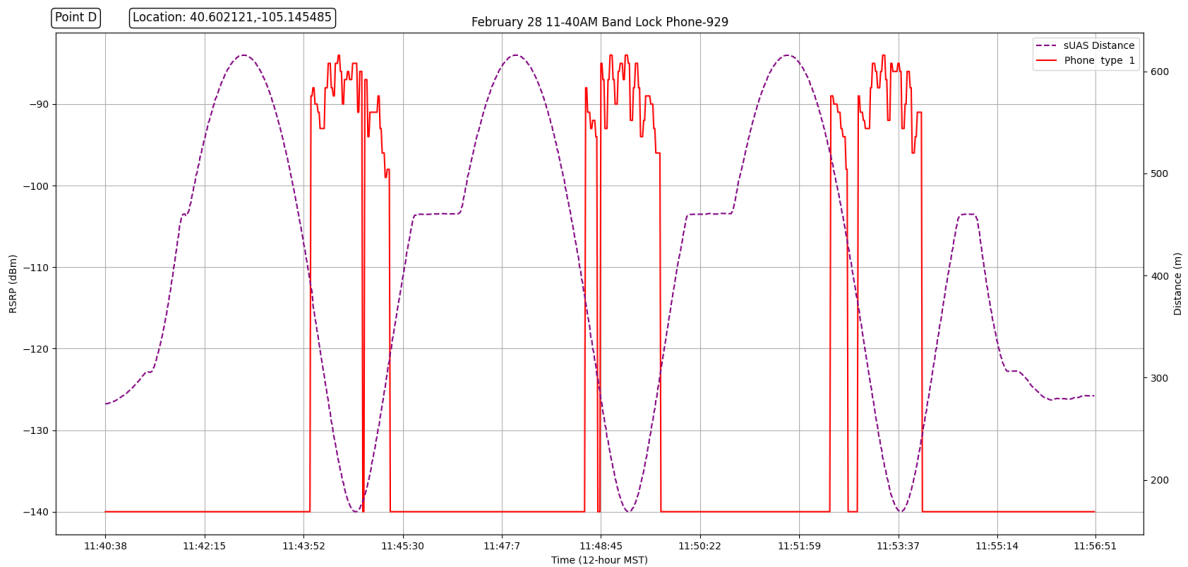
Fig. 34. 350-meter test with intermittent connectivity for a phone at point D

Figure 35 presents another case where a phone lost connectivity briefly when the drone was over 630 m away before reconnecting.
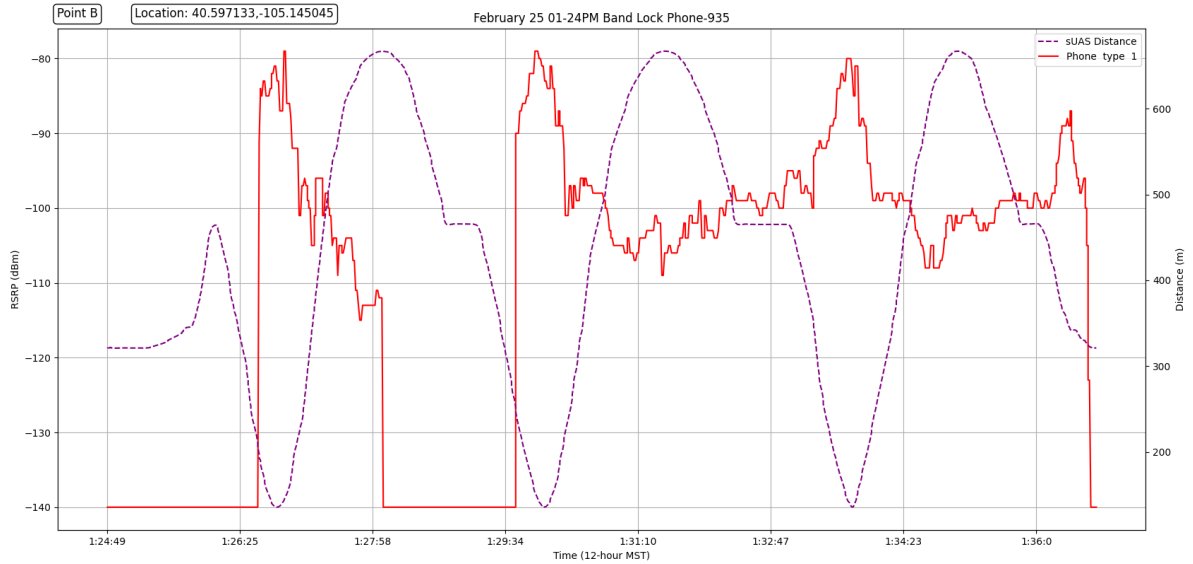
Fig. 35. 350-meter test with inconsistent connectivity for a phone at point B

Figure 36 shows results from a phone in the center of the orbit, where we see connectivity only when the drone is at its closest proximity to the phone. The phone detaches from the network at around -94 dBm. This phone was not mounted to a tripod but was lying horizontally on a table near the center. Although not comparable to the other plots due to its orientation, the results are still interesting and present a different connectivity pattern. We see this result repeated in Fig. 57, Fig. 60, and Fig. 66 of Appendix C, along with the remaining plots for the 350-meter flights.
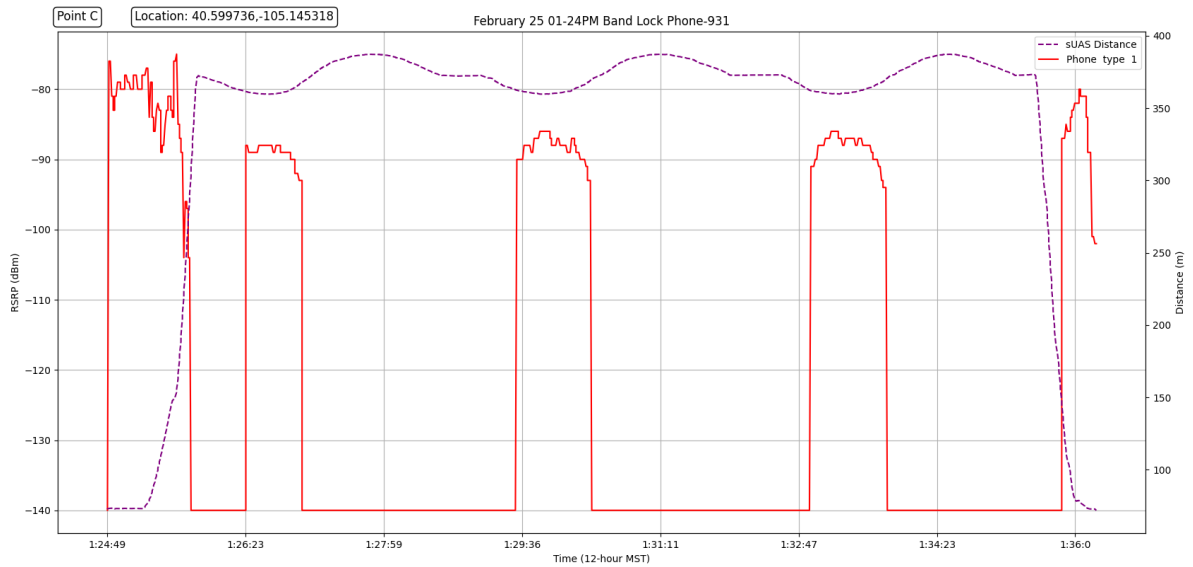
Fig. 36. 350-meter test for a phone at the center of the orbit, horizontal orientation

34

As noted above, neighboring AT&T cell site signals were present at Christman airfield in December and February, increasing the noise floor for phones trying to connect and maintain connectivity to the aerial LTE network. In December, PSCR staff observed only one AT&T cell site at the airfield with a measured RSRP value around -110 dBm. Interference levels were higher in February, with measurements between -95 dBm and -105 dBm for three different cell sites. Increased interference from the commercial network (operating by design at much higher power levels than the aerial network under test) is a likely cause for the inconsistent connectivity that was present in the data for the February experiments. Figure 37 shows a spectrum analyzer measurement from two commercial network cell sites (Cell IDs 331 and 332) and the PSCR system (Cell ID 97). A third commercial site (Cell ID 14) is not shown but was recorded with a similar RSRP level to site 332.

Fig. 37. February 25 LTE site survey of band 14 at Christman airfield

5.5.2. February 600-Meter Tests

Of the two 600-meter tests conducted, no phones would connect to the LTE network during any orbit. Even as the drone passed directly overhead, devices did not connect to the aerial LTE system. Based on limited investigation, it is assumed that the failure to connect resulted from insufficient time intervals for for completing the attach procedure. We have omitted the plots of the 600-meter tests due to the lack of meaningful data.

6. Summary of Results and Issues

Small fixed-wing aircraft flight operations with hosted LTE communication systems are difficult to conduct. Many challenges hinder the overall effectiveness of the concept, such as the mass of the LTE system, the output power available from small LTE systems, Part 107 drone restrictions, the nature of fixed-wing sUAS, and default smartphone network

attachment schemes. This report details our experience and response to each of those challenges as we prepared and executed the test plan for aerial LTE communications. Although initial tests were not conclusive, the test and drone teams worked through changes in the test design, configuration and hardware to collect meaningful and insightful data on orbiting aerial LTE deployments. Findings may be used to help guide future experiments and endeavors by public safety or public safety broadband service providers. This section provides an overview of some of the research issues and comments on the data gathered from the experiments.

6.1. Inconsistent Connectivity

A major problem encountered during the experiments was the lack of connectivity from phones to the LTE network when phones were expected to be connected. As noted previously, phones that were not configured to attach only to band 14 LTE systems would not connect consistently to the aerial LTE network. As a solution, most phones have the capability to lock to a specific frequency and technology. After applying this configuration, we found much more consistent connectivity to the aerial LTE network. Although connectivity improved after this change, we still observed some dropped connections. As noted in the report, AT&T commercial cell sites were operating near the airfield. The resulting increase to the noise floor increased the probability that phones would drop connections or fail to connect to our test network.

6.2. Sporadic Dropped Measurements

Another notable issue was the number of dropped connectivity points recorded at the top of each baseline test plot. Close-range baseline tests in both locations showed numerous dropped connections to the LTE system. Figure 17 in particular, shows phones in each row and across all phone types with several hundred dropped connection points during the test. As mentioned in the October close-range baseline test, these are points where the NetMonitor Pro tool could not decode LTE reference signals such as the eNodeB Cell ID. The expectation for these tests is that no dropped connections, or very few, should be recorded. This problem differs from the inconsistent connectivity issues mentioned in the previous section since the dropped points are interlaced with real measured points in the NetMonitor Pro tool.

PSCR staff observed the same phenomenon during earlier field experiments with the LTE system in September 2019 in Gypsum. In this field test, we used a Rohde and Schwarz FSH8 spectrum analyzer which has software to demodulate and analyze LTE reference signal information. In Fig. 38, the LTE system location is represented by the blue PSCR logo. The dots represent measurement points, and darker red dots correspond to higher RSRP values. Each red triangle reflects a failure to synchronize with or measure the LTE system.
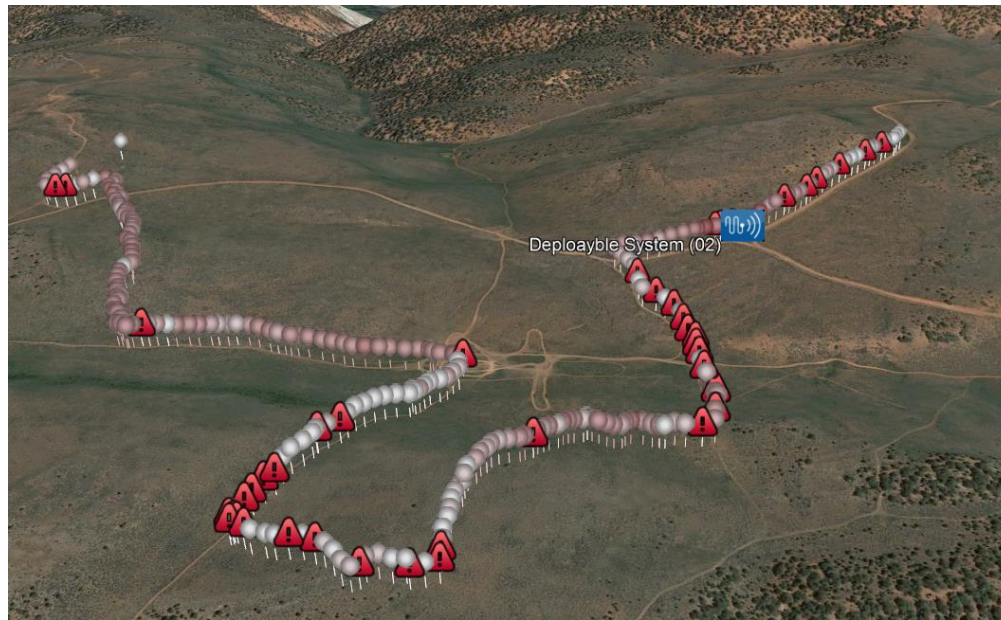
Fig. 38. September 2019 measured coverage area from LTE system

Figure 38 shows disconnectivity points adjacent to measured points with high RSRP values. Following the 2019 test, PSCR worked with the LTE system vendor to troubleshoot this issue, and after reconfiguration, the problem seemed to be resolved. Further testing on this system with the FSH8 in a lab environment showed no more desynchronization points, but field trials were not executed. PSCR staff has used the FSH8 on at least three other LTE systems in field trials, all from different vendors, without recreating this random loss of synchronization. However, it appears that the same issue seen in 2019 may have been present during the aerial experiment. Although the lapses in connectivity are a cause for concern, this problem may be attributed to the fact that the LTE system is still a prototype with some unresolved issues.

6.3. Coverage Footprint

The coverage area provided by a one-watt LTE system is difficult to determine, as demonstrated by widely varying results from different scenarios covered during these experiments. As detailed above in Sec. 4.1, for a one-watt total system, the reference signal power level is approximately 1.67 mW (2.22 dBm). Even with some antenna gain, the highest achievable RSRP is low compared to fixed LTE cell sites with more than an order of magnitude higher power. Relative to such sites, the coverage area for a low-power system is impacted disproportionately by variables in the transmission channel (e.g., terrain, distance, antenna orientation and obstructions).

Looking at the measured coverage from the two baseline tests, phones reliably attached to the network 20 meters away from the one-watt LTE system. In the Gypsum tests, we observed only one type of phone attach at 305 m and 605 m, whereas in Fort Collins, no phone would attach beyond 20 m. Given the small sample size for these tests and the notably different full range baseline test results between Gypsum and Fort Collins, we cannot determine with certainty the coverage range for reliable phone attachment. This baseline attachment result differs significantly from the walking tests at each site. In Gypsum, phones retained

37

connections to the system 600 m away, and in Fort Collins no phone would stay attached beyond 170 m. The shorter range in the walking test for Fort Collins may be attributed to the higher noise floor from the nearby AT&T network. In Fort Collins, we measured the nearby cell site RSRP at -110 dBm for the baseline tests, whereas in Gypsum we measured RSRP around -120 dBm.

Range determination was further obscured by the fact that phones maintained existing connections at distances significantly greater than the maximum ranges for initial network attachment. Devices which attached to the network for the baseline tests could be moved out from the system and maintain connections; however, once the connections dropped, they had to be moved closer to the system again to reattach. Even without introducing other variables, two methods were possible for specifying the range.

The points above illustrate a small part of the complexity inherent in attempting to state the range or coverage area provided by the one-watt system. On one hand, if we say the range is based on UE already attached to the system, then the range could be 600 m with visual line of sight. If we say the coverage area is based on attaching to the system, then it could vary from 20 m to 605 m since the baseline tests do not yield a consistent number.

Further complicating the range description, both flight experiments (with and without band locking) showed different ranges from the baseline tests. For aerial tests without band locked phones, we observed phones staying connected to the aerial LTE network at distances as far as 1100 m. Referring to Fig. 28, phone type 2 was able to attach to the LTE network at around 300 m, and as the drone continued its orbit, the phone stayed attached until the drone was around 1100 m away. In Fig. 25, we observed that phone types 1 and 3 attached while the drone was less than 200 m away and stayed connected until approximately 700 m. For the aerial tests with band locked phones, we observed results similar to the previous aerial tests where phones only connected to the aerial LTE network at close distances to the drone. Figure 34 and Fig. 35 show phones reattached to the network only when the drone was less than 400 m away. The band lock tests also showed phones maintaining connections to the LTE network at longer distances than in the baseline test. In Fig. 77, Fig. 81, and Fig. 89, we observed a phone staying connected up to 930 m away for each test. In both of these flight examples, we see the same phenomenon as in our baseline and walking tests. Specifically, phones can only attach at relatively close distances, under 400 m, but can maintain connections for a much longer distance. With a small coverage footprint for phones to attach, roughly 400 m in the aerial case and anywhere from 20 m to 605 m for the static case, phones have a much smaller window of connectivity when the sUAS passes over. A consequence of this low attachment radius is that phones miss their opportunities to connect. As the coverage area of an LTE system decreases, more connectivity problems appear.

A solution for increasing the UE attachment radius could be to increase the output power of the system. Unfortunately, this is not feasible with current technology solutions. The output power from an eNodeB is limited by the size of the LTE system, as explained in Sec. 2. Any increase in gain from using a larger power amplifier in an eNodeB would result in a much heavier system, which would likely exceed the payload weight limit for a Part 107 aerial platform. The LTE system used here has a mass of around 1.5 kg, which is already at the limit for the Albatross fixed-wing UAV. Since the input power to the antenna system is fixed, other options should be investigated to increase the system output power while keeping

the mass constant. One option would be to use higher gain antennas. The antennas used for this experiment were a consumer product that were not heavy enough to impact the sUAS endurance time. It would be beneficial to design a special-purpose antenna specifically for the frequency band being used. An ideal antenna should have high gain and a main lobe width anywhere between 90 degrees and 160 degrees. The beam width should be chosen to provide as much power to the ground as possible; hence power should not be sent toward the sky, as in the case of an omnidirectional antenna, or to the immediate left or right of the aircraft, as in the case of a 180-degree antenna. One could also make a tradeoff between data rates and output power to increase the attachment coverage area. In an effort to increase the coverage radius, one could decrease the channel bandwidth (e.g., from 10 MHz to 5 MHz), increasing the power in the reference signal and improving the signal-to-noise ratio at the receiver.

6.4. Fixed-wing Platform Complexity

Communications equipment was not the only difficult component encountered during testing. The fixed-wing delivery platform presented unique challenges which prohibited us from successfully flying the real LTE system (it only flew with the replica). The first issue with the fixed-wing sUAS came from constraints on where the drone could take off. The aircraft could not take off from a straight gravel runaway or uneven grassland—specifically, testing revealed that it required a paved runway for takeoff. Access to a paved runway near an incident is uncommon for a public safety operation, so this requirement hinders first responders from deploying a fixed-wing drone in a real scenario. This constraint in takeoff location also halted our experiment, requiring us to move to a new location.

Another issue was that the fixed-wing drone was damaged during a flight, causing us to switch platforms. Its autopilot system was not tuned correctly to the mass of the payload, which caused the landing gear to break on landing. Although problems often arise during flight operations, this single incident stopped all further testing. Multi-rotor sUAS can encounter issues where propellers break or an arm detaches; however, multi-rotor drone pilots expect breakage and often keep replacement parts on hand for quick repairs. The fixed-wing platform we chose, in contrast, did not have this replaceable parts capability; in more than one instance, operations stopped because of damage to the aircraft. Each flight operation poses a risk of damage; if first responders need a communications payload to serve a large area for several hours using multiple flights, the probability of losing the delivery platform during the mission is high. Learning from this experiment, a public safety entity that plans to move forward with a fixed-wing aircraft for a communications operation should be careful to ensure all components of the aircraft can be repaired on site. This finding is not necessarily a criticism of the fixed-wing aircraft design, but a recommendation to ensure the robustness of any fixed-wing vehicle.

An additional obstacle for using fixed-wing sUAS is that they are generally difficult to pilot, requiring significant levels of training and skills. In our case, the fixed-wing platform required two pilots. One of the operators had specific knowledge of the auto-piloting system, while the other had specific skills in manual flight operations. Any organization developing an sUAS program should consider fixed-wing platform constraints with runway conditions, required piloting skills, and aircraft fragility.

Although challenging, employing fixed-wing sUAS for communication systems can provide longer endurance times compared to other delivery platforms. In our experiment, the multi-rotor platform provided around 17 minutes of flight, which would not meet expectations for an actual public safety event. The endurance of the fixed-wing system was never verified due to the problems noted above, but the system was expected to provide around 30 minutes of flight time, almost doubling the endurance time of the multi-rotor sUAS.

7. Recommendations

Overall, we were able to address some of the questions posed at the beginning of the endeavor. We were able to validate that eNodeB motion did not cause severe link degradation to a UE. Although we did not characterize any level of link degradation due to eNodeB motion, we found that motion did not stop a smartphone device from carrying out basic functions. Phones were able to attach to the LTE network even as the system moved 9.8 m/s on average, and aerial trials with band locked phones showed data could be sent from one phone to another. We observed that rapidly varying distances between the eNodeB and the UE caused fluctuating link qualities, as illustrated by data showing effects on the links. These UE link fluctuations are a product of the range of the system and the size of the orbit. Because of the combination selected, we were able to view a realistic use case for system range and orbit size. Although the data would have been more consistent across tests with a better eNodeB antenna and less interference from commercial networks, several plots showed connectivity patterns of phones at various positions through RSRP values measured over time. We found that the expected coverage area was larger than anticipated. In general, the coverage area from the aerial network extended approximately 1000 m radially if a phone was already attached. It is important to note that although we saw this for multiple trials, there were instances where phones would detach from the aerial network when the distance was less than 1000 m. This result differed from the static tests where phones could not stay connected beyond 600 m. In general, the LTE network provided a larger coverage area when airborne than it produced on the ground. We validated that phones required several seconds to attach to the LTE network, leading to phones not attaching when the drone was passing overhead. In other words, because the phones took time to attach, the overall attachment coverage area was reduced. The network attachment delay was a factor for both the non-band locking tests and the band locking tests. Finally, we were able to show that an aerial LTE operation can be improved easily by locking phones to the incident LTE network. This configuration greatly improved the data collected during the experiment and would improve operations for a public safety agency.

In conclusion, many best practices resulted from this set of experiments. Below is a list of recommendations for public safety agencies or other stakeholders to consider before launching a fixed-wing sUAS based LTE network.

1. Find a way to lock the phones to a specific network. As stated above, phones spend critical time cycling through all possible networks instead of attaching directly to the aerial LTE network. This research demonstrated the improvements that resulted from this simple configuration.

2. Always coordinate with the primary spectrum holder before deploying an independent system. As stated before, commercial cell sites contributed to

inconsistent connectivity between the phones and our aerial network. In cases where sufficient LTE coverage is in place, it would be practical to rely on the commercial network rather than placing a deployable system on site.

3. Focus on increasing eNodeB gain by designing a specific antenna for the selected frequency band, with a propagation pattern optimized for the fixed-wing system scenario.

4. Consider LTE equipment that uses a narrower bandwidth, such as 5 MHz. There are implications for licensing and a tradeoff between bandwidth and data rates, but it may be worthwhile to pursue this avenue to increase the coverage area.

5. Ensure that the selected sUAS can take off from rough and uneven terrain. Often, public safety personnel do not choose where an operation will take place, so it is important that the sUAS can accommodate diverse terrain conditions.

6. Ensure that the sUAS can be easily repaired or replaced in the field. Although users should take measures to prevent damaging the system, breakage is often inevitable and poses a significant risk to sUAS flights.

Acknowledgments

References

[1] H. Nguyen, M. Maurice, S. Ray "Next Generation First Responder Deployables and IoT Technology" NIST PSCR, June, 2019 URL: https://www.nist.gov/ctl/pscr/2019-stakeholder-meeting-resilient-systems-sessions

[2] H. Nguyen, T. Manley, K. Saidi "Survey of Drone Usage in Public Safety Agencies" NISTIR 8305, April, 2020 URL: https://nvlpubs.nist.gov/nistpubs/ir/2020/NIST.IR.8305.pdf

[3] M. Maurice, S. Ray, M. Leah, "Use Case 1 Dynamic Incident Area Network with No Existing Coverage or Backhaul," PSCR, October 2017, URL:https://www.nist.gov/sites/default/files/documents/2017/10/17/deployable_networks_use_case_1.pdf.

[4] M. Maurice, S. Ray, M. Leah, "Use Case 2: Dynamic Coverage of Existing Network, Intermittent Backhaul," PSCR, October 2017, URL: https://www.nist.gov/sites/default/files/documents/2017/10/17/deployable_networks_use_case_2.pdf.

[5] T. Manley "FIRST RESPONDER UAS ENDURANCE CHALLENGE" NIST, August, 2020 URL: https://www.firstresponderuaschallenge.org/

[6] R. Öhlund "Drones and energy efficiency" Smart Planes, November, 2017 URL: http://smartplanes.com/drones-and-energy-efficiency/

[7] "Meet Albatross" August 2020 URL: https://www.appliedaeronautics.com/albatross-uav

[8] "EM-LTE Flexible LTE Internal Strip Antenna" Mobile Mark, Inc. December 2020 Itasca, IL URL: https://www.mobilemark.com/product/em-lte/

[9] "PLMN Selection in LTE (Idle Mode Action)" Techplayon.com, April 25, 2019 URL: http://www.techplayon.com/plmn-selection-in-lte-idle-mode-action/

[10] "LTE Cell Camping and Selection Procedure" Techplayon.com, May 5, 2019 URL: http://www.techplayon.com/lte-cell-camping-and-selection-procedure/

42

Appendix A: Prediction Plots

Prediction Plots: 350-meter Test
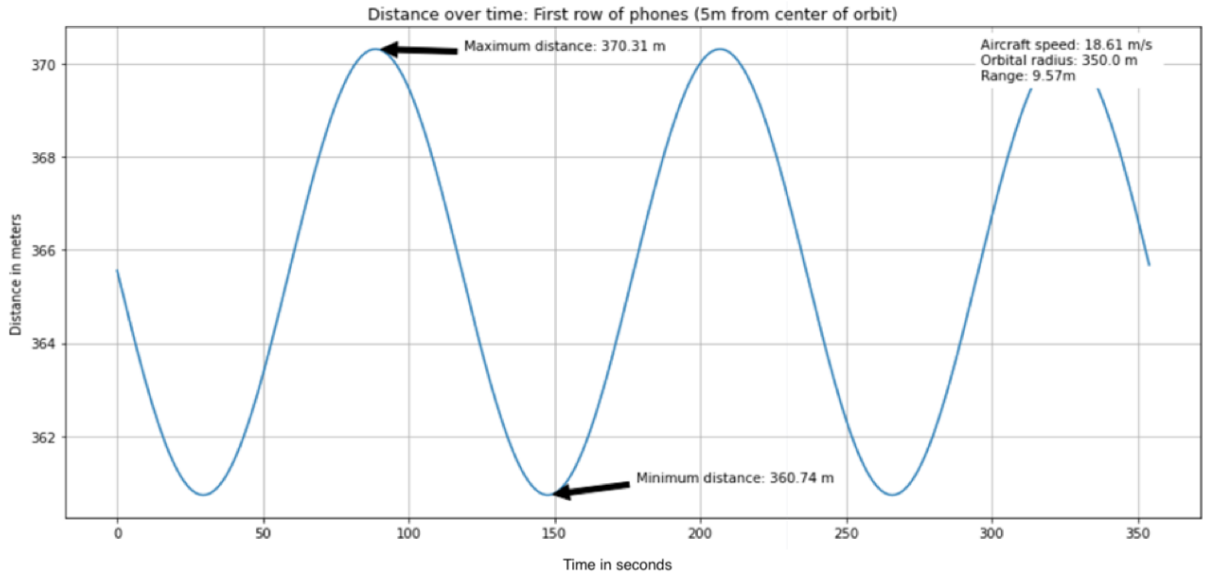
Fig. 39. Distance over time prediction plot of the 350-meter test aircraft to the first row
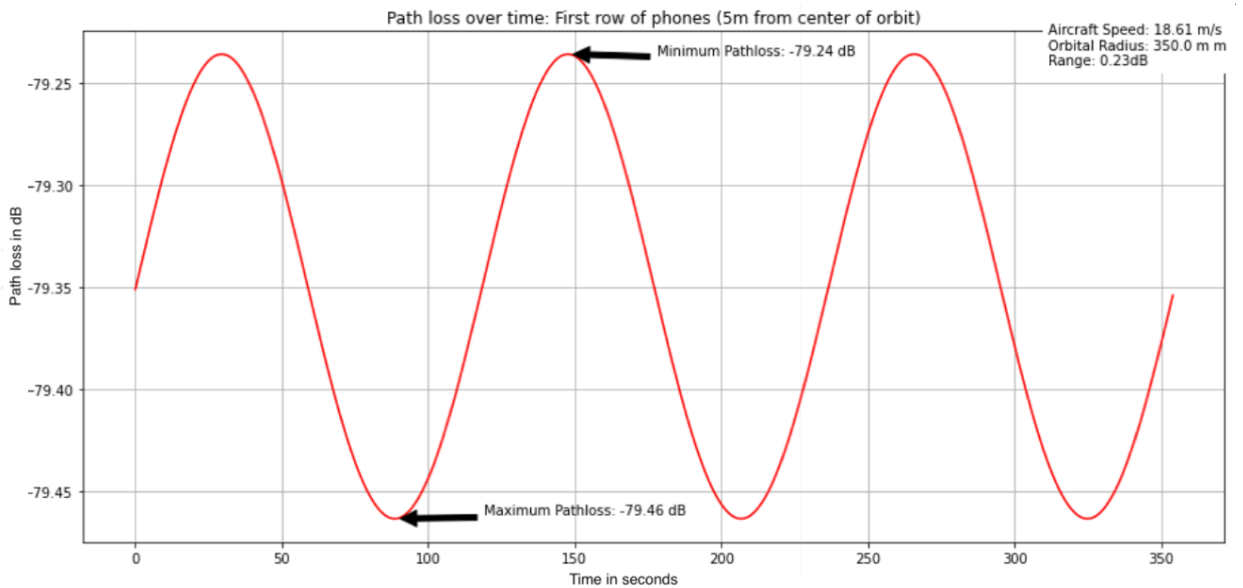
Fig. 40. Path loss over time prediction plot of the 350-meter test aircraft to the first row
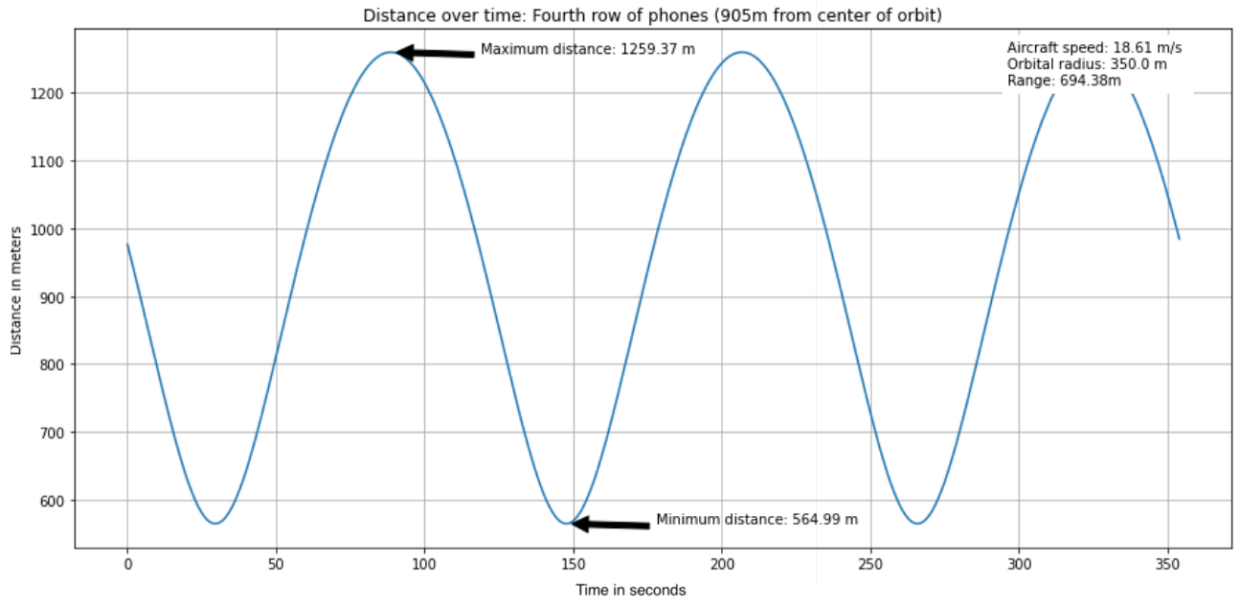
Fig. 41. Distance over time prediction plot of the 350-meter test aircraft to the fourth row
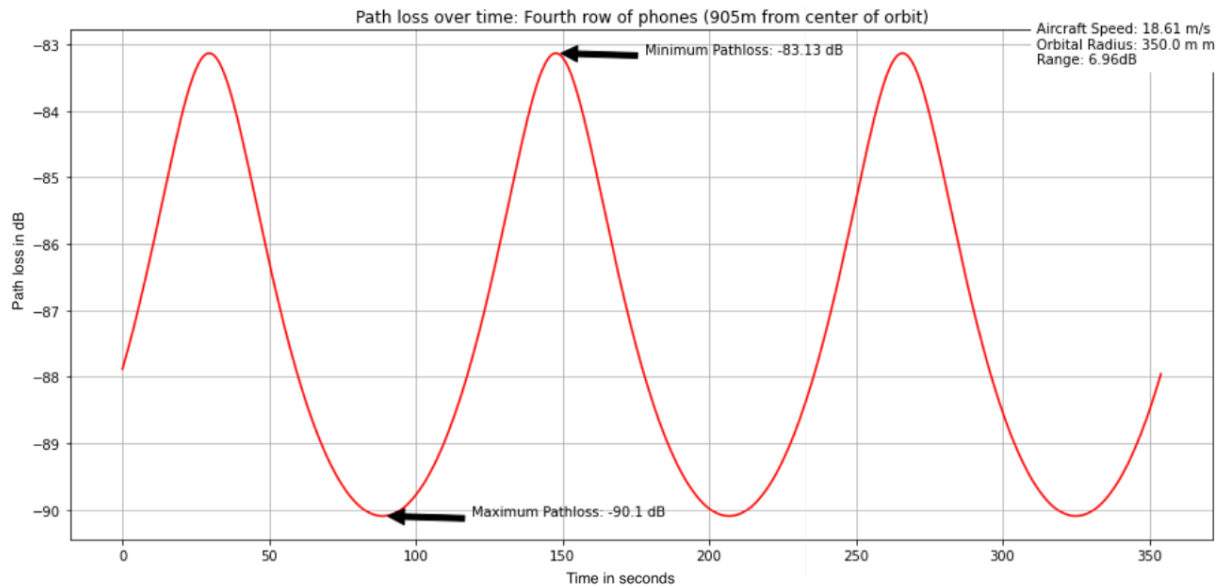
Fig. 42. Path loss over time prediction plot of the 350-meter test aircraft to the fourth row

44

Prediction Plots: 850-meter Test
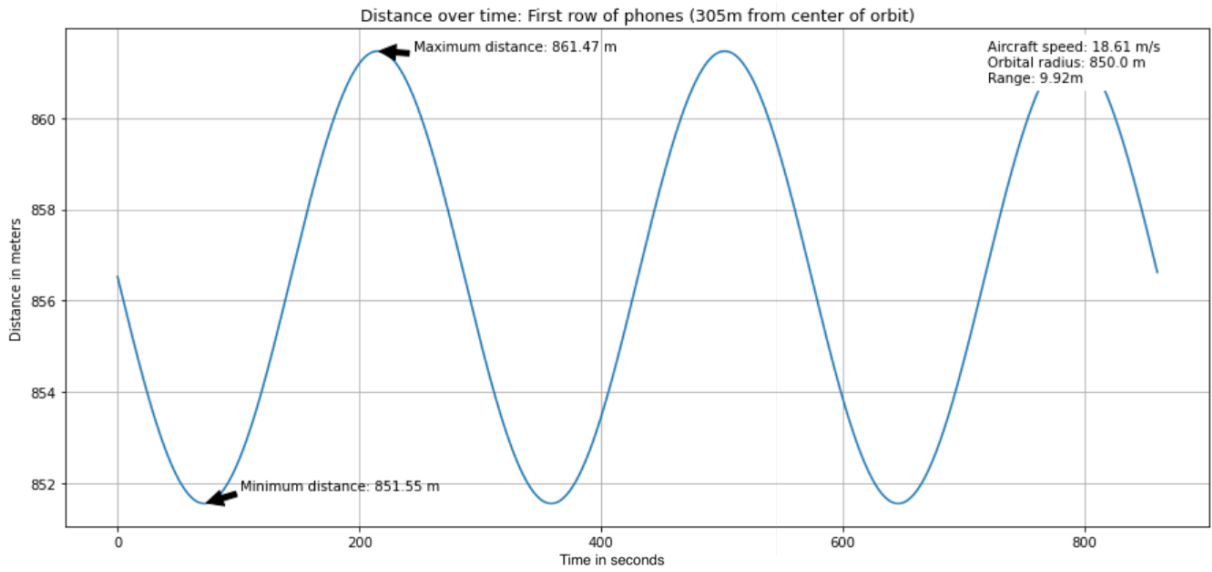
Fig. 43. Distance over time prediction plot of the 850-meter test aircraft to the first row
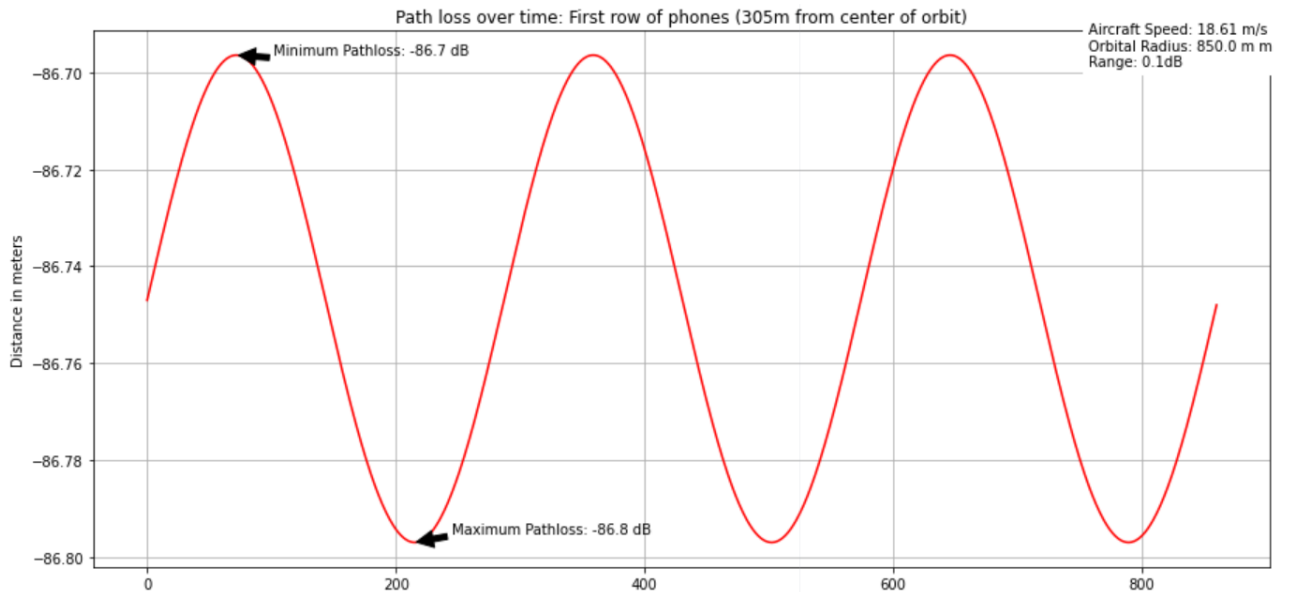
Fig. 44. Path loss over time prediction plot of the 850-meter test aircraft to the first row
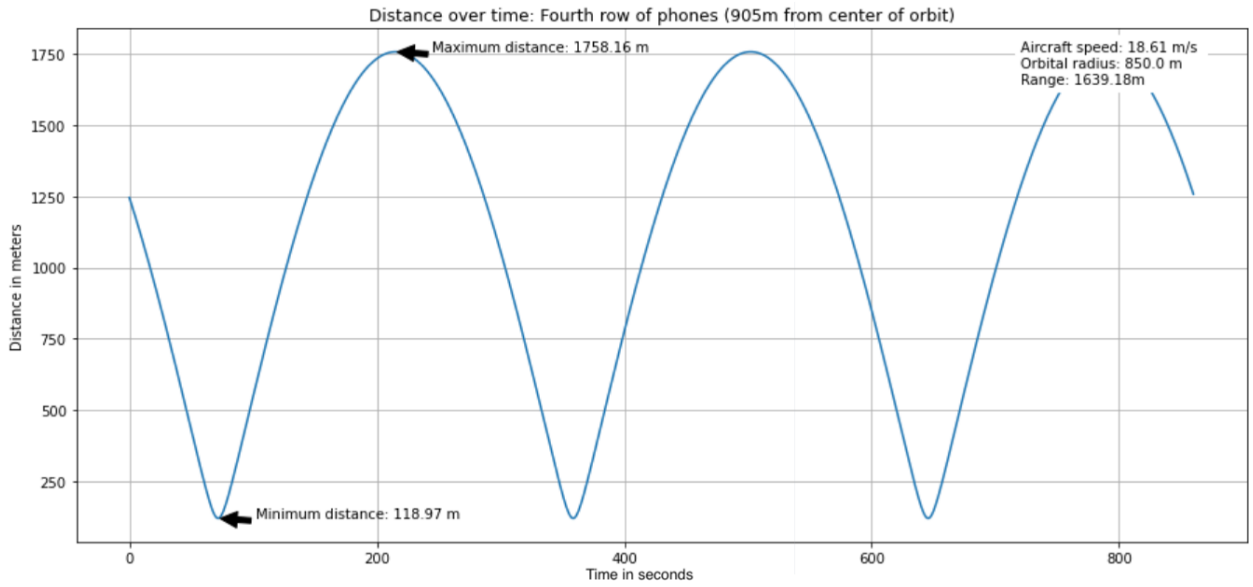
Distance over time: Fourth row of phones (905m from center of orbit)

Fig. 45. Distance over time prediction plot of the 850-meter test aircraft to the fourth row

Path loss over time: Fourth row of phones (905m from center of orbit)
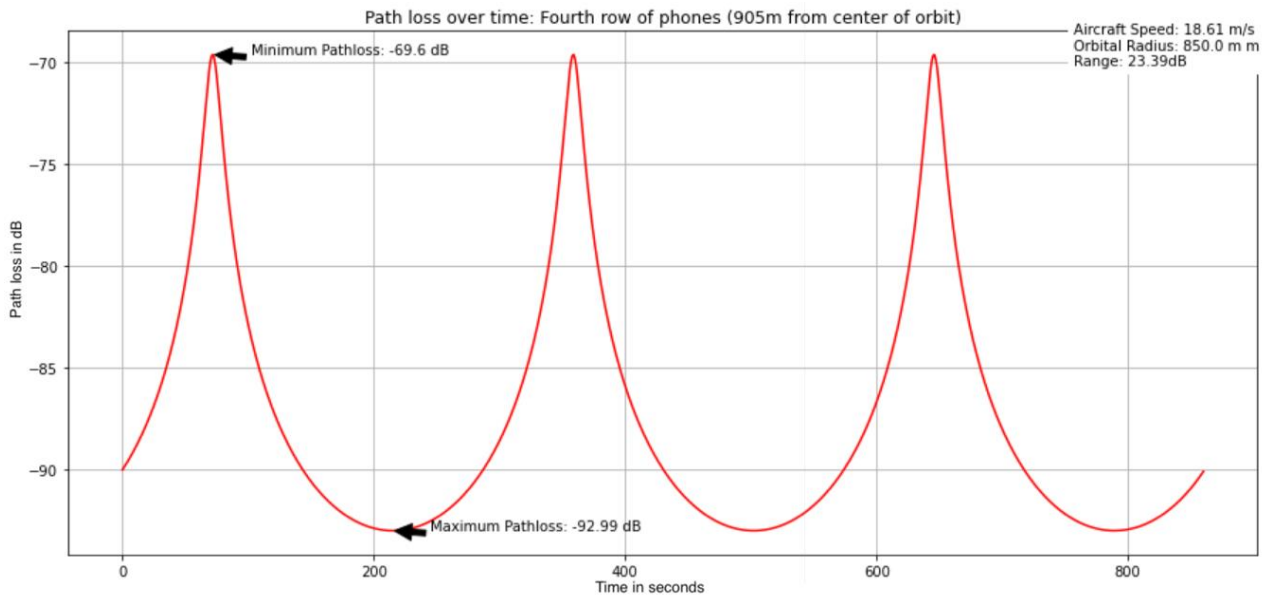
Fig. 46. Path loss over time prediction plot of the 850-meter test aircraft to the fourth row

Appendix B: Ground Tests by Phone

October Gypsum Site Close-range Baseline Test by Phone
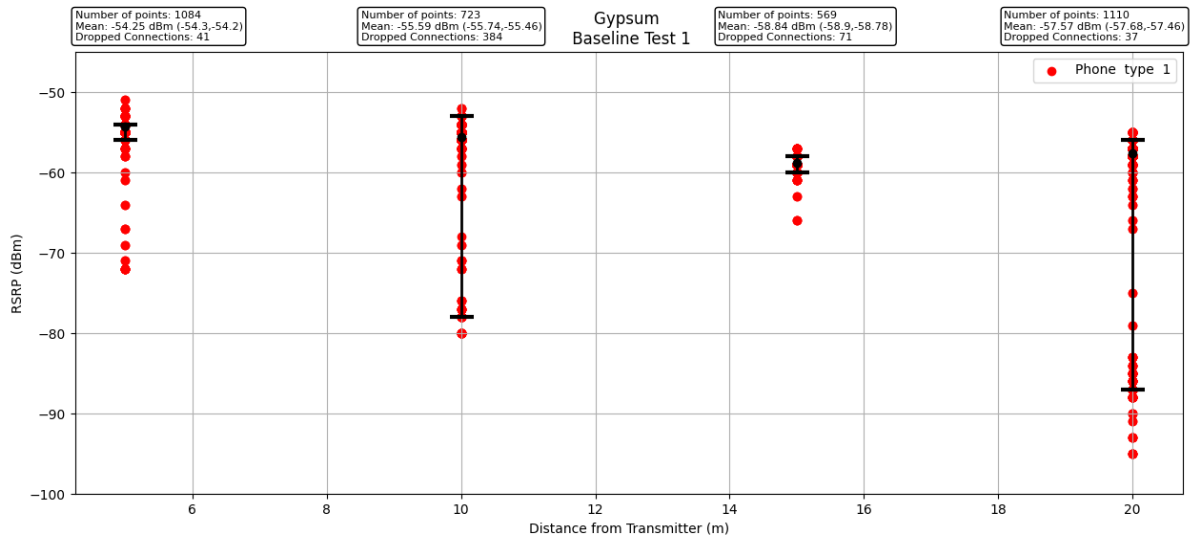
Fig. 47. Measured RSRP over distance of phone type 1
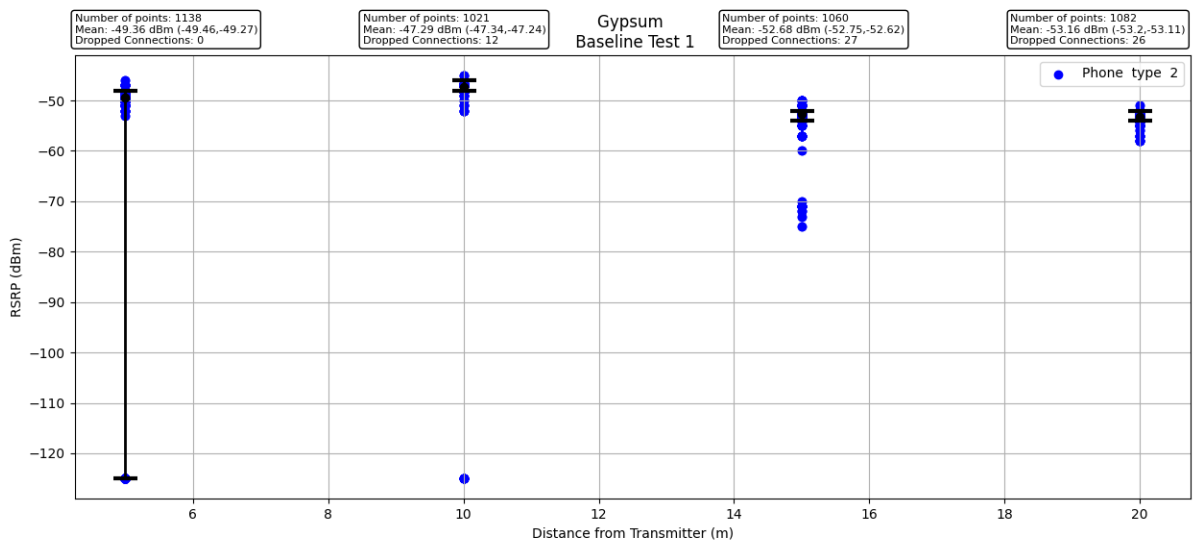
Fig. 48. Measured RSRP over distance of phone type 2
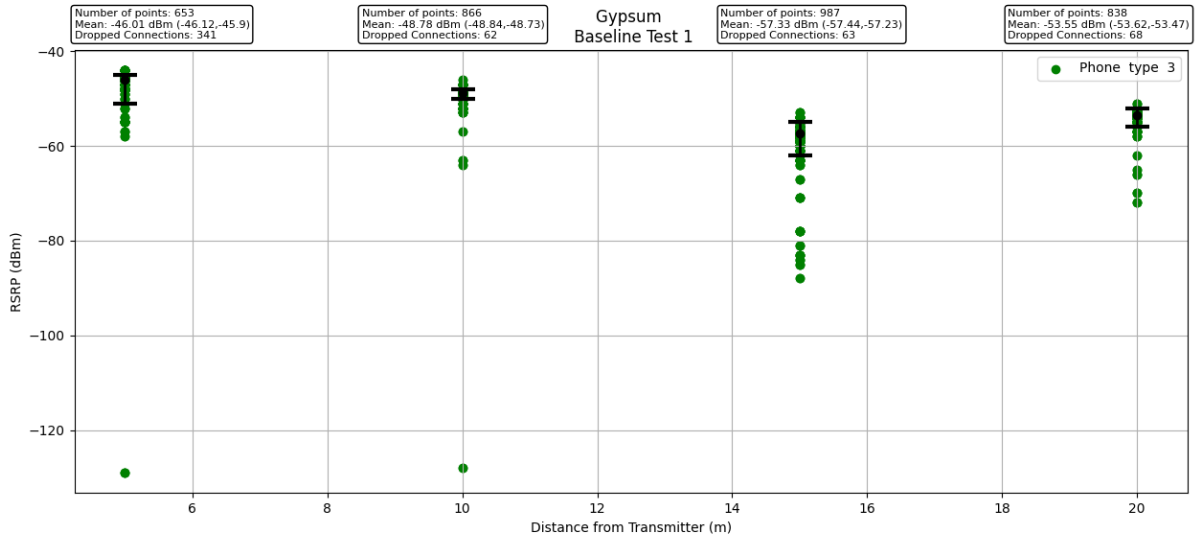
Fig. 49. Measured RSRP over distance of phone type 3

October Gypsum Site Walking Test by Phone
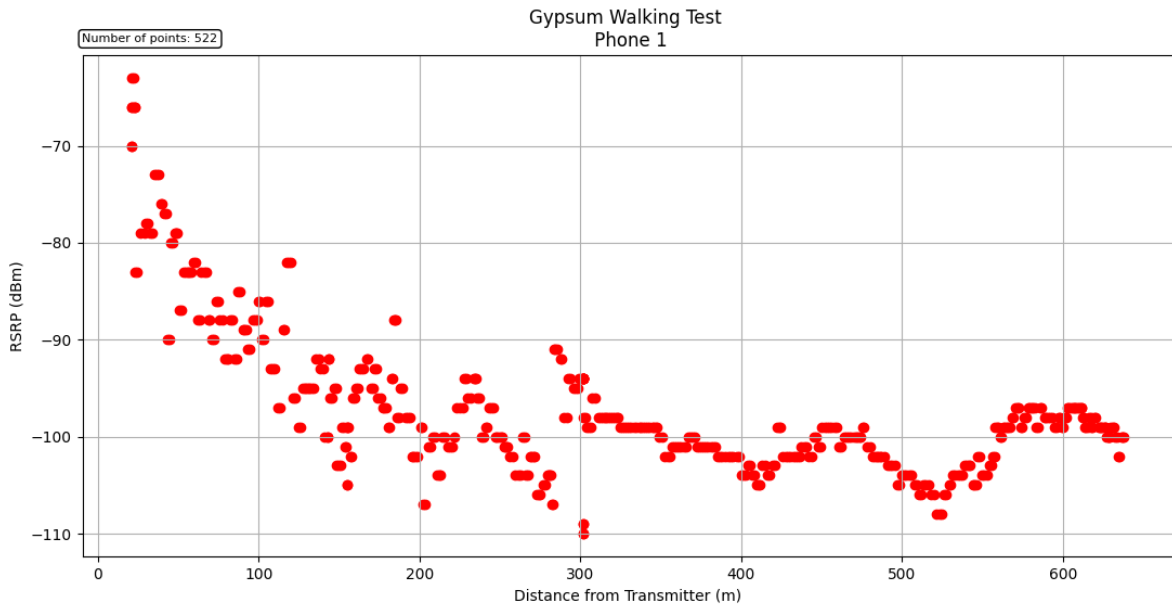
Fig. 50. Walking test measured RSRP over distance of phone type 1

48
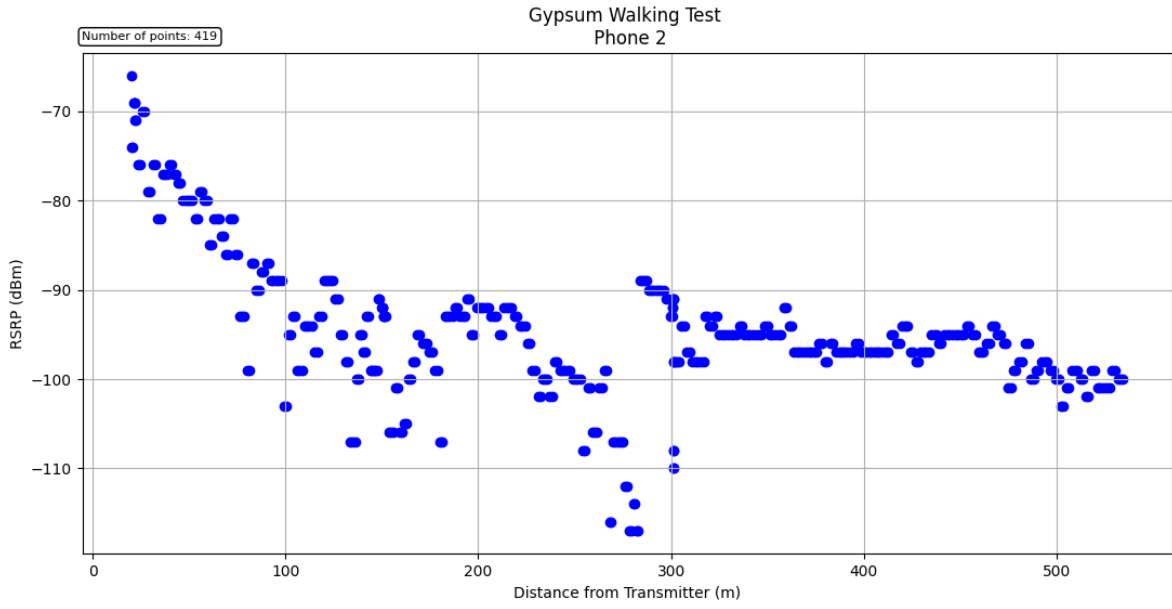
Fig. 51. Walking test measured RSRP over distance of phone type 2
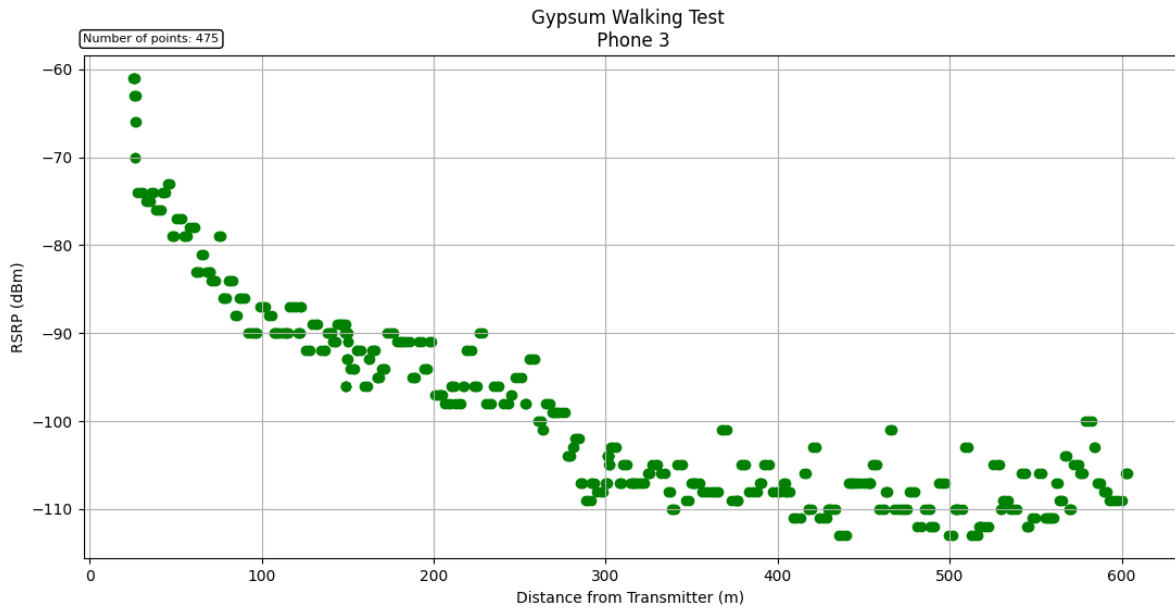
Fig. 52. Walking test measured RSRP over distance of phone type 3

December Fort Colins Site Close-range Baseline Test by Phone
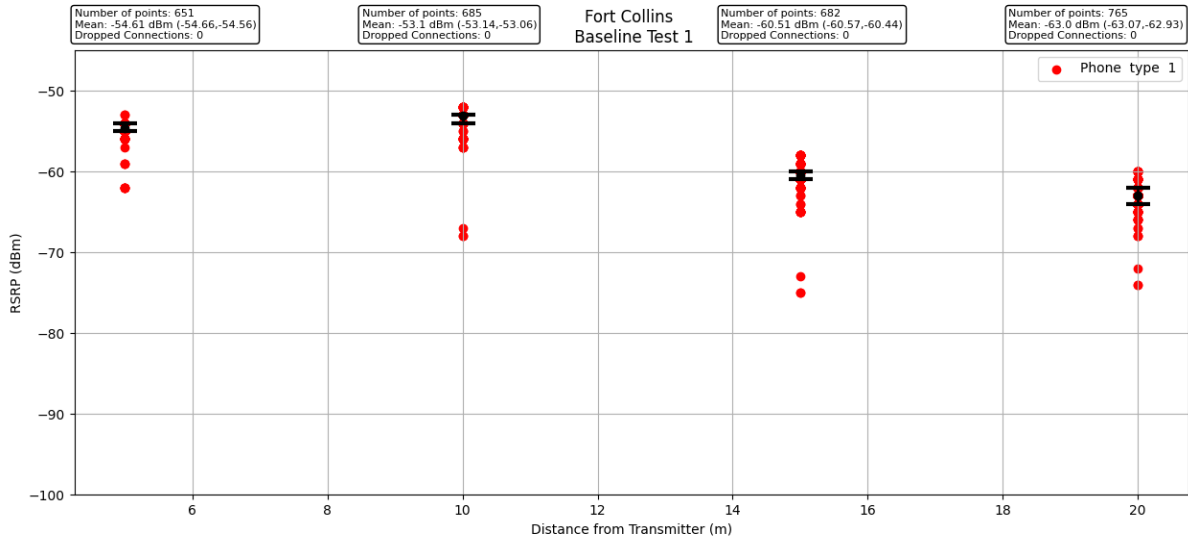
Fig. 53. Measured RSRP over distance of phone type 1
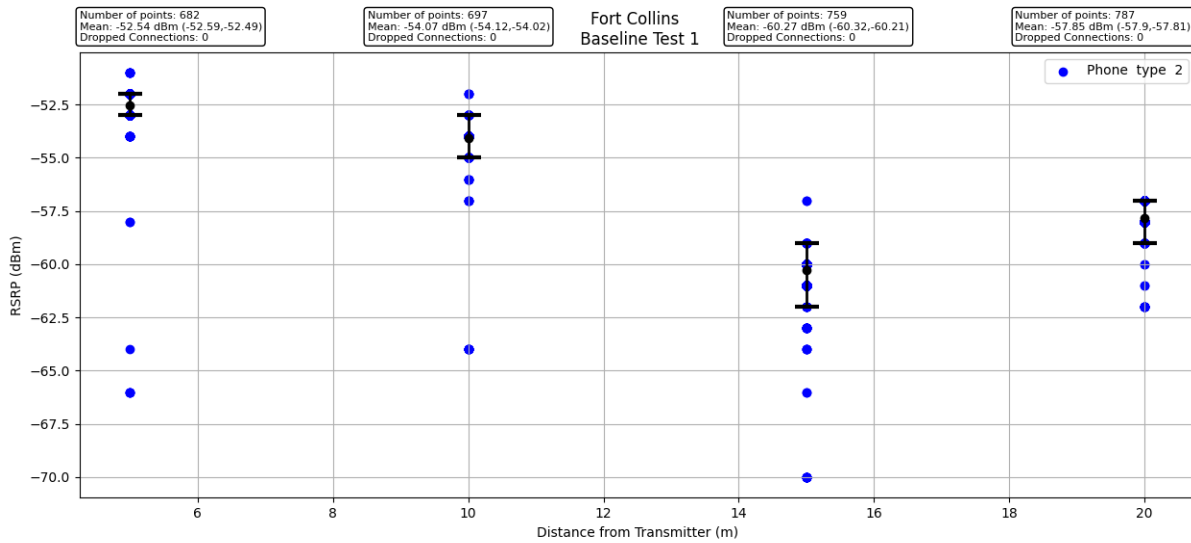
Fig. 54. Measured RSRP over distance of phone type 2
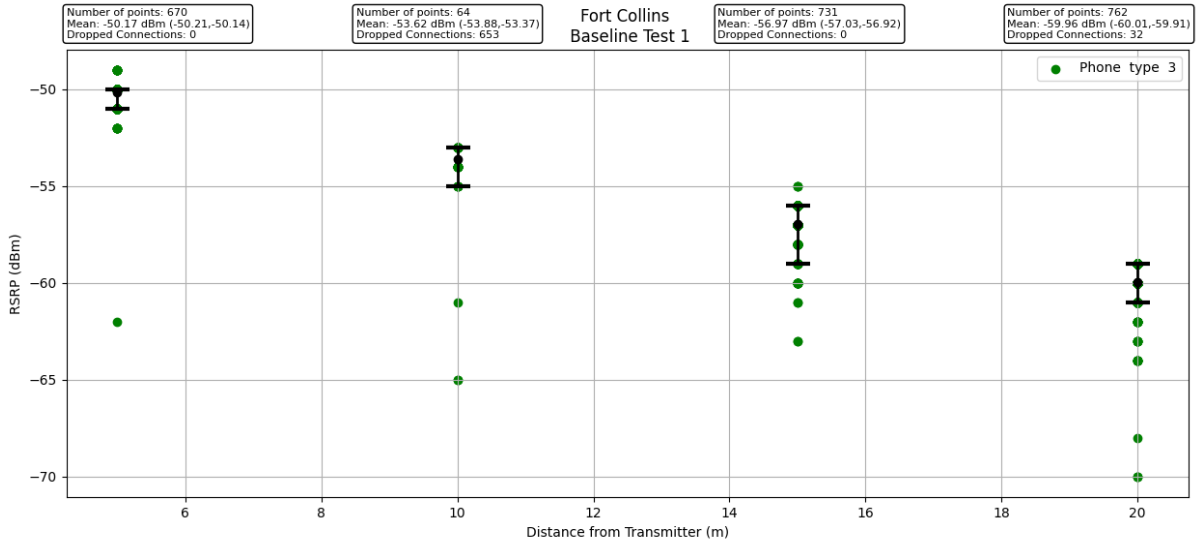
Fig. 55. Measured RSRP over distance of phone type 3

Appendix C: February Aerial Tests

February 25 350 Meter Flight Test 1
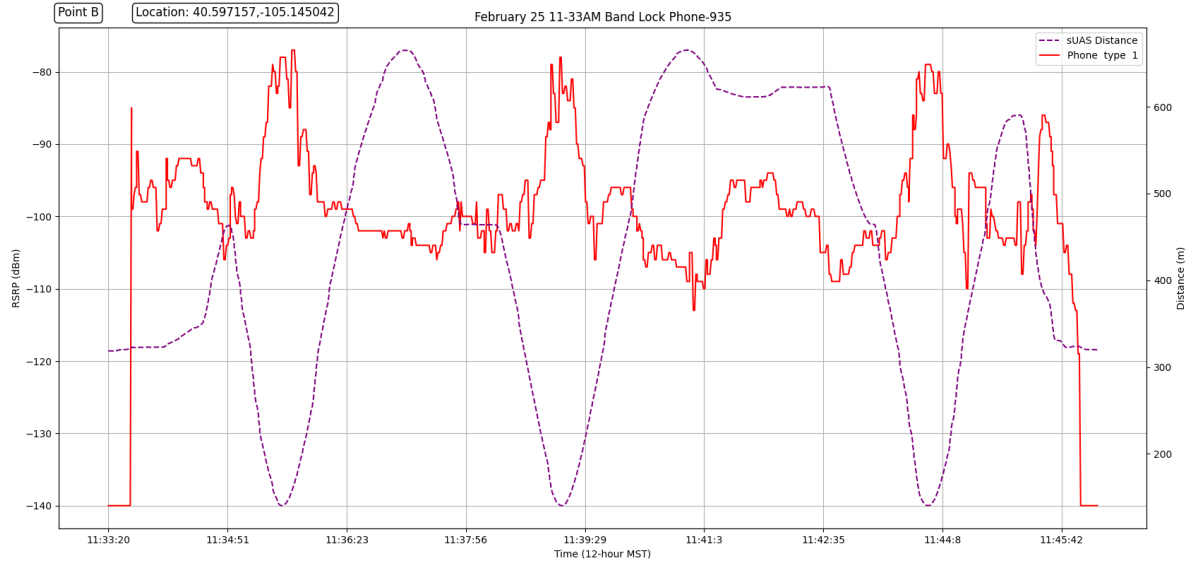
Fig. 56. 350-meter flight test 1 for band locked phone at point B
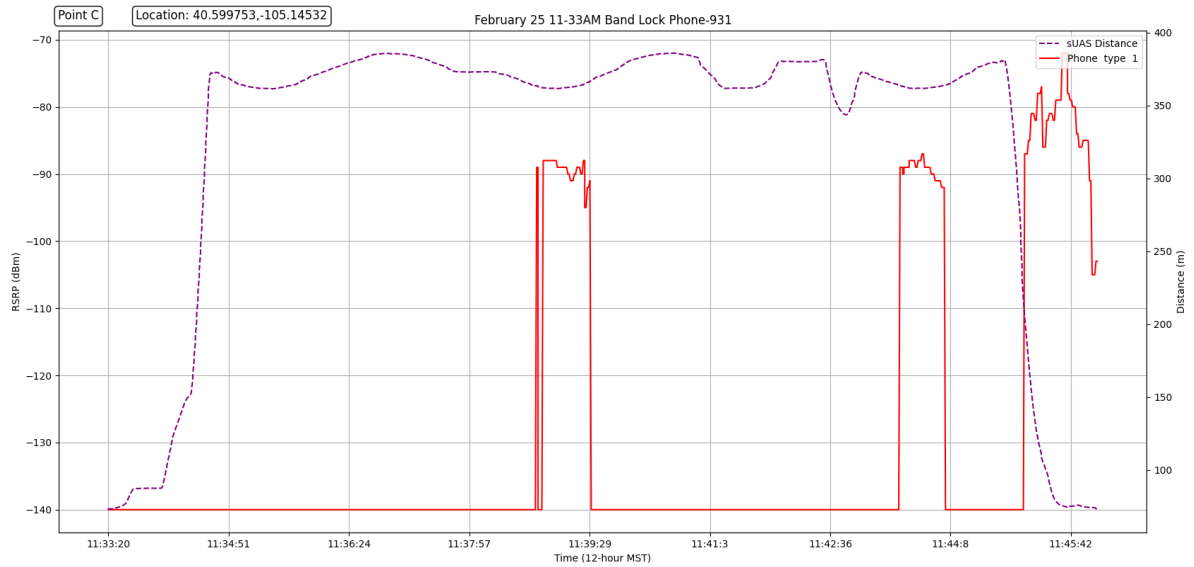
Fig. 57. 350-meter flight test 1 for band locked phone at point C
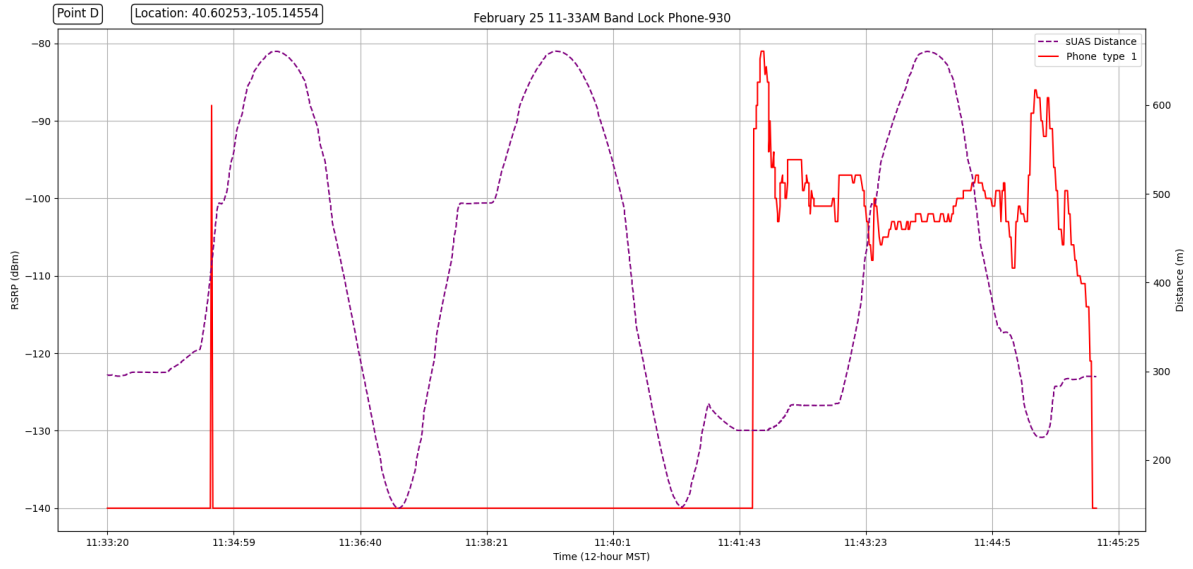
Fig. 58. 350-meter flight test 1 for band locked phone at point D

February 25 350-Meter Flight Test 2
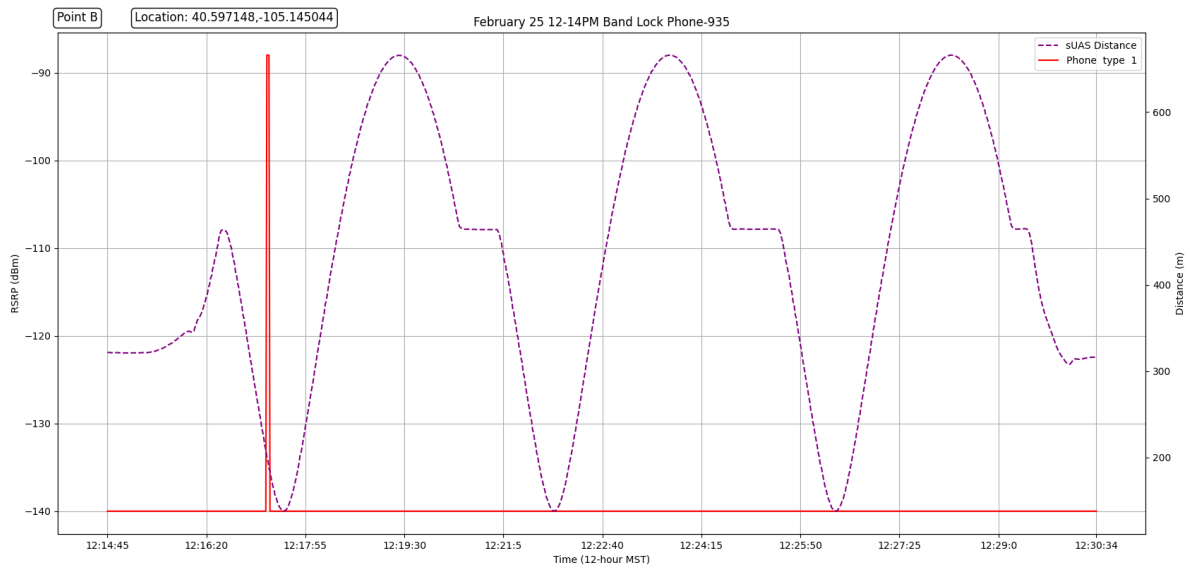
Fig. 59. 350-meter flight test 2 for band locked phone at point B

Fig. 60. 350-meter flight test 2 for band locked phone at point C

Fig. 61. 350-meter flight test 2 for band locked phone at point D

February 25 350-Meter Flight Test 3
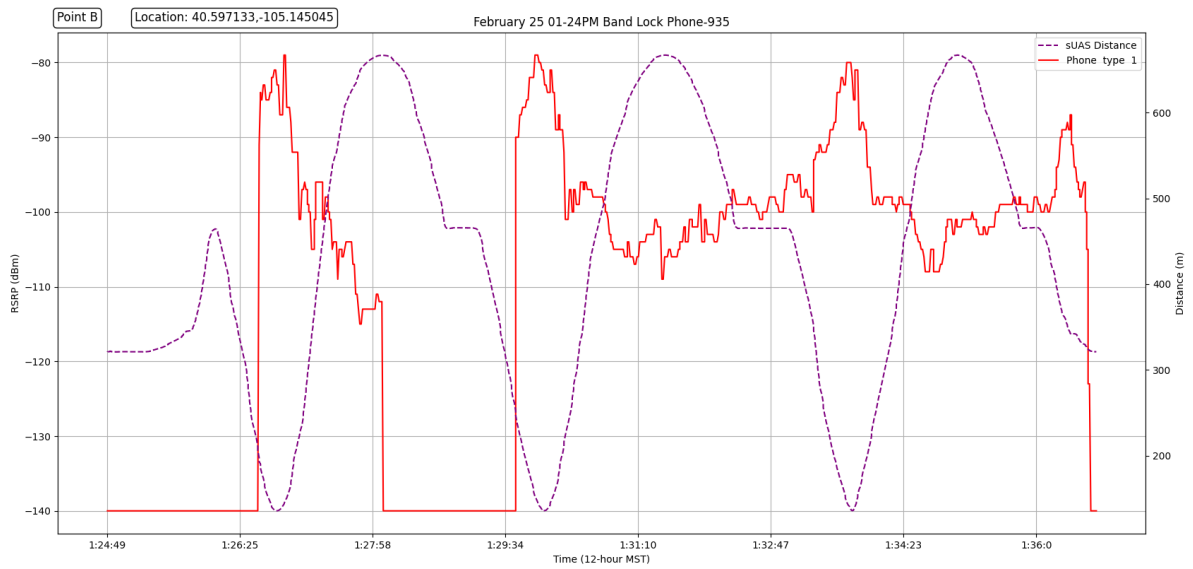
Fig. 62. 350-meter flight test 3 for band locked phone at point B
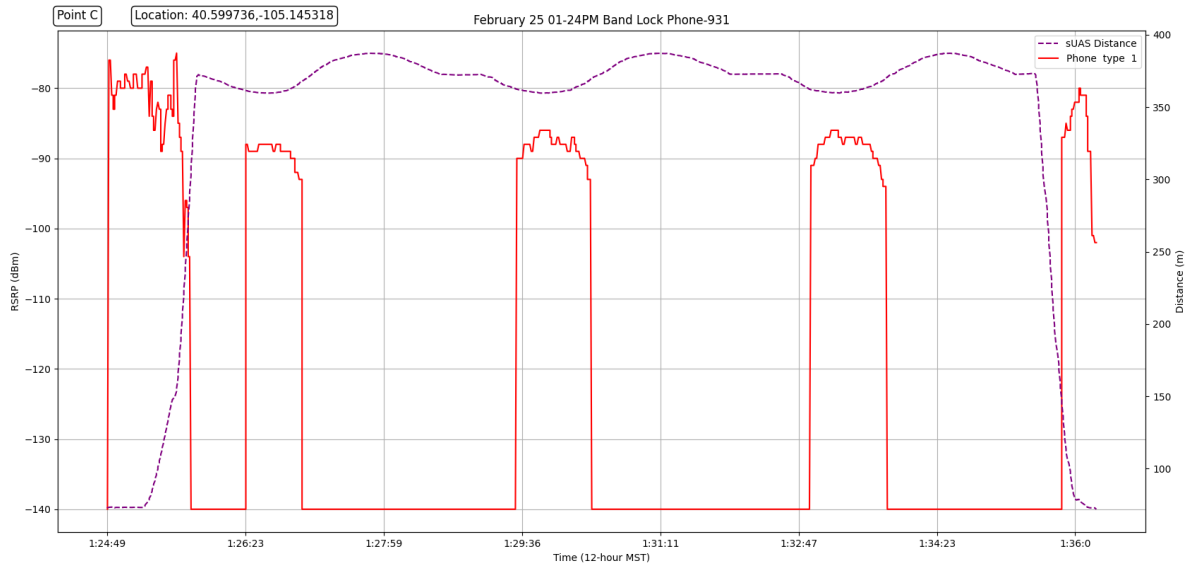
Fig. 63. 350-meter flight test 3 for band locked phone at point C

55
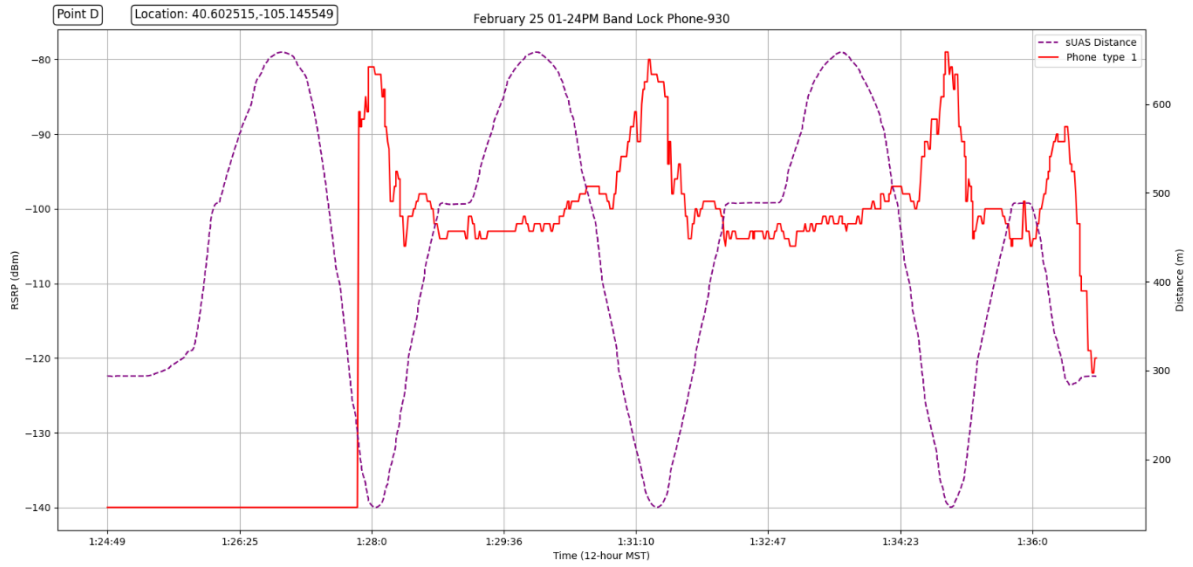
Fig. 64. 350-meter flight test 3 for band locked phone at point D

February 25 350-Meter Flight Test 4
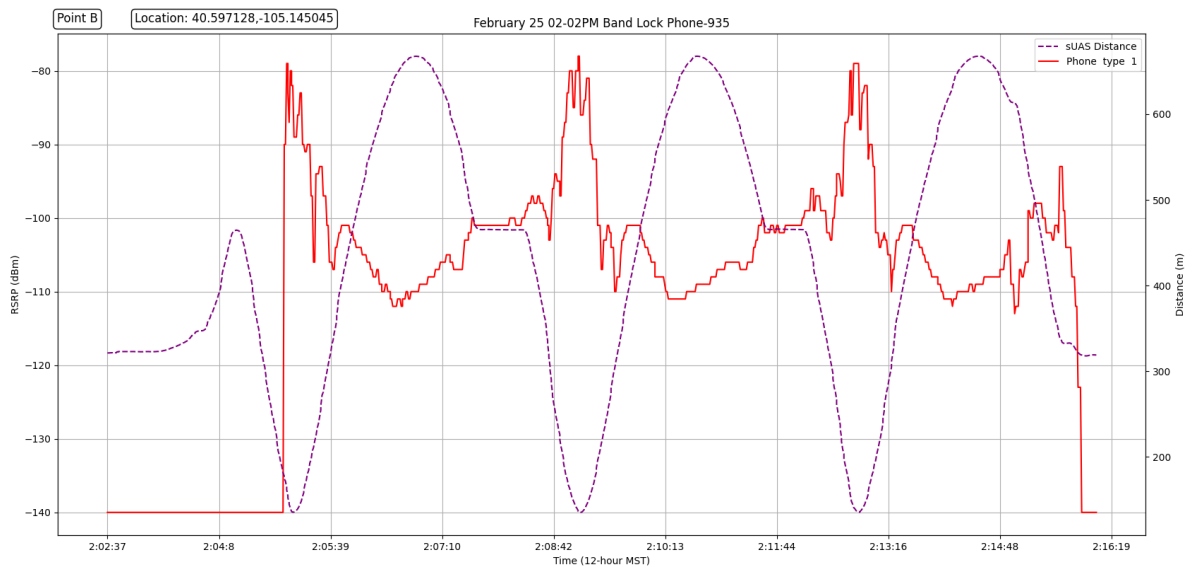
Fig. 65. 350-meter flight test 4 for band locked phone at point B
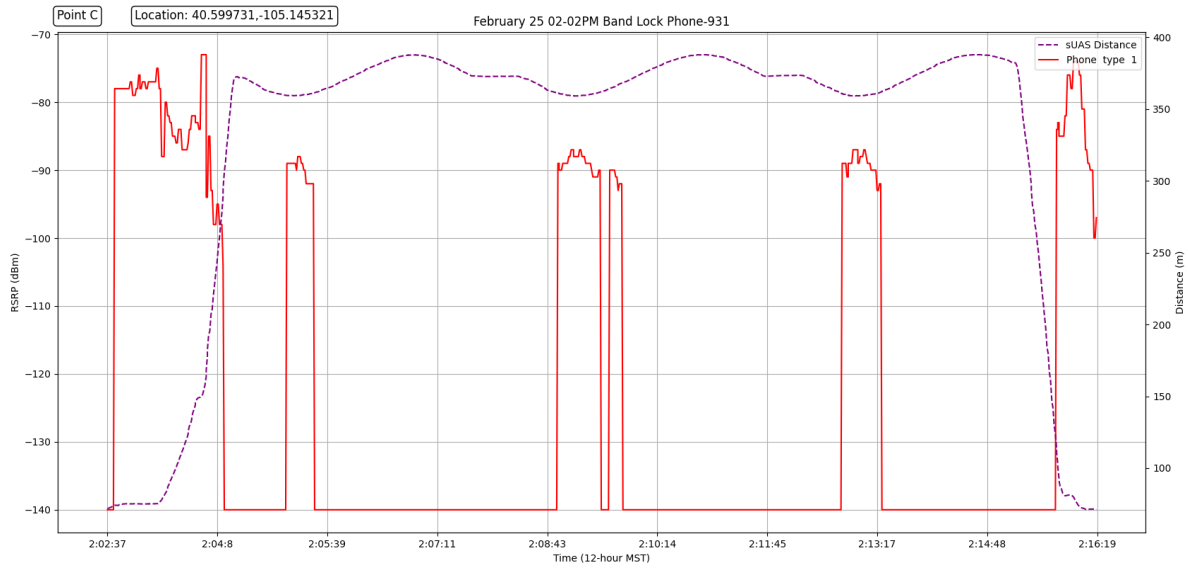
Fig. 66. 350-meter flight test 4 for band locked phone at point C
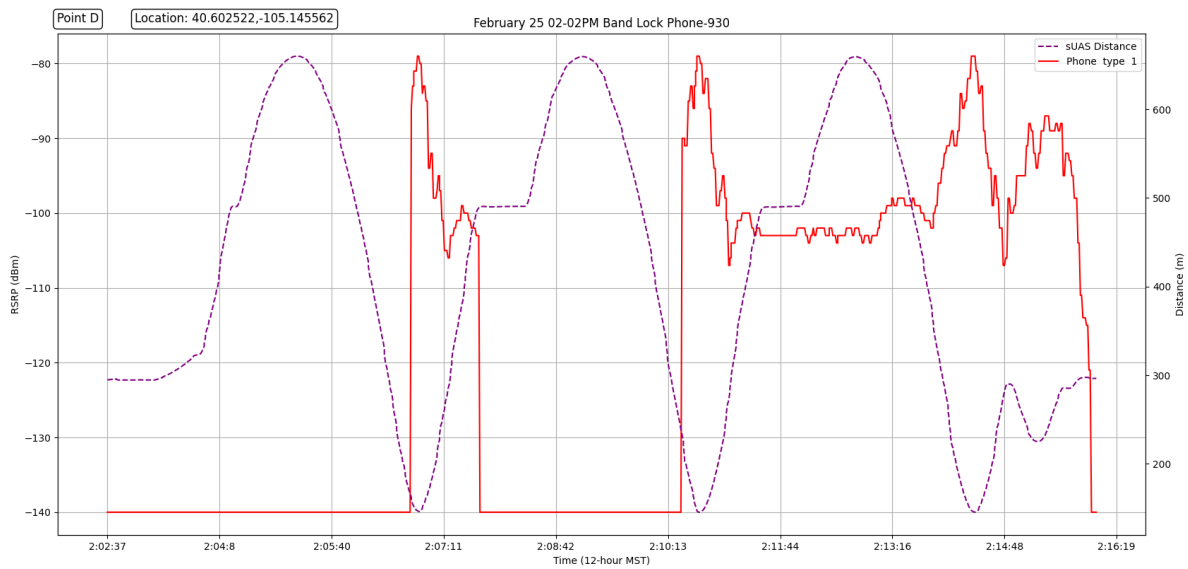
Fig. 67. 350-meter flight test 4 for band locked phone at point D

February 25 600-Meter Flight Test 1
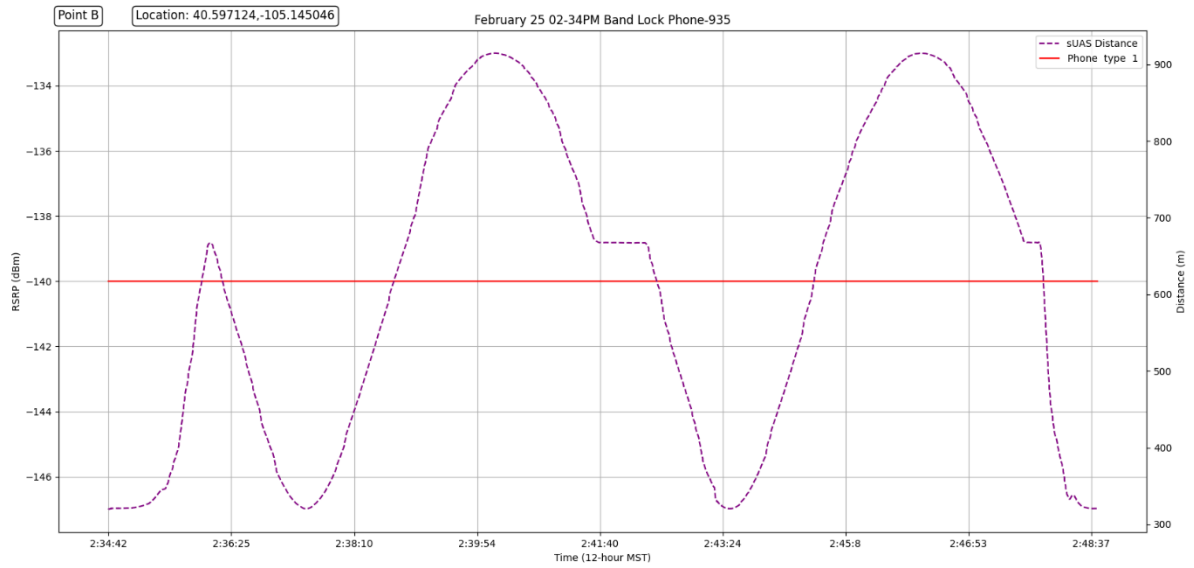
Fig. 68. 600-meter flight test 1 for band locked phone at point B
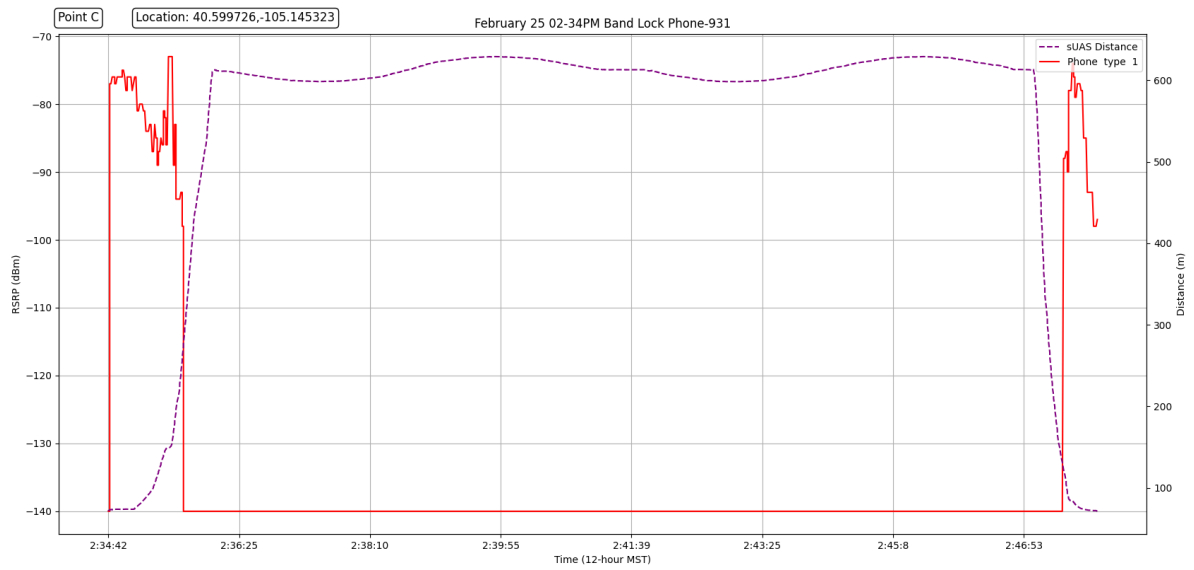
Fig. 69. 600-meter flight test 1 for band locked phone at point C
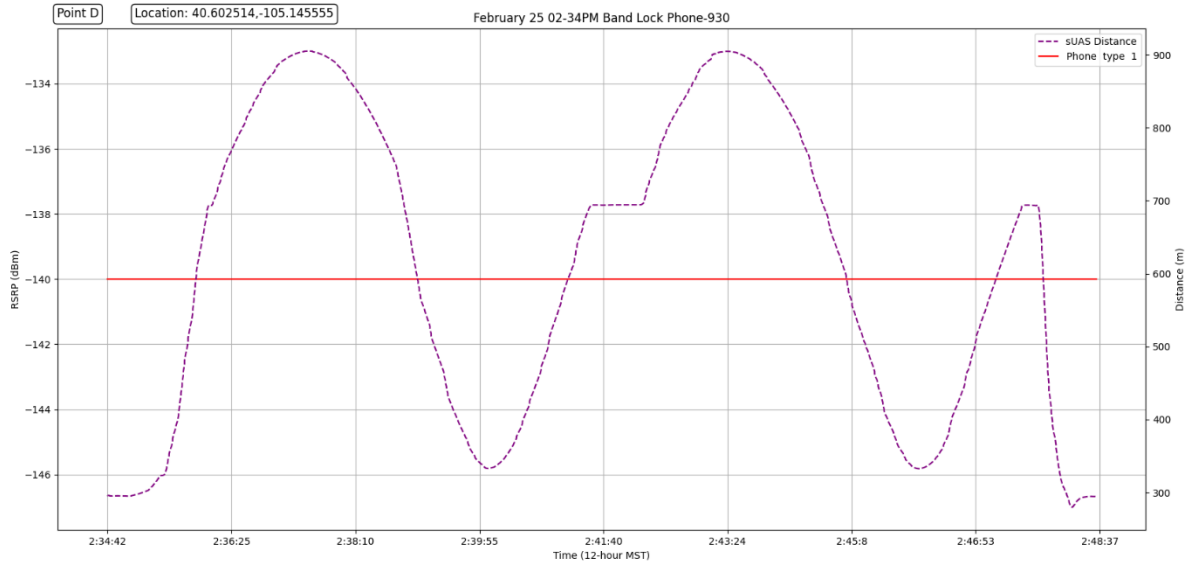
Fig. 70. 600-meter flight test 1 for band locked phone at point D

February 25 600-Meter Flight Test 2
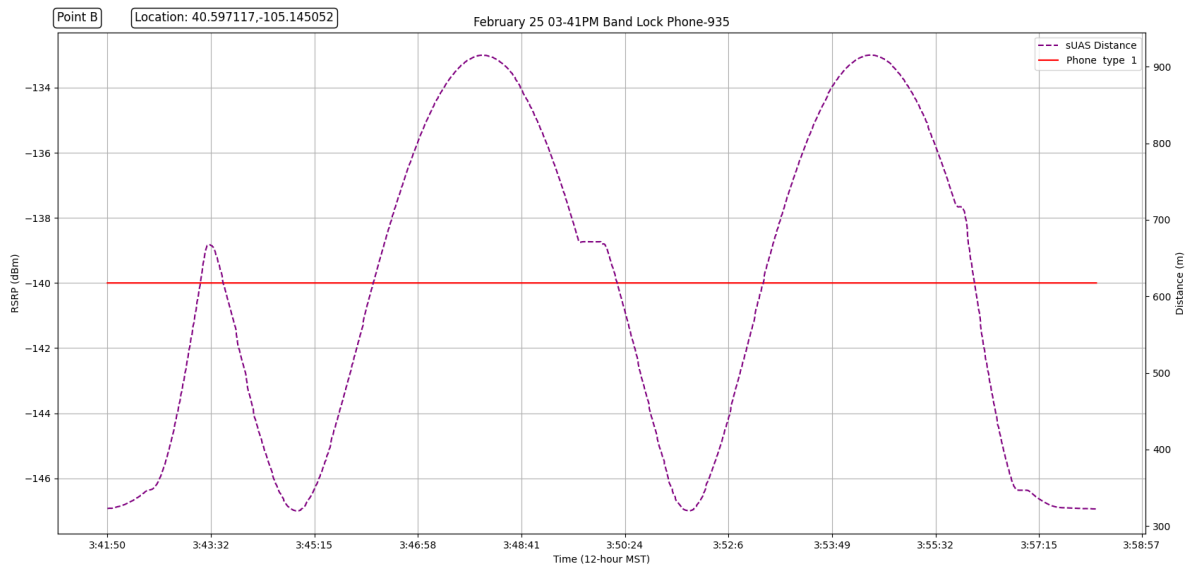
Fig. 71. 600-meter flight test 2 for band locked phone at point B

59

Fig. 72. 600-meter flight test 2 for band locked phone at point C
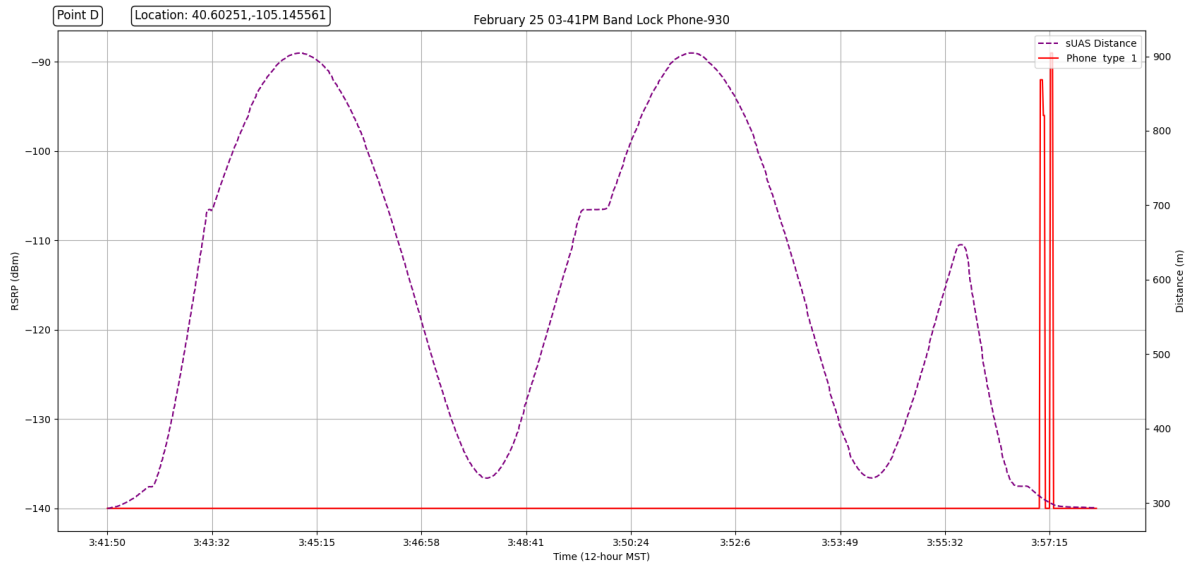
Fig. 73. 600-meter flight test 2 for band locked phone at point D

February 28 350-Meter Flight Test 5
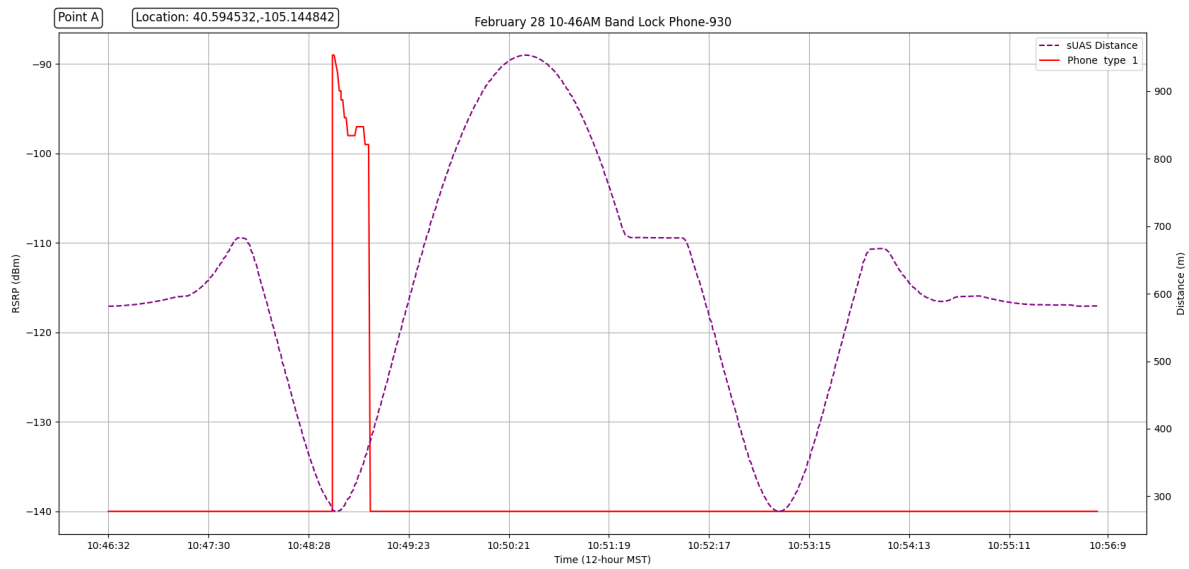
Fig. 74. 350-meter flight test 5 for band locked phone at point A
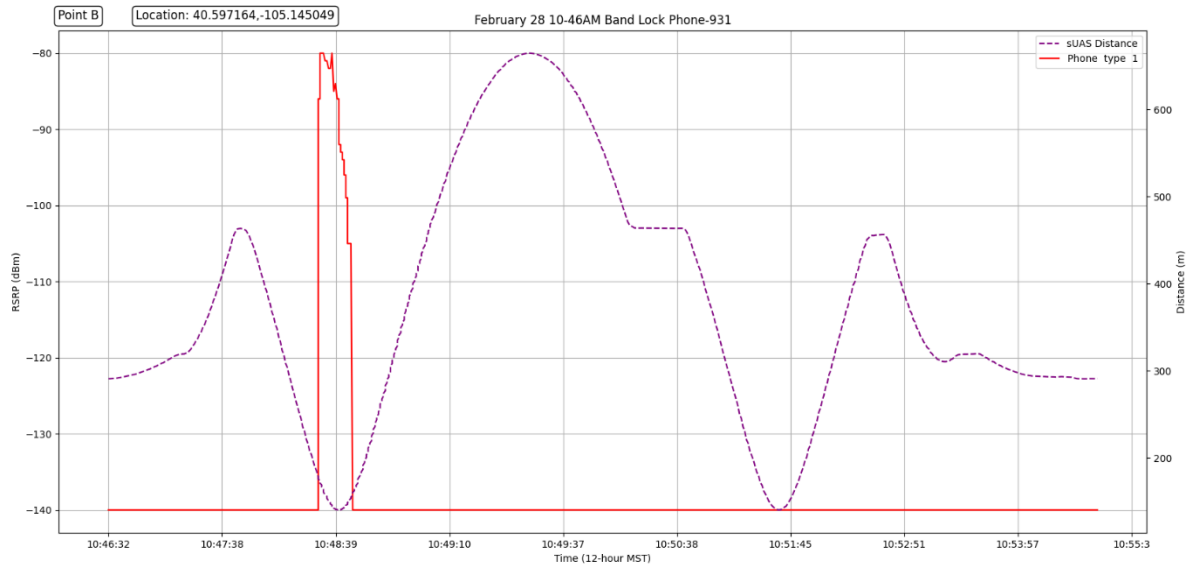
Fig. 75. 350-meter flight test 5 for band locked phone at point B

61
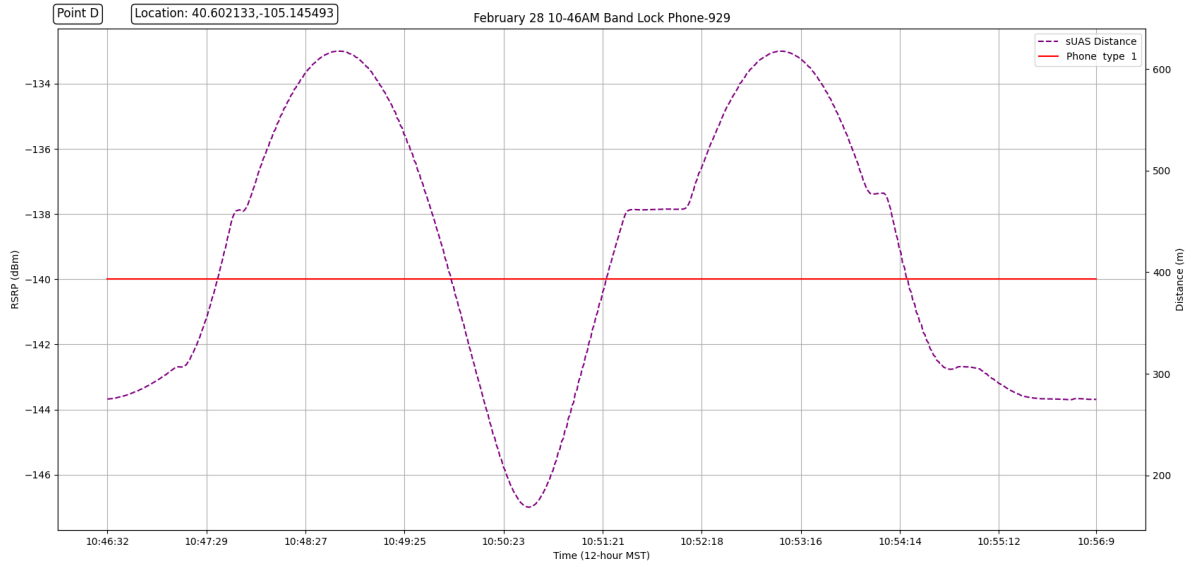
Fig. 76. 350-meter flight test 5 for band locked phone at point D

February 28 350-Meter Flight Test 6
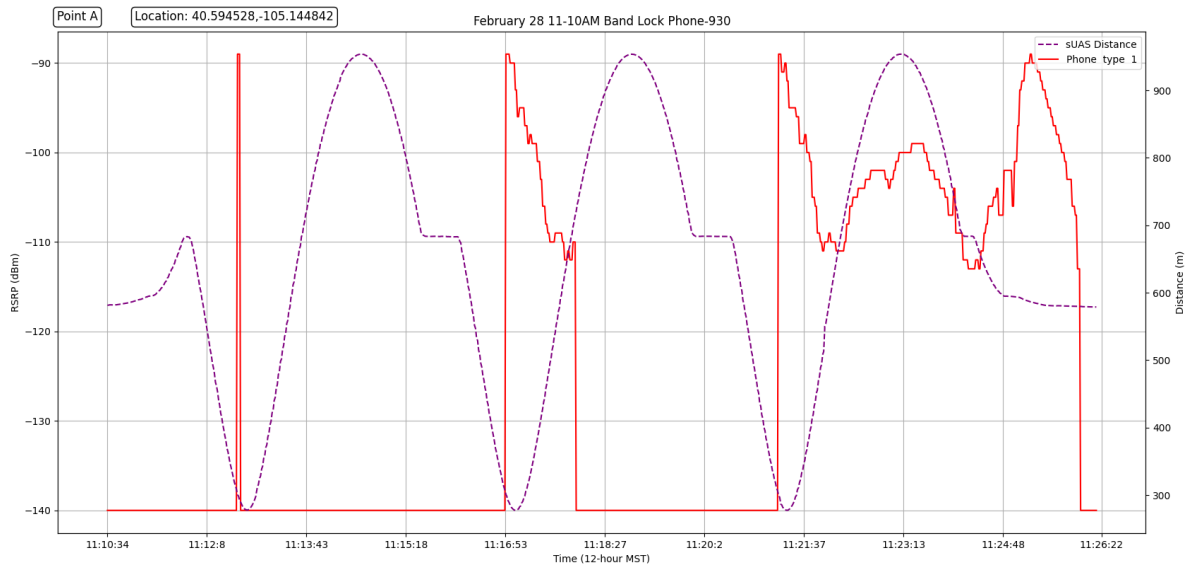
Fig. 77. 350-meter flight test 6 for band locked phone at point A

62
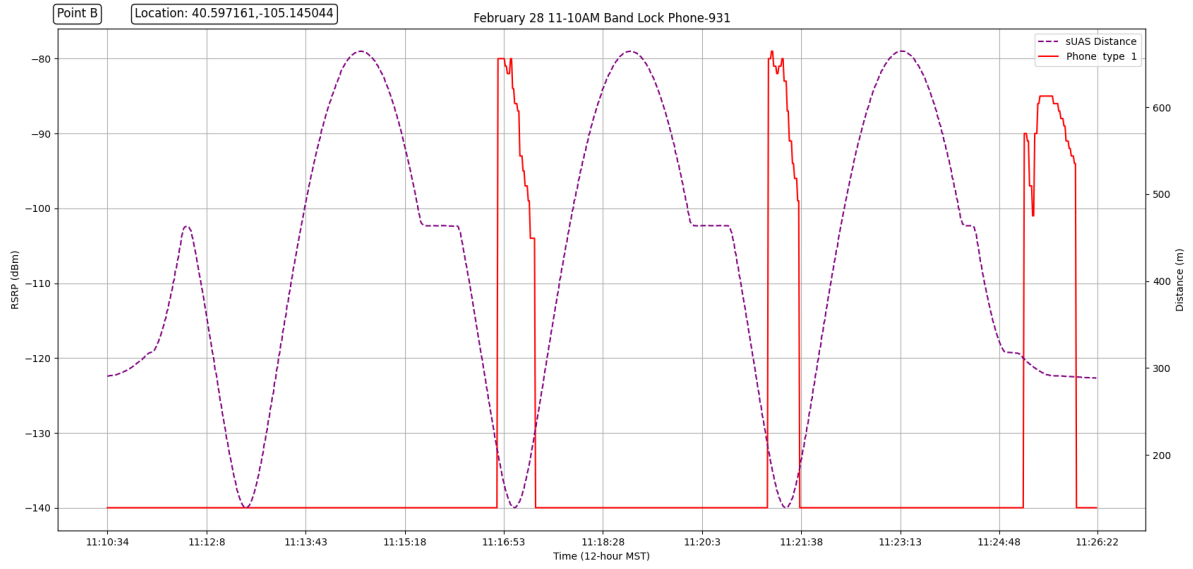
Fig. 78. 350-meter flight test 6 for band locked phone at point B
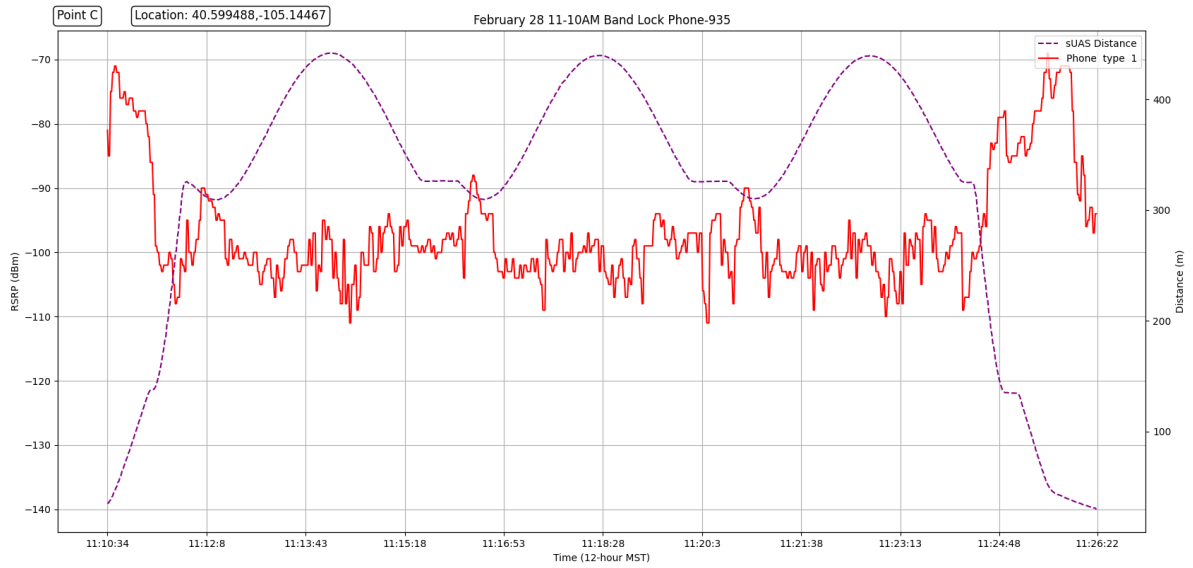
Fig. 79. 350-meter flight test 6 for band locked phone at point C

Fig. 80. 350-meter flight test 6 for band locked phone at point D

February 28 350-Meter Flight Test 7
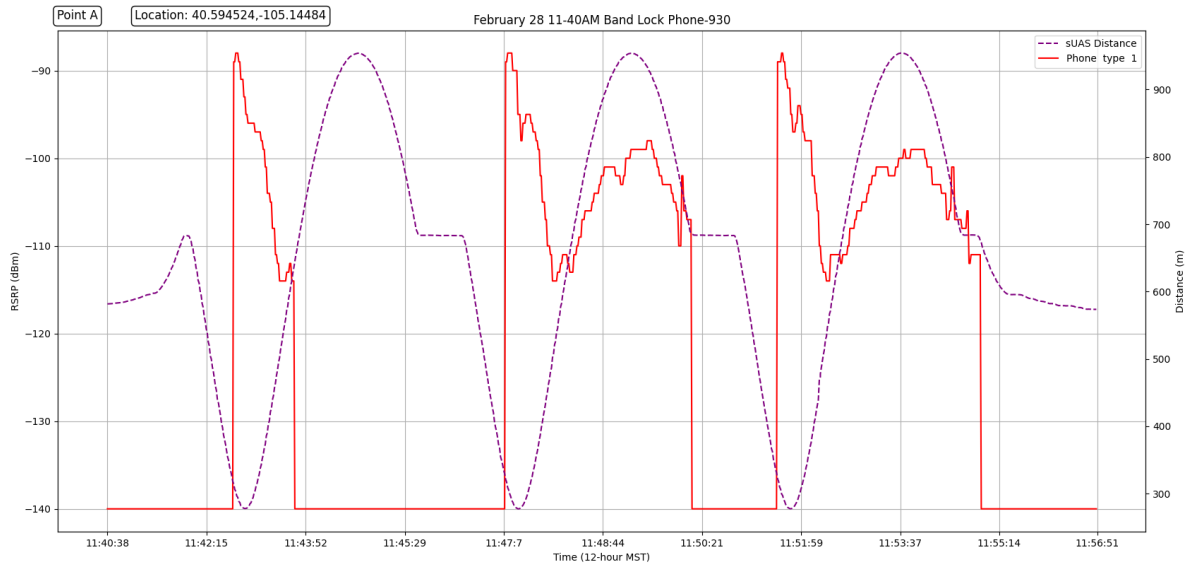
Fig. 81. 350-meter flight test 7 for band locked phone at point A
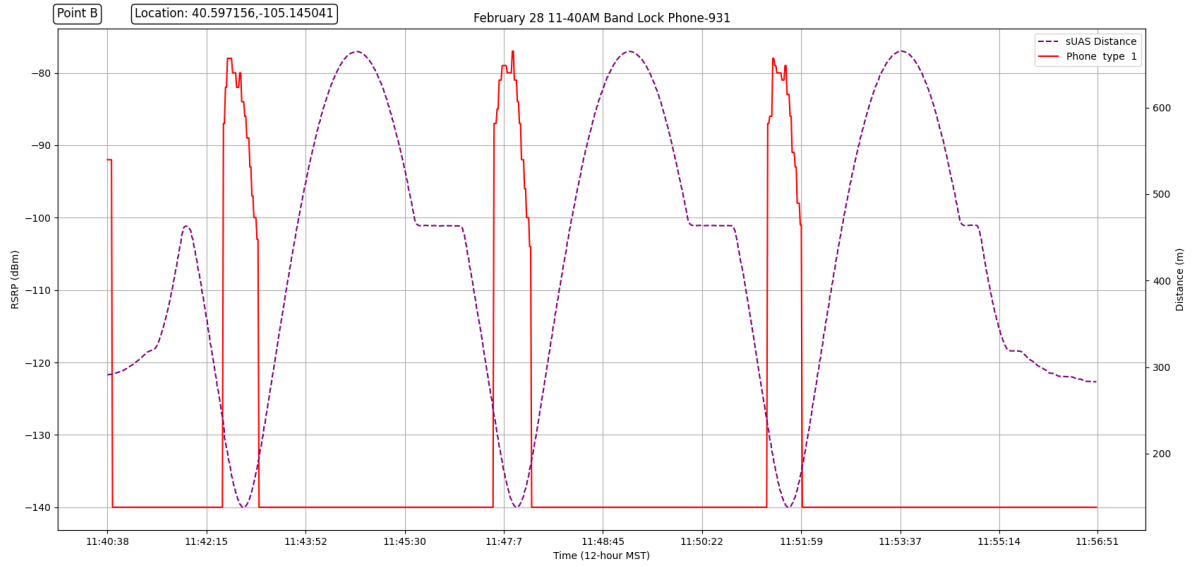
Fig. 82. 350-meter flight test 7 for band locked phone at point B
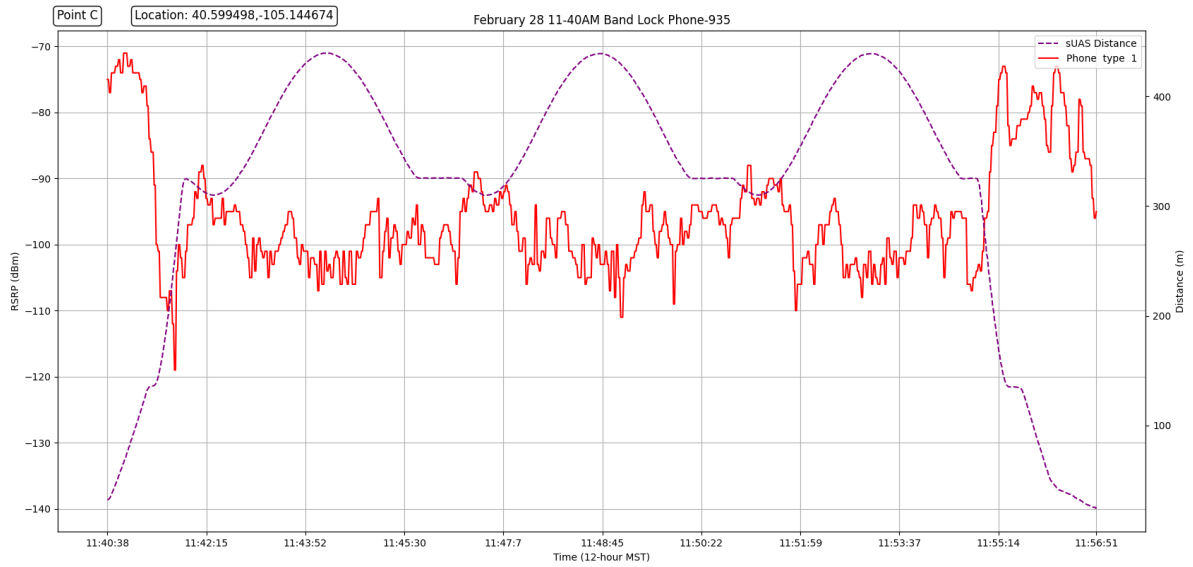
Fig. 83. 350-meter flight test 7 for band locked phone at point C
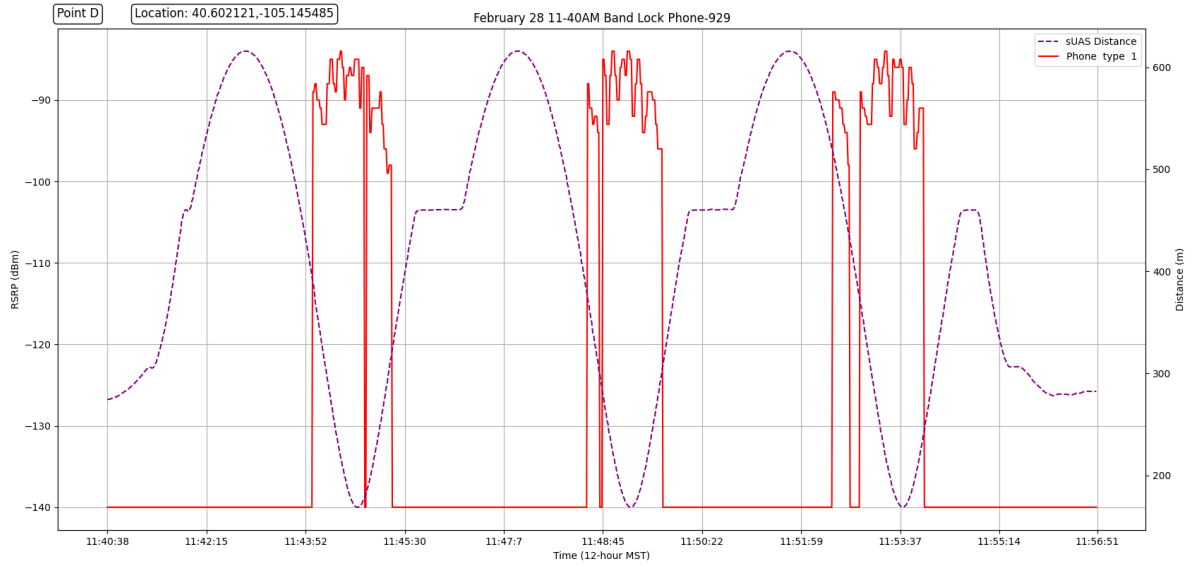
Fig. 84. 350-meter flight test 7 for band locked phone at point D

February 28 350-Meter Flight Test 8
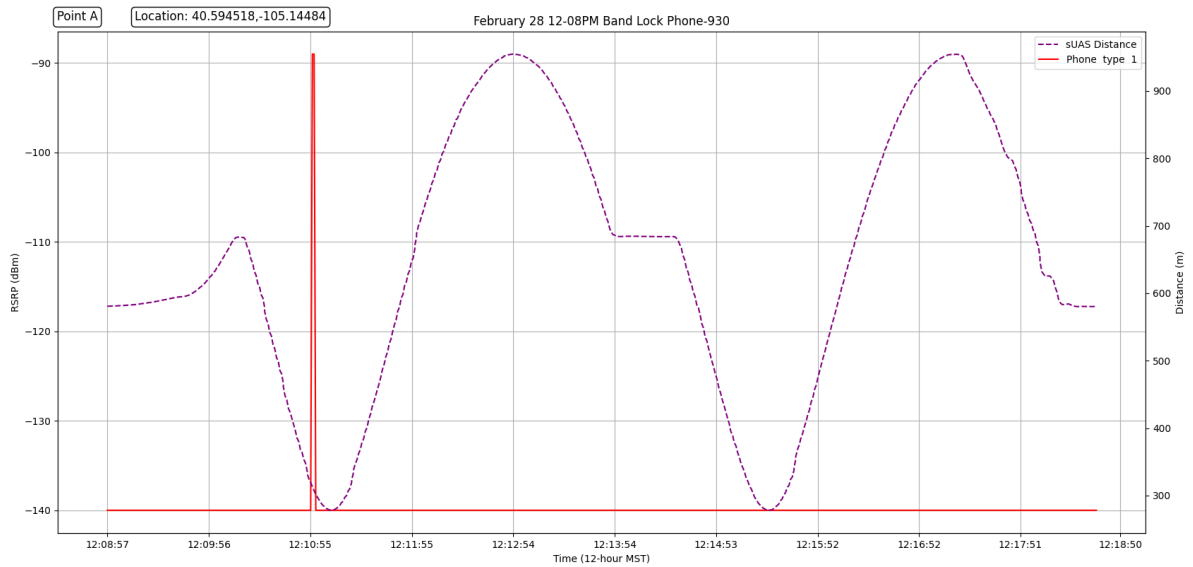
Fig. 85. 350-meter flight test 8 for band locked phone at point A

66
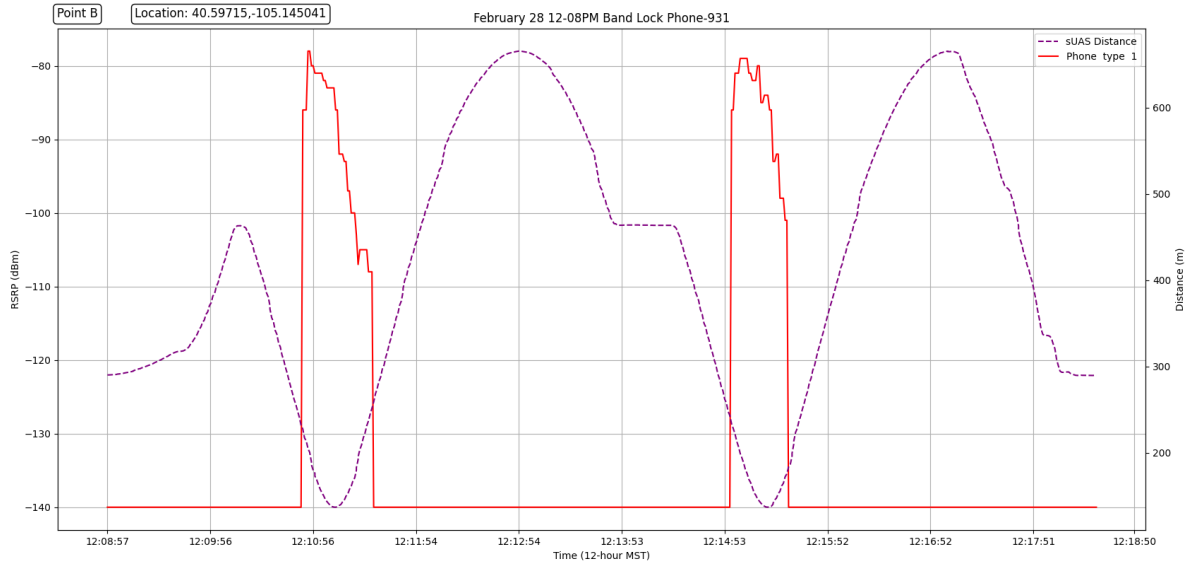
Fig. 86. 350-meter flight test 8 for band locked phone at point B
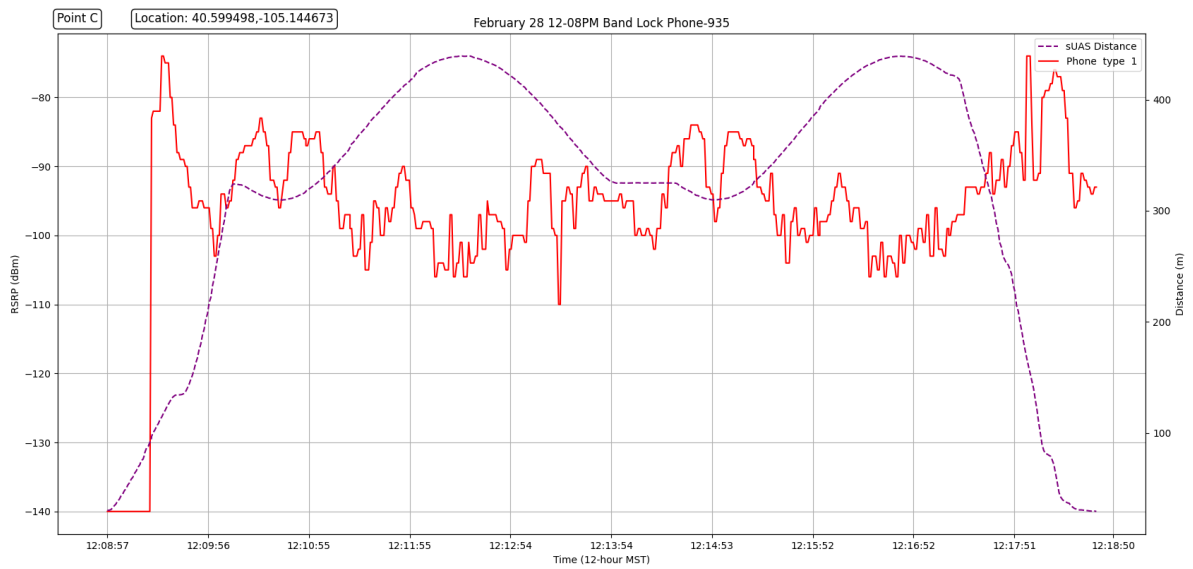
Fig. 87. 350-meter flight test 8 for band locked phone at point C
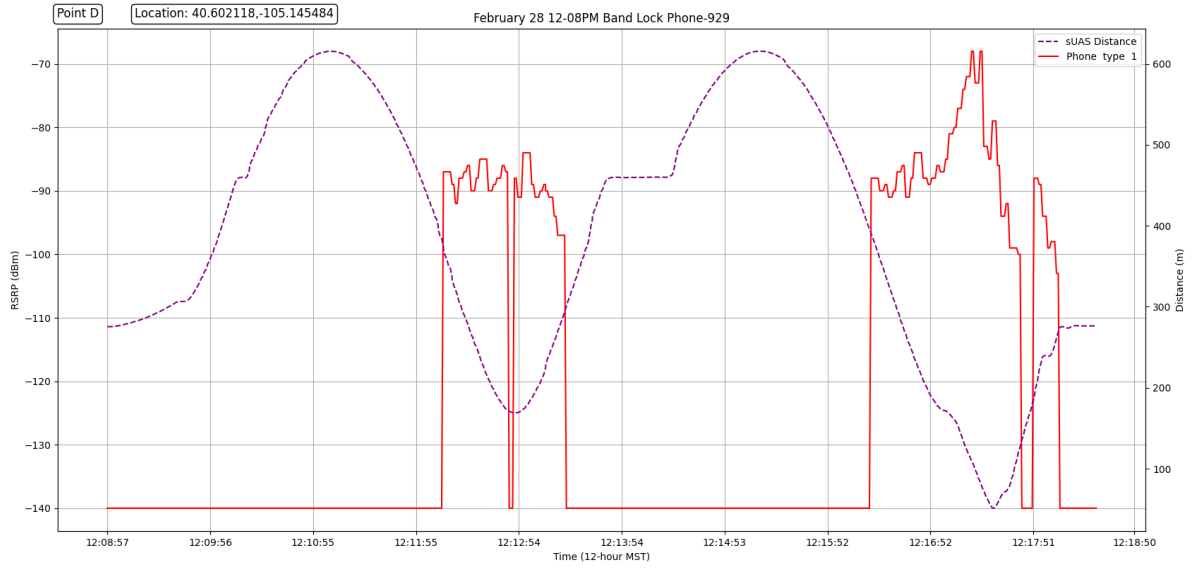
Fig. 88. 350-meter flight test 8 for band locked phone at point D

February 28 350-Meter Flight Test 9
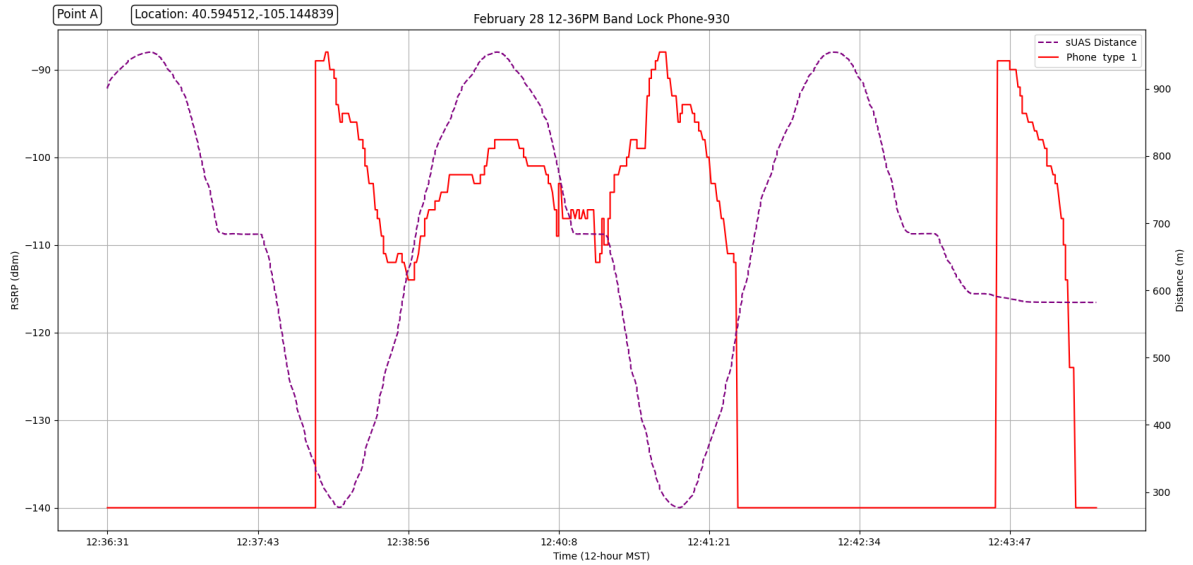
Fig. 89. 350-meter flight test 9 for band locked phone at point A
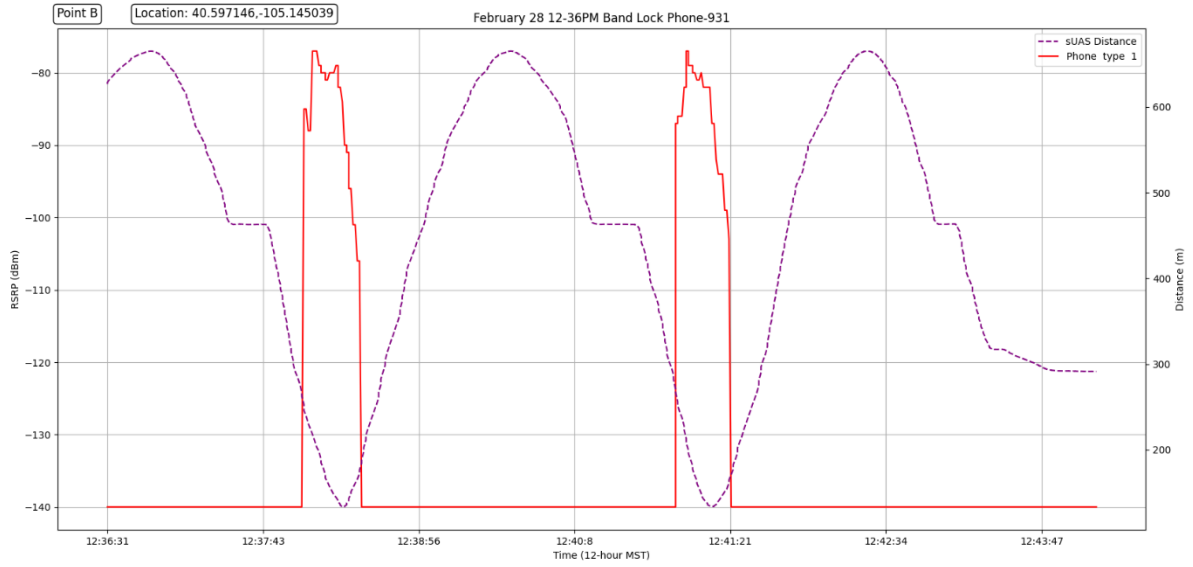
Fig. 90. 350-meter flight test 9 for band locked phone at point B
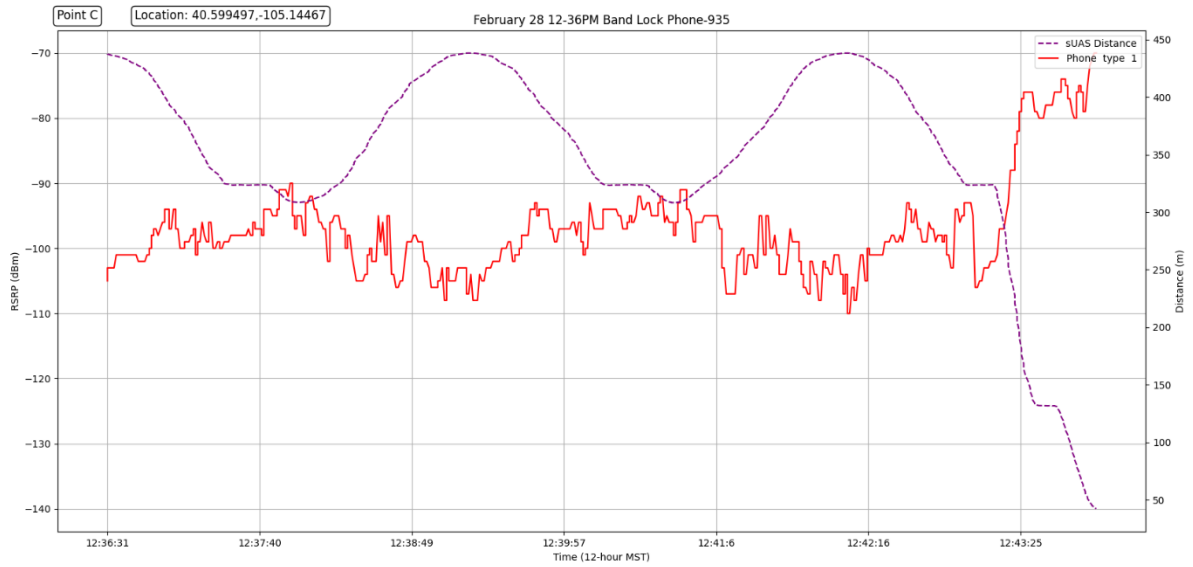
Fig. 91. 350-meter flight test 9 for band locked phone at point C

Fig. 92. 350-meter flight test 9 for band locked phone at point D